COMBINED CO_2/H_2O SOLID OXIDE ELECTROLYSIS

by

Christine Schroeder Iacomini

A Dissertation Submitted to the Faculty of the

DEPARTMENT OF AEROSPACE AND MECHANICAL ENGINEERING

In Partial Fulfillment of the Requirements
For the Degree of

DOCTOR OF PHILOSOPHY
WITH A MAJOR IN AEROSPACE ENGINEERING

In the Graduate College

THE UNIVERSITY OF ARIZONA

2004

The University of Arizona ®
Graduate College

As members of the Final Examination Committee, we certify that we have read the dissertation prepared by Christine Schroeder Iacomini

entitled COMBINED CO_2/H_2O SOLID OXIDE ELECTROLYSIS

and recommend that it be accepted as fulfilling the dissertation requirement for the Degree of Doctor of Philosophy

Cho Lik Chan	4/8/04 date
K. R. Sridhar	April 8, 2004 date
Matthias Gottmann	4/8/04 date
Bruce Bayly	8 April 2004 date
Robert Indik	date

Final approval and acceptance of this dissertation is contingent upon the candidate's submission of the final copies of the dissertation to the Graduate College.

I hereby certify that I have read this dissertation prepared under my direction and recommend that it be accepted as fulfilling the dissertation requirement.

Dissertation Director: Cho Lik Chan / K. R. Sridhar — 4/8/04 / 4/5/04 date

STATEMENT BY AUTHOR

This dissertation has been submitted in partial fulfillment of requirements for an advanced degree at The University of Arizona and is deposited in the University Library to be made available to borrowers under rules of the Library.

Brief quotations from this dissertation are allowable without special permission, provided that accurate acknowledgment of source is made. Requests for permission for extended quotation from or reproduction of this manuscript in whole or in part may be granted by the head of the major department or the Dean of the Graduate College when in his or her judgment the proposed use of the material is in the interests of scholarship. In all other instances, however, permission must be obtained from the author.

SIGNED: 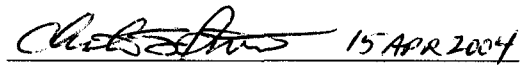 15 APR 2004

ACKNOWLEDGEMENTS

I would like to thank the National Aeronautics and Space Administration of the United States for having the vision and foresight to pursue the research endeavors presented in this dissertation. The willingness of Dr. Mark Kliss and Dr. John Finn of the Astrobiology Technology Branch, NASA Ames Research Center, to sponsor the effort allowed for the work to be mostly funded by the NASA Graduate Student Researchers Program (GSRP) through NASA-Ames Grant No. NGT 2-52268, "ISRU Technologies for Human Mars Exploration".

I would like to thank Dr. K. R. Sridhar, my principle advisor, for providing to me the opportunity to pursue research that supports human exploration of space, particularly Mars. His past work has created a legacy that justifies the pursuit of solid oxide electrolysis as a viable and enabling technology for space exploration.

I am very grateful to the other Dissertation Committee members from the Aerospace and Mechanical Engineering Department. Dr. Cho Lik Chan co-advised this dissertation, giving much advice over the years, and acted as Director of the Dissertation Committee. Dr. Matthias Gottmann always made himself available, providing invaluable feedback regarding experimental and theoretical investigations.

I would like to acknowledge the efforts of my minor Dissertation Committee members from the Department of Mathematics. Dr. Bruce Bayly offered much appreciated support and enthusiasm. Dr. Robert Indik, with whom I enjoyed working, granted me guidance in mathematical modeling.

Dr. David Lynch of the Materials Science and Engineering Department deserves special recognition for his completely voluntary involvement with this dissertation. His dedication and valuable instruction allowed me to better visualize and analyze the thermodynamics of reactive multi-component systems.

My colleagues must also be acknowledged contributors to this work: Ian Russell for teaching me how to work effectively in a lab and conduct electrolysis experiments; Dave Lyle for helping me troubleshoot odds and ends of test beds; Darren Hickey for donating his higher fidelity test bed to my research; Dr. Gege Tao for teaching me how to build my first electrolysis cells and reviewing this dissertation; Richard Cetner for assistance in collecting experimental data; Dien Nguyen for his expertise in electrolytes; and finally, but definitely not least, Dr. Tomo Oishi for the many debates over hypotheses and theoretical derivations as well as his time in reviewing this dissertation.

Special thanks go to AME departmental staff. Barbara Heefner's support not only made the experience fun, but easier as she always ensured I fulfilled all graduate study requirements on time and correctly. Lynda Silvain's professionalism and follow through ensured I was never left unsupported. And with Nelson Zabik and Jim Blair in charge, the machine shop provided me with top quality parts while never delaying my experiments.

Finally, I need to thank my husband Ross for brining me here to Tucson. Words can not express the importance of his encouragement in my pursuit of my dreams.

TABLE OF CONTENTS

TABLE OF CONTENTS - *Continued*

TABLE OF CONTENTS - *Continued*

TABLE OF CONTENTS - *Continued*

TABLE OF CONTENTS - *Continued*

LIST OF FIGURES

LIST OF FIGURES - *Continued*

LIST OF FIGURES - *Continued*

LIST OF FIGURES - *Continued*

LIST OF TABLES

ABSTRACT

Solid oxide electrolysis of a mixture of water and carbon dioxide has many applications in space exploration. It can be implemented in propellant production systems that use Martian resources or in closed-loop life support systems to cleanse the atmosphere of facilities in extraterrestrial bases and of cabin spacecrafts. This work endeavors to quantify the performance of combined water and carbon dioxide electrolysis, referred to as "combined electrolysis", and to understand how it works so that the technology can be best applied.

First, to thoroughly motivate the research, system modeling is presented that demonstrates the competitiveness of the technology in terms of electrolysis power requirements and consequential system mass savings. Second, to demonstrate and quantify the performance of the technology, experimental results are presented. Electrolysis cells were constructed with 8% by mol yttria-stabilized zirconia electrolytes, 50/50 by weight platinum/yttria-stabilized zircona electrodes and chromium-alloy or alumina manifolds and tubing. Performance and gas chromatograph data from electrolysis of many different gas mixtures, including water, carbon dioxide, and a combined mixture of both, are presented. Third, to explain observations made during experiments and theorize about the phenomena governing combined electrolysis, data analyses and thermodynamic modeling are applied.

Conclusions are presented regarding the transient response of combined electrolysis, the relative performance of it to that of other mixtures, how its performance depends on the water to carbon dioxide ratio, its effect on cell health, and its preference to water

versus carbon dioxide. Procedures are also derived for predicting the composition of combined electrolysis exhaust for a given oxygen production rate, humidity content, and inlet flow rate.

The influence of the two cell materials proves to be significant. However, in both cases it is proven that combined electrolysis does not encourage carbon deposition and the make-up of its products is governed by the water gas shift reaction. It is shown that the chromium-alloy system achieves water gas shift reaction equilibrium whereas the alumina system does not. Experimental observations support the argument that chromium oxide inside the chromium alloy cell forces its water gas shift reaction to equilibrium during electrolysis, influencing combined electrolysis performance.

1 INTRODUCTION

1.1 Motivation

A closed-loop oxygen regeneration system for life support would greatly benefit the International Space Station in low Earth orbit as well as any extended duration human mission to the Moon or Mars. Neither low Earth orbit nor the moon has an atmosphere. Mars' tenuous atmosphere can not sustain life as we know it because it is comprised of 95% CO_2. Thus for human space exploration of all these frontiers, a system to provide life support is needed.

Currently, the biggest power consumer of the station's carbon dioxide removal system is the water/carbon dioxide separator. A water electrolysis unit is used to reclaim oxygen from the separated water alone. Alternatively, solid oxide electrolysis can utilize both carbon dioxide and water simultaneously to make up for the metabolic oxygen needs. This application of combined electrolysis of water/carbon dixoide obviates the need for the energy intensive water/carbon dioxide separator.

As early as 1970, a Hamilton Standard trade-off study for NASA identified solid oxide electrolysis as the most promising option for long duration closed-loop life support [1]. Several significant factors are cited: solid oxide electrolysis's flexibility to handle carbon dioxide and water mixtures of any ratio, relative simplicity of the system, elimination of the need to separate liquid-gas mixtures in reduced- and micro-gravity environments, and elimination of the need for a separate water electrolysis unit.

Solid oxide electrolysis is also a technology well suited for the utilization of *in situ* resources to provide propellant for robotic/human extraterrestrial missions. In 1978, the

seminal paper by Ash *et al.* first proposed using oxygen and methane generated from Mars resources and earth-sourced hydrogen as the return-vehicle propellant for a robotic Mars Sample Return Mission [2]. Consequently, several *in situ* propellant production plant designs have been investigated [3]-[9].

One idea under consideration [10] is to use solid oxide electrolysis to simultaneously electrolyze both carbon dioxide, from the Martian atmosphere, and water, a by-product of methane fuel production. Again, the application of combined electrolysis of water/carbon dioxide allows for a simple and light weight system while achieving the optimal propellant mixture ratio for oxygen to methane ratio of 3.5:1.

Therefore, whether the application is closed-loop life support in low earth orbit and beyond or propellant production on the surface of Mars, the operation and performance of combined carbon dioxide/water electrolysis using solid oxide electrolysis technology needs to be investigated.

1.2 Solid Oxide Electrolysis

Solid oxide electrolysis (SOE) is based on the observable fact reported by Nernst in 1899 that ion conduction can be used to transport oxygen through non-porous stabilized zirconia [11]. A detailed description of SOE technology can be found elsewhere [11]-[13]. However, a brief description is provided here to define terms used throughout this work.

SOE is a process that is used to strip oxygen from "oxygen-providing" molecules. Oxygen-providing is used in this work to define any molecule that can be electrolyzed to provide oxygen, such as carbon dioxide (CO_2) or water (H_2O). The SOE structure can be

described as a cell generally made up of a solid oxide electrolyte sandwiched between two electrically conducting porous electrodes as illustrated in Figure 1-1.

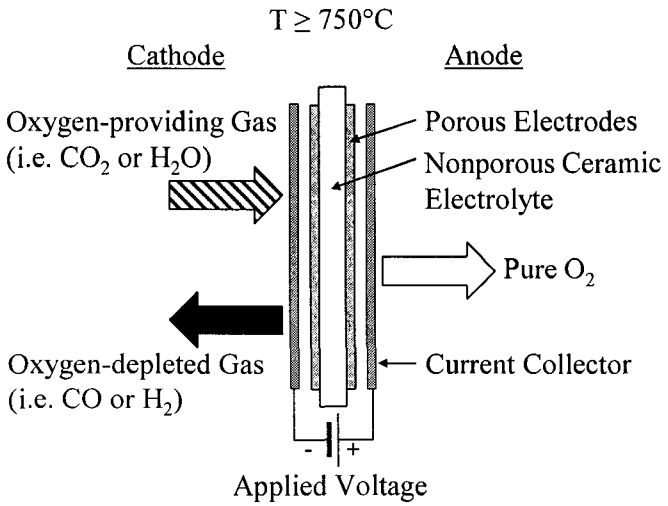

Figure 1-1 Illustration of SOE

At elevated temperatures (≥ 750°C), when enough electrical potential is applied across the cell, oxygen-providing molecules at the cathode are electrolyzed. One oxygen atom is removed from the oxygen-proving molecule and then doubly ionized. The oxygen ion ($O^{=}$) is then transported through the non-porous electrolyte to the anode where it gives up its electrons and recombines to produce pure, dry oxygen (O_2). The electrons travel through the electrode and to the current collector. The half-cell reactions at the cathode for CO_2 and H_2O electrolysis are, respectively:

$$\text{Cathode:} \quad CO_2 + 2e^- \rightarrow CO + O^{=} \tag{1.1}$$

$$\text{Cathode:} \quad H_2O + 2e^- \rightarrow H_2 + O^{=} \tag{1.2}$$

The half-cell reaction at the anode for both electrolysis reactions is:

$$\text{Anode:} \quad 2O^{=} \rightarrow 4e^- + O_2 \tag{1.3}$$

Thus the total reactions are:

$$CO_2 \rightarrow CO + \tfrac{1}{2}O_2 \tag{1.4}$$

$$H_2O \rightarrow H_2 + \tfrac{1}{2}O_2 \tag{1.5}$$

The electrons (carried through the electrolyte by the oxygen ions and then given up to the current collector) create a measurable current. Thus, the current that is produced by an electrolysis cell is an independent measure of the oxygen production rate. 100% ionic efficiency is achieved when the "transference number", or ratio of calculated (from measured O_2 production) to actual measured current, is one. The oxygen production (mol/s) is related to the measured current via Faraday's law [14] as represented in equation (1.6). The 4 refers to the number of electrons required to make a diatomic molecule of oxygen as shown in equation (1.3).

$$\dot{N}_{O_2} = \frac{I}{4\Im} \tag{1.6}$$

In order to drive this current, an applied electrical potential in the form of a voltage is required. The applied voltage is a function of operating temperature, pressure, and system irreversibility. For an ideal system that experiences no losses (also called a thermodynamically reversible system) the theoretical minimum voltage required to drive the current (V_{min}) is related to Gibbs free energy of the overall reaction [15]. However, in a real cell, the required applied voltage is greater than the theoretical V_{min} and the extra amount is called "overpotential" [16]. Example reasons for overpotential in real cells include 1) concentration gradients that develop as molecules diffuse to the reaction sites at the interface between the electrode, electrolyte and oxygen-providing gas as

demonstrated in Figure 1-2, 2) ohmic heating due to cell resistance and 3) slow reaction kinetics.

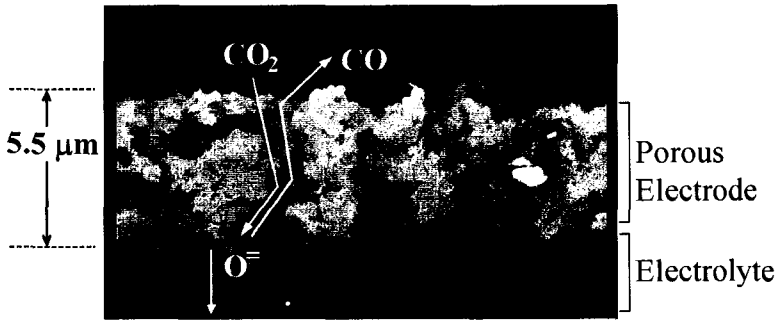

Figure 1-2 SEM image of an electrode cross section demonstrating a possible path to a CO_2 electrolysis reaction site.

Performance of electrolysis cells is typically described in terms of "current density" versus cell voltage required to induce the current. Current density is current divided by the physical electrode area. Current density, rather than current alone, facilitates easier comparison between cells of different sizes (and oxygen producing capacity). Plots of current density versus voltage are called "IV" curves in this work.

The cathode of electrolysis cells must be sealed to guarantee the composition of the gas to be electrolyzed. Tubes are provided for the inlet of fresh gas and the outlet of gas depleted of O_2. The gas is supplied at a pre-determined oxygen-providing molar flow rate. The flow forces the gas to move along the electrode and then to exhaust out of the exhaust tube. This allows for a constant supply of fresh oxygen-providing molecules while flushing away the electrolysis products (i.e carbon monoxide (CO) or hydrogen (H_2) in the case of CO_2 or H_2O electrolysis, respectively).

For pure O_2 production, the anode should be sealed such that nitrogen (N_2) contamination is avoided. For other applications (i.e. H_2 production from H_2O), the

anode can be exposed to air. The voltage required for electrolysis is directly dependent upon the O_2 partial pressure at the anode [11]. If the anode of an electrolysis cell is not properly sealed or exposed to the atmosphere, N_2 can alter the O_2 partial pressure. The actual O_2 partial pressure would be difficult to determine since the magnitude of N_2 diffusion would have to be quantified. Thus when performing experiments to quantify voltage requirements, if the anode is not sealed, it is flushed with air to guarantee a fixed, known O_2 partial pressure.

A mass limiting condition evolves in an electrolysis cell when electrolysis reactions are slowed due to a lack of available oxygen-providing molecules [17]. In this case, if the oxygen-providing molar flow rate into the cell is increased, a significant increase in performance can incur. This dependency on flow rate can complicate interpreting experimental results. Therefore, in order to minimize the influence of the oxygen-providing molar flow rate, tests are carried out above a cell's "mass limiting flow rate". Mass limiting flow rates are cell dependent and thus are usually determined experimentally.

"Utilization" refers to the percentage of oxygen-providing molecules supplied to a cell that is electrolyzed. Utilization increases as oxygen-providing molecules spend more time on the cathode before being swept away by the flow. Thus utilization can be increased with either increasing electrode area or decreasing oxygen-providing molar flow rate.

1.3 Previous Work

SOE has long been considered in Martian propellant production plant designs to electrolyze the mostly CO_2 atmosphere into pure O_2 and CO [2], [8], [9]. Water SOE was studied extensively as early as 1969 and into the mid-eighties [18]-[31] as an alternative to making H_2 from fossil fuels because SOE was deemed possibly the next cheapest method over solid polymer or conventional H_2O electrolysis [32]. Investigations into the combined electrolysis of CO_2 and H_2O are lacking.

Since 1969, it has been widely accepted that high performance electrolytes are made with zirconium dioxide (ZrO_2) stabilized by the addition of 8 – 15% by mol of yttrium oxide (Y_2O_3), commonly called YSZ for yttria-stabilized zirconia. Electrical conduction of such electrolytes is quite low exhibiting close to 100% ionic efficiency. All the experimental results cited here use YSZ electrolytes of various thicknesses: from 1.5 mm to 0.03 mm, which must be noted to account for the increased overpotential to overcome higher ohmic losses in the thicker electrolytes.

Platinum (Pt) is an effective catalyst that is used as a cathode material for electrolysis of both CO_2 and H_2O. For high concentration H_2O SOE, nickel (Ni) and cobalt (Co) also work. Copper (Cu) is chemically stable in a H_2O/H_2 environment however it has a low melting point of 1085°C (1358 K), which could, depending upon the local temperature distribution, be problematic. The other melting points of proven H_2O electrolysis electrodes, along with other materials found in the construction of electrolysis cells, are shown in Table 1-1. Iron (Fe) and manganese (Mn), though viable electrodes for H_2O electrolysis, prove to be chemically unstable in H_2O concentrations above 30%

[19]. It is uncertain the applicability in SOE, but in advanced alkaline technology, molybdenum (Mo) added to Ni caused a 10% decrease in the applied voltage for a given current [25]. Mo has a high melting temperature and could thus be investigated as a possible additive for SOE cathodes. Anode materials initially originated from fuel cell investigations and consisted of perovskite oxides. The first studies in 1969 used 0.2 – 0.3 mm thick $PrCoO_3$ but could not be thermally cycled due to its thermal expansion coefficient mismatch between it and YSZ [19]. Other successful anode materials now include Pt [21], [29]. YSZ can be added to either electrode in up to 50% by weight to prevent sintering and growth of electrode particles [13].

Table 1-1 Melting temperatures of electrolysis materials.

Material	**Melting Point, °C (K) [33]-[34]**
Zirconia	1855 (2128)
Chromium	1907 (2180)
Platinum	1772 (2045)
Cobalt	1496 (1769)
Nickel	1455 (1728)
Copper	1085 (1358)
Molybdenum	2623 (2896)

Planar configurations, where the electrolyte is flat, were not used in H_2O electrolysis experiments until after the mid 90's [30]-[31] due to the uncertainties in their capability to tolerate the temperature gradients suspected in electrochemical cells [20]. Therefore, most of the H_2O electrolysis data were collected using cells constructed out of YSZ tubes. The cathode and anode are placed on the inner and outer side of the tube, respectively. Water vapor is sent along the inside of the tube while the outside is exposed to air. Because the electrodes have marginal electrical conduction due to added YSZ or

porous structure, several little cells are connected in series along the tube (rather than one long electrode). The increased surface area enables high utilization but the many connections add resistance to the overall cell.

Figure 1-3 is a typical example of published H_2O electrolysis performance at 1000°C for various levels of humidification achieved through use of H_2 as a carrier gas. The rest of the data presented in the literature seems to fall within the range of the two slopes presented in Figure 1-3. There are many contributions to overpotentials. The difference in voltage for a given current between Barbi *et al.* [24] and the others [18], [21] is probably a classic example of ohmic losses due to cell resistance. For example, Erdle's electrolyte thickness was 0.5 mm whereas Barbi *et al.*'s was three times that at 1.5 mm. Additionally, Barbi used pure electrodes (Pt) where the others used mixed electrodes (Ni and zirconia), which have shown to perform better [13].

Planar cell configurations have been tested in the electrolysis of CO_2 [35]-[36]. Recent developments in cell materials and construction have lead to increased performance. A typical example of today's state of the art 100% CO_2 electrolysis using 50/50% by wt Pt/YSZ electrodes with a planar geometry is shown in Figure 1-4 [37].

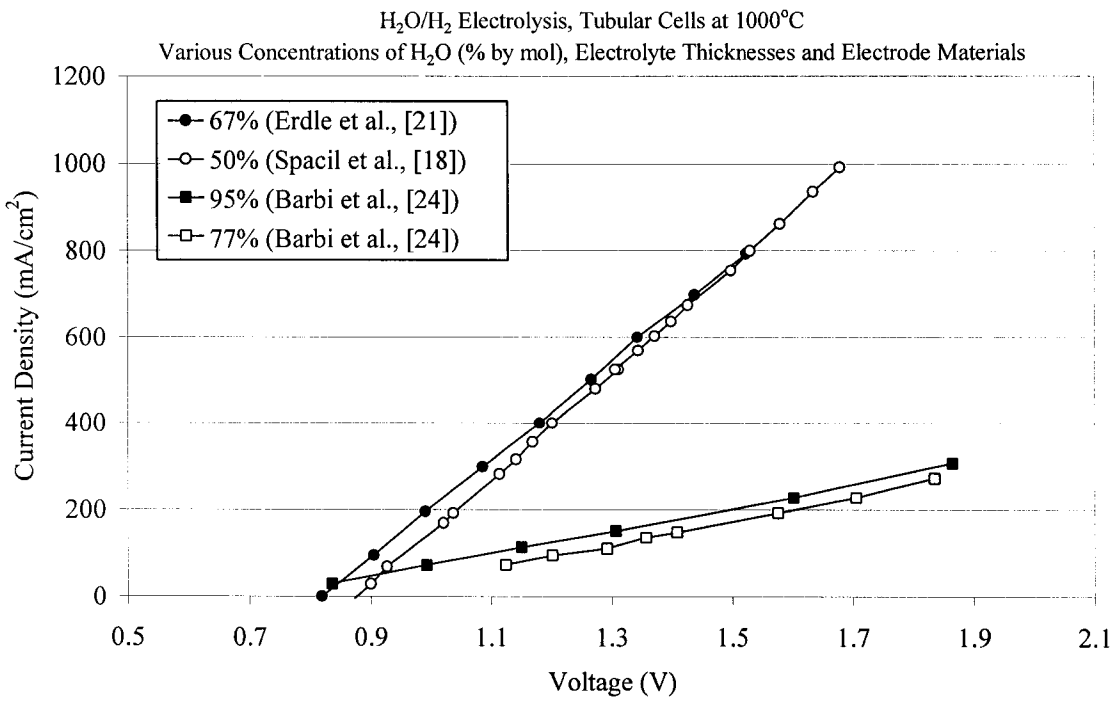

Figure 1-3 Past H_2O/H_2 electrolysis performance.

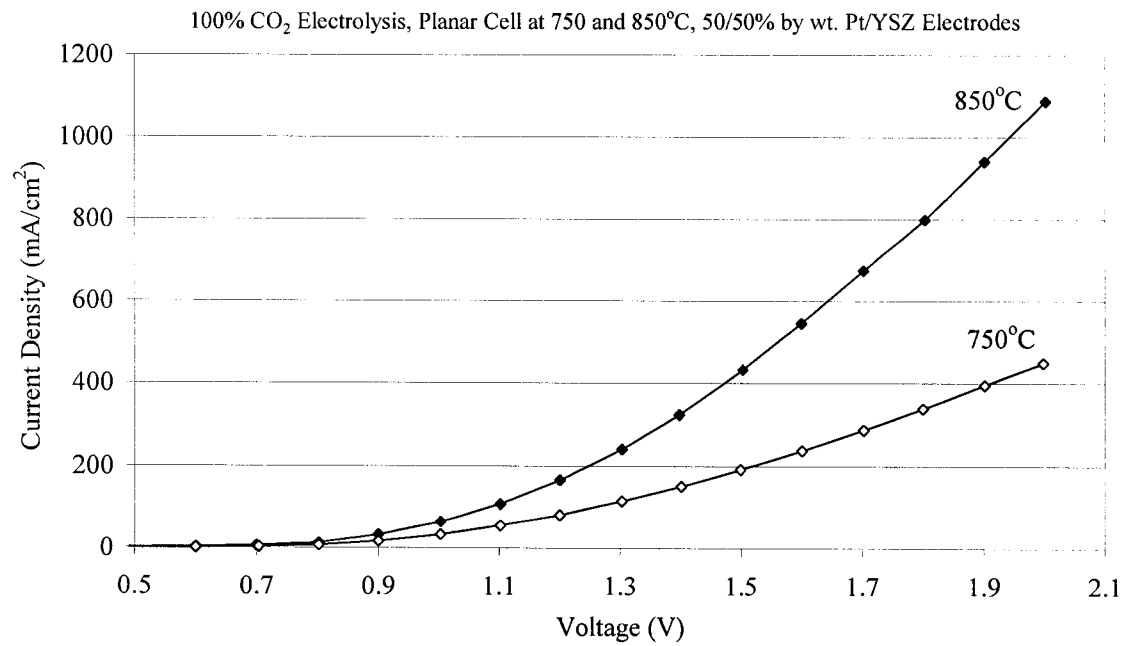

Figure 1-4 Hickey's CO_2 electrolysis performance [37].

In 1980 Isenberg [20] used Ni/Zr electrodes to electrolyze CO_2 and H_2O, though not together. It is not specifically mentioned, but further analysis of his data as recompiled in Figure 1-5 shows that at 1000°C, H_2O electrolyzes more easily than CO_2. It is uncertain whether this same conclusion can be made for Pt/YSZ electrodes. Furthermore, comparing Figure 1-5 to the state of the art performance in Figure 1-4, it can be seen that recent developments in cell technology are enabling the same CO_2 performance but at lower temperatures (1000°C vs. 850°C). There are no data yet as to whether H_2O electrolysis will do as well at moderate temperatures.

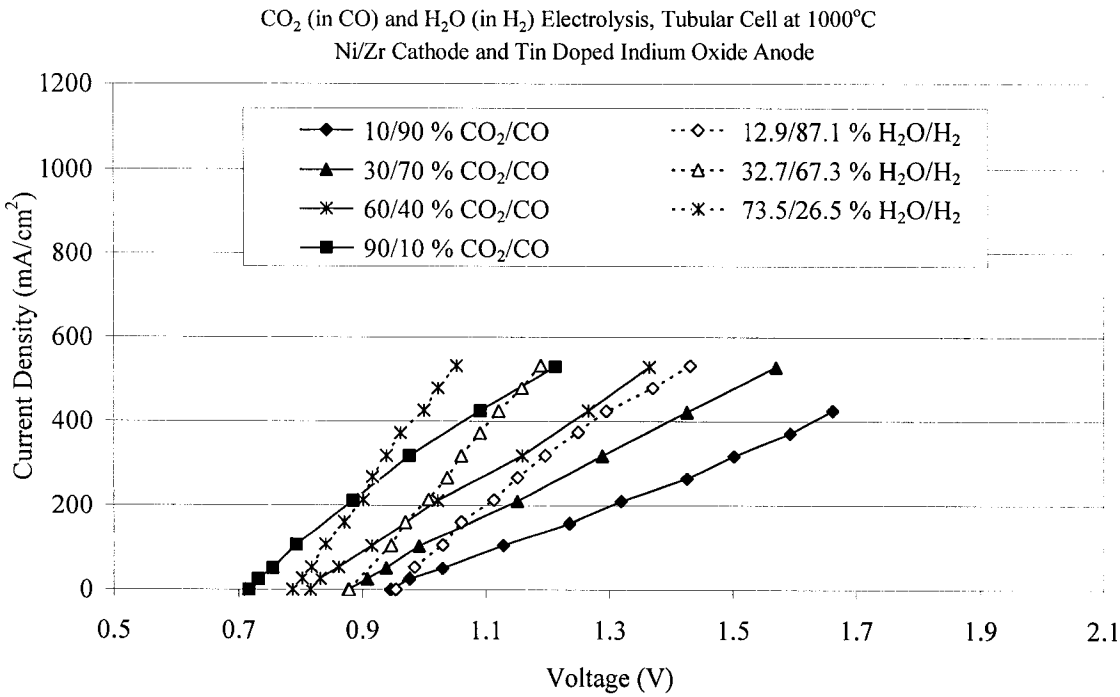

Figure 1-5 Isenberg's H_2O versus CO_2 electrolysis data [20].

Maskalick [23] publishes H_2O electrolysis of different flow rates at 1000°C. He states that the higher flow rate causes an increase in performance. If this is true, this has

a tremendous impact on system design and should be further qualified at moderate temperatures.

In 1971, Elikan *et al.* [38] performed combined electrolysis of H_2O and CO_2 at 900°C in an oxygen regeneration system for life support applications. The SOE unit used Pt/YSZ electrodes on 10% mol YSZ electrolytes. The SOE housing was made entirely of Inconel 600. To prevent against carbon deposition in temperature gradient areas, Inconel parts were clad with copper. Gas inlet and discharge tubes were also lined with deoxided copper. H_2 was removed from the SOE exhaust using palladium membranes. CO in the exhaust was converted to CO_2 in a carbon deposition reactor. The CO_2 was then recycled back to the SOE unit. Nothing was mentioned about undissociated H_2O leaving the SOE unit. Therefore, the actual H_2O/CO_2 ratio that the SOE unit saw can not be certain due to the recycle loop.

Elikan *et al.*'s data show a change in SOE performance over the first 30 days of the 180 day test as the oxygen regeneration system was adjusted even though SOE operating temperature and applied voltage remained constant. This change in performance could be due to the input mixture levels changing from the recycled stream as the overall system reached equilibrium. Eventually 160 mA/cm^2 was achieved with about 1.8V. This is low compared to today's CO_2 performance shown in Figure 1-4, especially considering Elikan *et al.*'s experiment operated at a higher temperature of 900°C. Regardless, over 180 days six stacks of seven cells were tested without one cell failure and less than a 6% increase in voltage was required to maintain a fixed oxygen production rate.

Later in 1998, 800°C combined electrolysis of H_2O and CO_2 with Pt electrodes was performed in 1998 by Hibino *et al.* [39] in investigating concepts for detecting NO in the presence of excess oxygen. However, the concentrations were small (a mixture of 500 ppm NO, 1-7% O_2, 3-10% water vapor, and 0-10% CO_2 in argon at a flow rate of 10 ml/min).

What has not appeared to be done by either Hibino *et al.* or Elikan *et al.* was that exhaust gas composition was not strictly analyzed for CO or H_2 to establish platinum's preference to H_2O or CO_2 (if at all). It is still unknown whether, when electrolyzed together, if one molecule inhibits the electrolysis of the other, a fact that could complicate system design. Nor can any conclusion be made regarding mixture ratio and its effect on performance. However, Hibino does note that, in keeping voltage constant, "the current signal slightly increased with increasing concentration of water vapor".

1.4 Objectives

Clearly little has been presented in the literature concerning the specific study of combined solid oxide electrolysis of H_2O and CO_2, or "combined electrolysis" as referred to hereafter. Therefore, the main objective of this dissertation is to better understand combined electrolysis. Specifically, the aim is to answer the following.

1) Can stable combined electrolysis be verified? Elikan *et al.* [38] does show that stable combined electrolysis can be achieved. With today's current technology, possibly the performance will exceed those results even at lower temperatures such as 750°C.

2) How does flow rate affect stable combined electrolysis? Mastilick [23] indicates higher flow rates increased H_2O electrolysis performance. Will the same affect be observed for combined electrolysis?
3) Does combined electrolysis performance depend upon H_2O/CO_2 mixture ratio? Whether it is dependent upon inlet mixture has yet to be investigated and is important to quantify. Engineers need to know how much oxygen production to expect if only a given mixture can be fed to the SOE unit.
4) Does combined electrolysis preferentially electrolyze H_2O over CO_2 or visa versa? If so, it must be understood as to what degree. A strong preference to either could cripple recycling intentions causing a buildup of the un-preferred constituent in the system.
5) What exhaust does combined electrolysis produce? Understanding the exhaust composition of H_2, CO, undissociated H_2O and CO_2 as well as any other formations such as hydrocarbons allows engineers to better implement combined electrolysis. For example, the ratio of CO to CO_2 may permit carbon deposition depending upon temperatures and materials down stream. Additionally, knowing how much H_2 is in the exhaust stream allows for the design of H_2 removal systems or Sabatier reactors.
6) How does combined electrolysis affect subsequent cell performance of CO_2 electrolysis and H_2O electrolysis? Such an evaluation of how combined electrolysis affects cell health will determine the flexibility of the technology to

be implemented in systems that may require instances of just CO_2 electrolysis or just H_2O electrolysis.

7) How does combined electrolysis performance compare to CO_2 electrolysis and H_2O electrolysis? This information is good as a general gauge to the technology's performance. More importantly, it allows the system engineer to optimize its implementation into a system.

1.5 Dissertation Outline

Chapter 2 justifies the motivation behind the objectives presented in the preceding section. Two studies are presented to exemplify the many advantages in implementing combined electrolysis. Chapter 2 also aims to review real applications such that the significance of conclusions later drawn is more evident.

Chapter 3 describes the equipment used in collecting the data presented in this dissertation. Special attention is given to testing procedures and apparatus specific to combined electrolysis. Materials, configuration and operation of the two different types of SOE cells used are also described.

Chapter 4 is dedicated to presenting experimental results. A detailed account of observations is presented with supporting examples of data. Some assessments are conducted but the majority of analysis and discussions are presented in chapter 5. It is intended that chapter 4 be used as a source to look up observations made for a given specific experiment. Electrolysis performance data, gas chromatograph analyses of cell exhaust as well as postmortem scanning electron imaging of cell structures are all provided.

Chapter 5 analyzes the data via inspection and comparison. Thermodynamic modeling is also used to explain observed phenomena. The particulars of some of the theoretical development and details of sample calculations can be found in the appendices.

Finally, conclusions and recommendations for future work are given in chapters 6 and 7, respectively.

2 CONVINCING THE CRITICS

In the introduction, SOE is described as a technology with many useful applications. But are such applications feasible and worth the effort of implementation? This section provides evidence that indeed SOE and its application towards combined electrolysis are very worthwhile.

2.1 A Competitive Technology

In general, electrolysis is a necessary tool in the business of space exploration. For Mars exploration, whether the objective is to send humans or return samples, electrolysis is an indispensable technology for the production of breathable air and/or propellant on Mars using the Martian resources. It also is as indispensable in life support regeneration systems like those used on the International Space Station or that required by future lunar habitats.

Electrolysis can be accomplished in different ways but over the years there have been two processes that have been used extensively in various system designs [7], [8], [40]. These are Proton Exchange Membrane (PEM) electrolysis [41], [42] and SOE. Regardless of the system design, the primary function of each is to provide O_2 for propellant oxidizer or air.

PEM electrolysis is used to electrolyze liquid H_2O exclusively, whereas SOE is capable of electrolyzing water vapor and/or CO_2. For Mars applications water could be obtained from the planet, for data from Mars Odyssey and Mars Global Surveyor both suggest the presence of ice near the surface [43] and in the polar caps [44], respectively. Regardless of H_2O availability on the planet, propellant systems usually produce H_2O as

a byproduct of fuel production. Carbon dioxide is obtained from the 95% CO_2 Martian atmosphere [45] anywhere on the planet. For life support systems, water vapor and CO_2 exist in the atmosphere of spacecraft cabins and surface bases, both expelled from humans.

There are pros and cons to using either technology. For instance, PEM electrolysis has been used extensively in industry [41]. It also operates at relatively low temperatures between 25 and 150°C [42]. However, as applied in Martian oxygen/methane propellant production plants, it can only produce a 2:1 oxidizer to fuel (O/F) ratio without wasting resources [46]. As applied to life support systems, the water needs to be condensed out of the atmosphere. On the other hand, SOE can produce an optimal 3.5:1 O/F ratio [10] and readily electrolyze water vapor but the technology is not as well established and as described in section 1.2 operates at much higher temperatures.

Performance data for PEM electrolysis are not widely available due to the proprietary nature of the technology. However, studies claim that it operates "very near the theoretical minimum voltage" [46]. As it turns out, current technology in SOE can achieve the same utilization for the same voltage – and, as will be shown in the next section, it is not even near the SOE theoretical V_{min}.

2.1.1 Theoretical Minimum Voltage

Iacomini *et al.* [47] describe in detail how to calculate the theoretical V_{min} for both SOE and PEM electrolysis. They show that the theoretical V_{min} for PEM electrolysis at operating conditions suggested for Mars propellant designs (25°C) is 1.23 to 1.3 V depending upon operating pressure. Due to the nature of electrolyzing liquid H_2O, this

calculation is for "low" utilization of less than 5%. Section 5.2 shows that SOE current technology operated at only 750°C can achieve 5% utilization of H_2O at a voltage under 1.3V.

What is even more promising is that SOE has not yet been fully optimized to operate near theoretical V_{min}. Iacomini *et al.* show that the SOE V_{min} is directly proportional to utilization and that even so, 100% utilization SOE operated at 850°C has a theoretical V_{min} between 0.96 – 1.0 V. The methodology presented by Iacomini *et al.* was used to generate calculations presented in Figure 2-1. The theoretical V_{min} for 5% utilization (η) at 850°C is 0.77 – 0.86V.

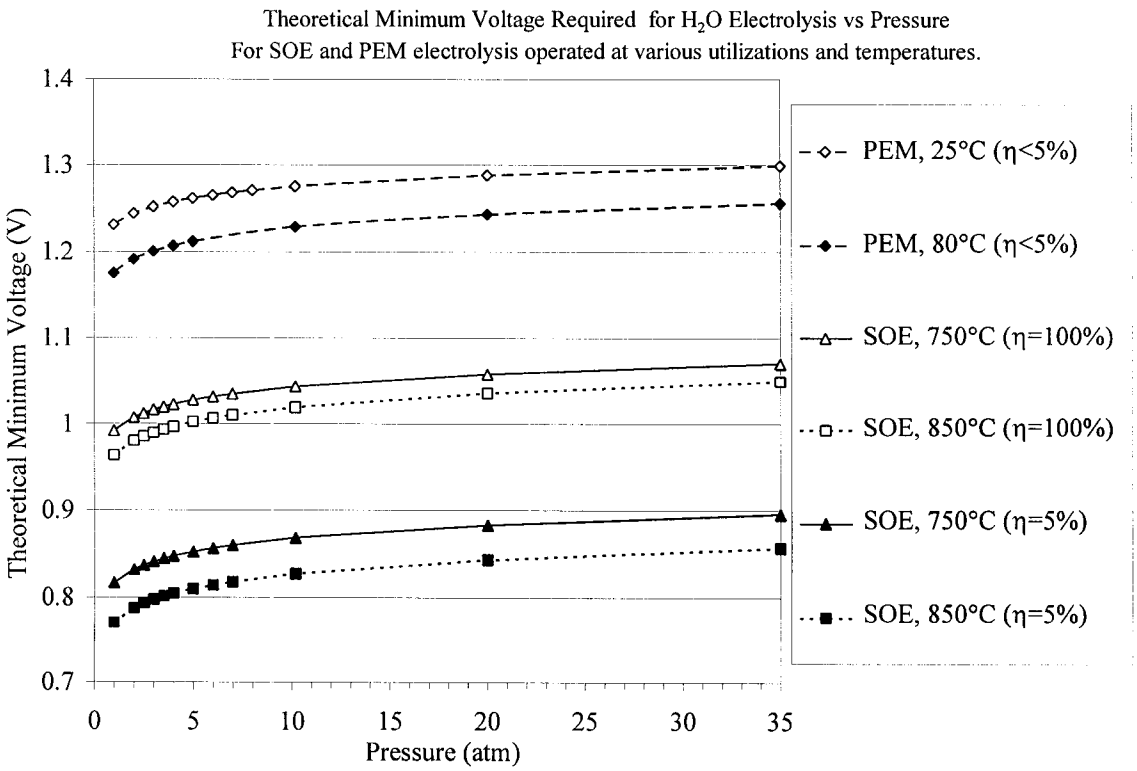

Figure 2-1 SOE vs. PEM: Theoretical V_{min} required for H_2O electrolysis.

To be fair, PEM electrolysis can actually be run at temperatures as high as 150°C [42], though most advocates of the technology suggest 80°C as the optimal temperature given the materials used. Because the dissociation of H_2O is enthalpy-driven, higher temperatures reduce the energy required by the endothermic reaction (see equation (1.5)). Figure 2-1 shows that increasing the temperature from 25°C to 80°C is helpful, reducing the theoretical V_{min} to 1.18 – 1.26V. However at the lowest SOE operating temperature of 750°C, even at 100% utilization the SOE theoretical V_{min} remains under 1.07V.

2.1.2 Total Heating and Power Requirements

Literature has reported that PEM electrolysis requires less power than SOE [40] because of its significantly higher operating temperatures. What have been overlooked are the heat transfer needs of PEM electrolysis. When tested on Earth, the ambient functions as an unlimited source of heat. Thus the heat required by PEM electrolysis to sustain the electrolysis reactions goes unnoticed. On Mars, the ambient temperature varies from -143 to 27°C (130 to 300K), with a mean temperature of -58°C (215K) [45]. Thus, for low temperature environments, heat transfer requirements need to be accounted for in power calculations.

Applying the first law of thermodynamics, neglecting potential and kinetic energy contributions and changes, and assuming a steady state system, Appendix A.1 shows the general expression for the total heat transfer and work applied to an electrolysis system is:

$$\dot{Q} - \dot{W} = \sum_{out} \dot{N}_o \bar{h}_o - \sum_{in} \dot{N}_i \bar{h}_i \qquad (2.1)$$

The work rate can be written as a function of the applied voltage and current (or oxygen production using equation (1.6)):

$$\dot{W} = -V_{applied} I = -V_{applied} 4\Im \dot{N}_{O_2,out}$$
$$= -V_{applied} 4\Im \frac{\eta}{2} \dot{N}_{CO_2,in} \quad (2.2)$$

It is informative to write the heat transfer rate per mol of CO_2 input as follows:

$$\frac{\dot{Q}}{\dot{N}_{CO_2,in}} = \frac{\eta}{2}\left[-V_{applied} 4\Im + \bar{h}_{T\,O_2} - \bar{h}_{298\,O_2} + 2\left(\Delta\bar{h}^{o}_{f298,CO} + \bar{h}_{T\,CO} - \bar{h}_{298\,CO}\right) - 2\left(\Delta\bar{h}^{o}_{f298,CO_2} + \bar{h}_{T\,CO_2} - \bar{h}_{298\,CO_2}\right)\right] \quad (2.3)$$

The quantity in the square brackets determines the sign of the heat transfer. If it is positive, the system requires heat. If it is negative, the system will release heat. For a given operating temperature, this quantity inside the brackets is only a function of applied voltage. The sign of heat transfer is not a function of current or utilization. The applied voltage for a given temperature that results in zero heat transfer is called the "thermal neutral" voltage. A common misconception about electrolysis is that producing a lot of oxygen (current) will generate heat. However, equation (2.3) proves that, regardless of the amount of current, heat will not be produced if the system is operated under the thermal neutral voltage.

Iacomini *et al.* [47] explain assumptions in using equation (2.3) to calculate the total heating and power requirements for oxidizer production by both SOE and PEM electrolysis required for a typical Mars sample return mission. They show total power and heating requirements for CO_2 SOE at 850°C and 1 atm to produce 389 g of O_2 per 12 hour day (3.5:1 oxidizer-to-fuel ratio) is 159W. The total power and heating

requirements for H_2O PEM electrolysis at 25°C at 1 atm to produce the same amount of oxygen is 161W. The thermal neutral voltages are 1.46 and 1.48V for the SOE and the PEM electrolysis, respectively.

The methodology and assumptions presented by Iacomini *et al.* are applied to the calculations presented in Figure 2-2. Even at 750°C, total power and heating required by SOE is practically the same as PEM electrolysis. When either electrolysis is operated at its theoretical V_{min}, Figure 2-2 shows that the electrolysis will require additional power in the form of heat. Such calculations performed by Iacomini *et al.* are corroborated in section 5.4.

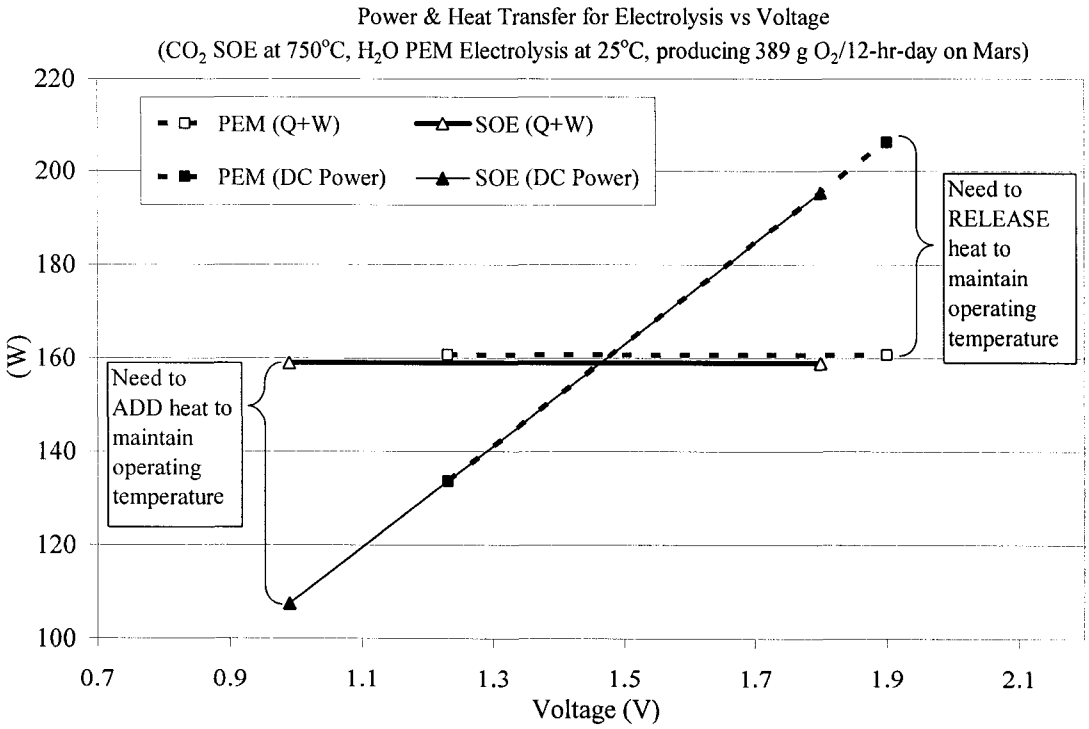

Figure 2-2 SOE vs. PEM: Power and heat transfer requirements.

It is worth noting that if either electrolysis process is operated at voltages above the thermal neutral voltage, the extra DC power will be converted to heat. This heat in turn would be available for other processes within a plant. Operating at the thermal neutral voltage implies electrolysis can be operated at pure DC power with no additional heating requirements. If no alternative heating source is available, this scenario is most effective since DC power can be generated more efficiently than heating. However in the real world, heat losses can not be avoided. Since SOE operates at a higher temperature than PEM electrolysis, a real design will require more insulation to minimize losses.

2.2 Mars Application Case Study

The application of SOE to combined electrolysis of H_2O and CO_2 allows for incredible mass savings in propellant production plants as well as life support generators which translates directly to costs in the realm of space exploration. It should be noted that PEM electrolysis does not have the flexibility to perform such a "combined" electrolysis.

One of the many propellant combinations that can be made on Mars is gaseous O_2 and gaseous methane (CH_4). The specific impulse of CH_4 (about 370 sec) is comparable or higher than alternatives, while still being relatively easy to produce on Mars [2]. The optimal O/F mixture ratio by mass for this propellant combination is around 3.5.

There are two *in situ* propellant production (ISPP) architectures that produce O_2 and CH_4 that have been given much consideration in the past [3]-[5],[7]. These are a Sabatier Reactor/Liquid Water Electrolysis (SWE) system and a Reverse Water Gas Shift Reactor/SWE (RWGS/SWE) system.

A flow chart of a SWE architecture is depicted in Figure 2-3. The inlet process stream is composed of compressed CO_2 mixed with earth-sourced H_2. The mixture enters a Sabatier reactor, which is a well proven, simple technology based on the exothermic Sabatier reaction:

$$CO_2 + 4H_2 \rightarrow CH_4 + 2H_2O \tag{2.4}$$

In the presence of excess H_2, the only constituents in the reactor's outlet are CH_4, H_2O and unreacted H_2, which are sent to a condenser. The resulting CH_4/H_2 process stream is then sent to a H_2 separator. The separated H_2 is recycled into the process stream. The H_2O is electrolyzed to produce wet O_2 that needs to be dried.

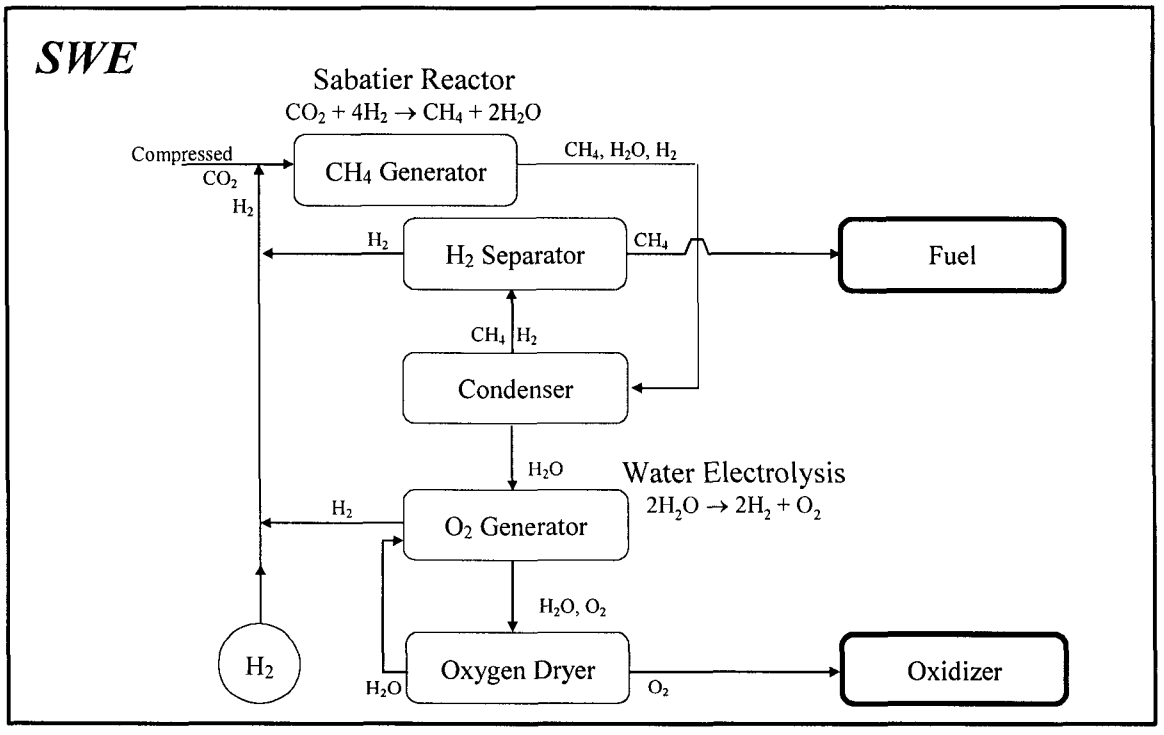

Figure 2-3 Schematic of a SWE propellant production plant.

The resulting O/F mixture ratio of the SWE architecture is 2:1. As previously noted, the optimal O/F ratio for O_2 to CH_4 is near 3.5. Therefore, though the SWE system is

designed around mature technology, it cannot achieve an optimal O/F mixture ratio or supplement life support consumables without producing excess CH_4. In order to boost the O/F ratio, a SWE system can be augmented with a RWGS reactor.

A flowchart of the RWGS/SWE system is shown in Figure 2-4. A SWE system, as described above, generates oxygen along with the exact necessary amount of CH_4 as dictated by a specific mission. This modified system has the potential to supply O_2 for life support needs also.

The inlet process stream of the RWGS system contains compressed CO_2 mixed with recycled H_2 from a H_2O source brought from Earth. The process stream enters a reactor that produces CO and H_2O from CO_2 and H_2 in the presence of a catalyst in accordance with the Reverse Water Gas Shift reaction:

$$CO_2 + H_2 \rightleftharpoons CO + H_2O \tag{2.5}$$

When the reaction is run at temperatures at 400°C and above, the reaction is slightly endothermic with a low equilibrium constant (K_p) of values from 0.1 to around 1. Thus it can be difficult to drive towards completion. However, conversions of 8 – 20% of the available CO_2 have been achieved with no undesired by-products such as CH_4 [5].

The RWGS/SWE system can produce an optimal O/F ratio and produce extra O_2 without wasting valuable H_2, but is more complicated and less mature. It also relies upon a source of H_2O to produce the optimal O/F ratio. If the H_2O source were to be depleted due to an accident or leakage, mission objectives could not be met. The RWGS also operates at about 10 bar pressure which increases the power requirements considering the Martian atmosphere is about 8 mbar.

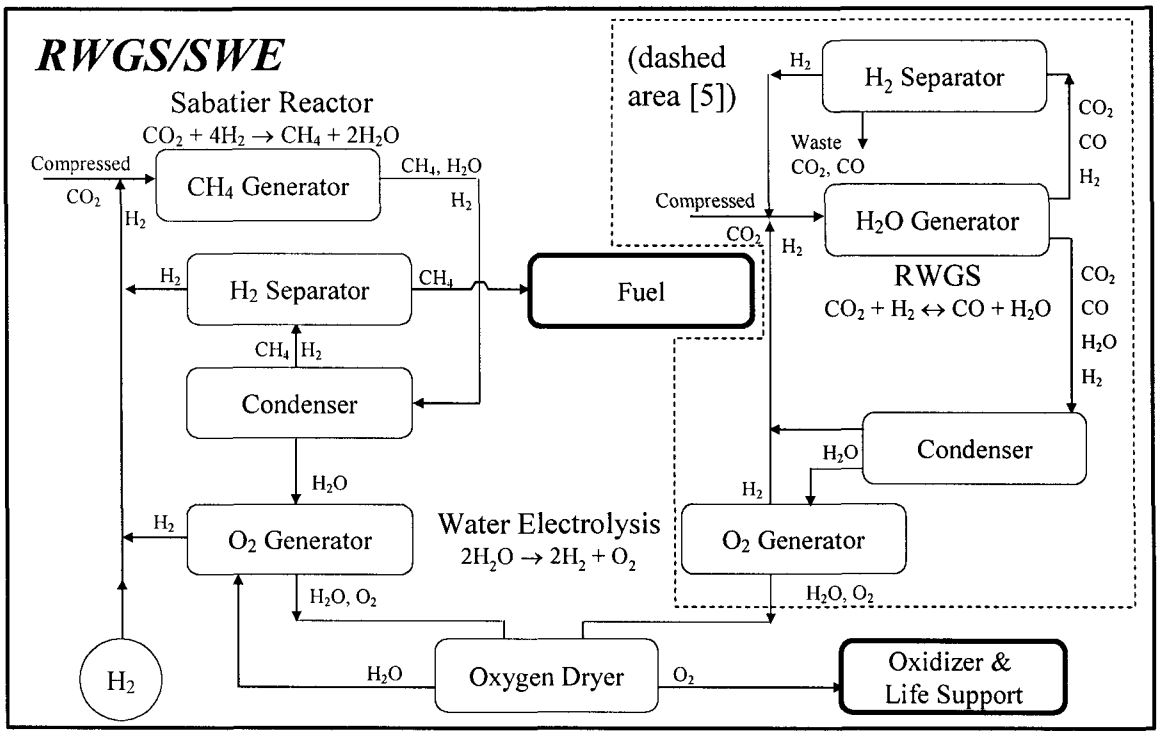

Figure 2-4 Schematic of a RWGS/SWE life support and propellant production plant.

With a Mars sample return mission on the horizon [48], the space program needs an architecture that is proven and simple yet still satisfies all mission requirements. In answer to this, an alternative system to producing O_2 and CH_4 is to employ Combined CO_2/H_2O solid oxide Electrolysis (CSOE) with a Sabatier reactor, called a CES system [10].

SOE has long been considered in ISPP plant designs to electrolyze the mostly CO_2 Martian atmosphere into pure O_2 and CO [2], [7]-[9],[16]. SOE of H_2O has also been studied to aid life support systems [49]-[50]. In fact, NASA confidence in SOE applications for Mars exploration is evident in its selection of SOE technology to fly on the Mars 2001 Lander [51], though the mission was cancelled in 2000. So SOE is

considered a proven technology but how does it satisfy all mission requirements in a simpler fashion than the alternatives?

The CES architecture is shown in Figure 2-5. Compressed CO_2 combines with recycled water vapor and H_2 before entering the SOE unit. The exhaust of the CSOE unit, which contains CO, H_2 and undissociated CO_2 and H_2O, is sent to a Sabatier reactor. When the system is run H_2-rich, the Sabatier reactor produces only CH_4, H_2O and excess H_2. These products are sent to the separator side of an electrochemical pump and separator which uses PEM technology [52]. On the separator side, when hydrogen protons are pumped through the membrane, H_2O molecules are drawn along providing H_2O removal from the stream. The CH_4 is stored as fuel. On the pump side of the electrochemical pump and separator, more H_2 is metered in to the H_2O/H_2 recycle stream to achieve the necessary amount of H_2 for the Sabatier reactor.

Once enough CH_4 is produced to fulfill mission requirements, the CH_4 generator can be turned off and the CSOE unit can be run solely using the CO_2 collected from the atmosphere. O_2 can be produced until the 3.5:1 O/F ration is achieved, with out wasting or depending upon any valuable resources. Furthermore, the SOE unit can be operated at any time to supplement O_2 for life support needs, again without wasting any valuable resources.

Comparing Figure 2-3, Figure 2-4, and Figure 2-5, it becomes evident that employing combined electrolysis reduces the complexity of an ISPP plant architecture without jeopardizing mission requirements. But are the advantages lost when system power and mass are considered?

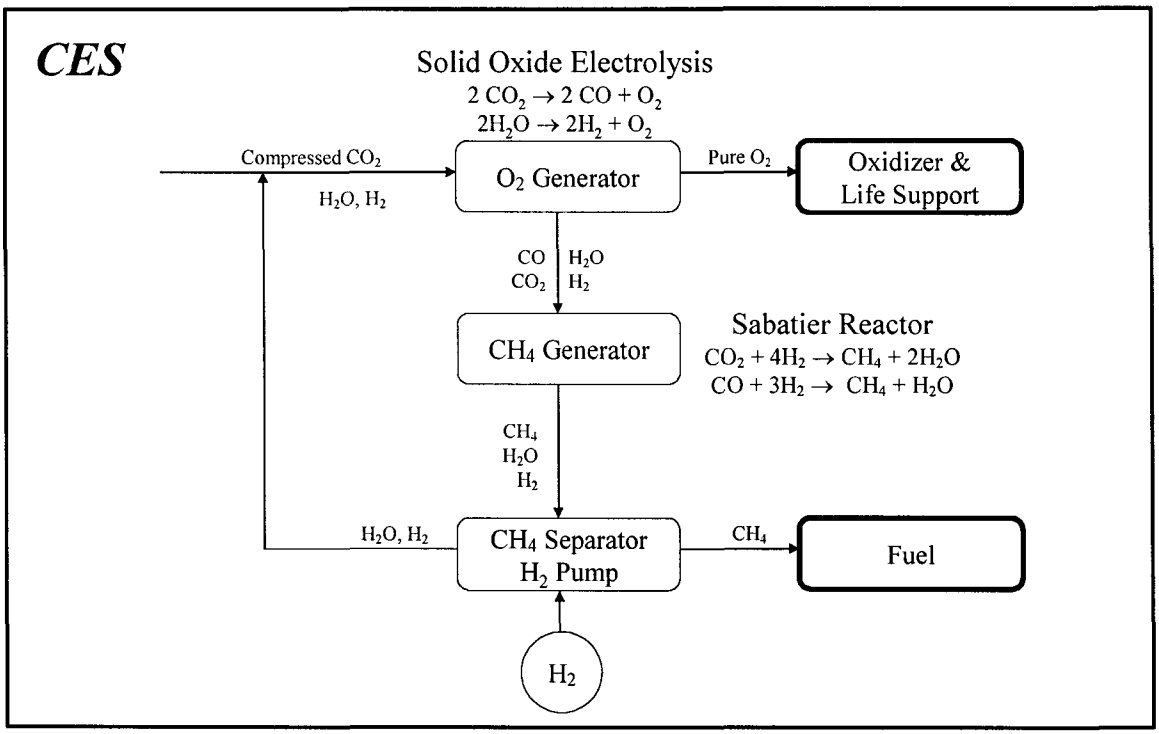

Figure 2-5 Schematic of a CES life support and propellant production plant.

Sridhar *et al.* [10] models the CES architecture and compares its total mass and power to the other two systems for a Mars sample return and human mission. They show that regardless of the scope of the mission (small sample return versus large human crew mission), the energy required to run the plant per O_2 produced per hour is relatively the same. Furthermore, they show the system employing combined electrolysis is over two times lighter for human missions and three times lighter for a sample return. An example of their calculations as compared to systems cited in the literature is presented here in Table 2-1 for a typical Mars sample return mission. It should be noted that Sridhar *et al.* assumes an SOE operating voltage above the thermal neutral voltage thus the heating requirements for the unit are shown to be zero.

Table 2-1 Comparison of SWE and RWGS/SWE Components to CES for a Sample Return Mission

Source	Zubrin, *et al.* [5]		Reddig, *et al.* [3]	Sridhar, *et al.* [10]
Plant	SWE	RWGS/ SWE	SWE	CES
Propellant Production Rate	0.5 kg per12 hr	0.5 kg per 12 hr	0.7 kg per "day"[a]	0.5 kg per 12 hr
O/F Ratio	2	3.5	2	3.5
Specific Energy (kWh/kg O_2 produced)	**5.9**	**5.7**	**5.6**	**5.7**
RWGS (W)	--	150	--	--
Electrolysis (W)	120		120	184.6
Electrolysis Heater (W)[b]	43	36	98	0
System Specific Mass (kg/kg O_2 produced/hr)	**108**	**123**	**309[a]**	**28**
RWGS (kg)	--		--	--
Sabatier (kg)	3	4	9	0.12
Electrolysis (kg)			3	0.8

[a] Assume production "day" is 12 hours.

[b] Calculated by authors assuming PEM electrolysis operated at 55°C and same heat losses as CES.

In theory, the concept of applying combined electrolysis to ISPP plant design allows for the production of 1) propellant in the optimal O/F mixture ratio and 2) extra oxygen for life support, irrespective of the resources brought from Earth. It is impressive to see the suggested mass savings, especially when one considers that the analysis used data collected from a SOE unit not optimized for performance. What is even more promising is that a system using combined electrolysis appears to scale easily and reasonably for either a sample return or human mission. This means systems engineers can use the technology now for sample return missions and not have to develop something entirely new for human missions later.

3 EXPERIMENTAL APPARATUS

Various experiments were conducted in order to gain knowledge that will help to accomplish the advantages of implementing combined electrolysis as presented in section 2.2. The following chapter describes the experimental equipment as well as any special considerations that are required when testing combined electrolysis.

3.1 Test Bed Description

Figure 3-1 is a schematic representing the gas flow and instruments of a typical test bed configured for combined electrolysis. A two-way valve allows for the selection of He or CO_2 carrier gas for pure H_2O or combined electrolysis, respectively. An MKS type 1179A Mass-Flo Controller meters the flow of the chosen carrier gas. A two-way valve directs the flow through the humidifier or directly to the SOE cell. The humidifier is a water filled glass flask that contains a glass frit through which the carrier gas is bubbled. To set the humidity, the flask is heated to a control temperature with an Omega STH051 Heating Tape controlled by a Watlow Series 96 Controller. In order to avoid condensation in the lines, the humidified gas flows through +100°C lines heated with more heater tape controlled by Omega CN350 Series controllers. A Vaisala HMP237 records actual humidity and temperature of the inlet gas before entering the cell.

The cell is heated in a Paragon model Q-11A (max temperature 1260°C) furnace controlled by a Watlow Series 942. An Agilent E3633A (0-8V,20A/0-20V,10A) DC power supply applies voltage across the cell. Current is independently measured via a shunt resistor.

If the anode is unsealed, it is flushed with air using an MKS type 1179A Mass-Flo Controller. Otherwise, O_2 production is measured with an MKS Type 1179A Mass-Flo Meter. H_2O is removed from the cell exhaust via a condenser. It is helpful to have a second humidity sensor to ensure adequate H_2O removal. Both the cell exhaust and oxygen production can be sent to either an Alltech soap film flow meter to verify flow rates or an Agilent 6890 gas chromatograph (GC) to verify oxygen purity (in the event the anode is not flushed with air) or exhaust composition. The exhaust is vented through a fume hood.

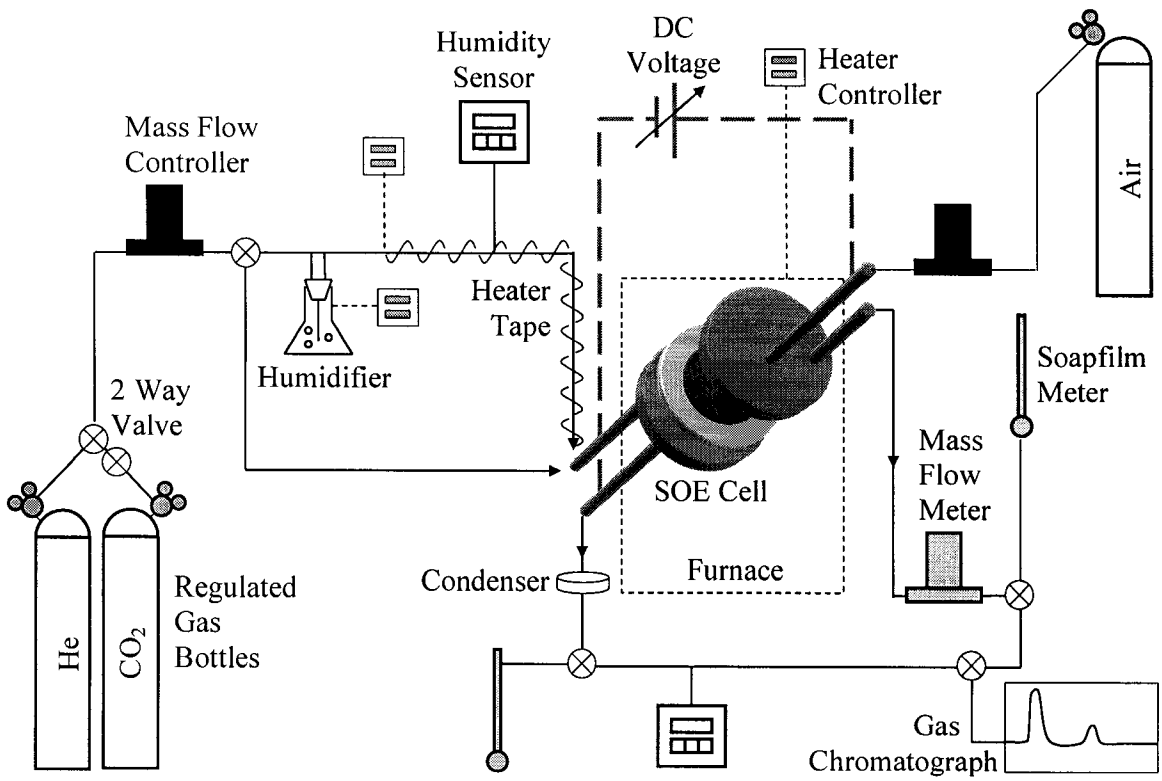

Figure 3-1 Schematic of a combined electrolysis test bed.

3.2 Data Collection and Labeling

Carrier gas flow rate, O_2 flow rate or anode flush rate, humidity data, humidifier temperature, tubing temperatures, furnace temperature, anode and cathode pressure, cell voltage, and current are all collected via an Agilent 34970A Data Acquisition/Switch Unit and HP Benchlink Data Logger V.1.3 software. Sufficient data collection rates for quantifying steady state performance are usually on the order of 0.05 Hz. Voltage settings can take anywhere from 5 minutes to 2 hours to achieve steady state current. In general, steady state was considered achieved when the rate of change of current density was less than approximately 0.1 mA/cm^2-min. Performance curves of current density versus voltage are sequentially catalogued for each cell as IV##. For example the first test of a given SOE cell would be labeled IV01. This label is used throughout this work to aid in providing a sense of sequence amongst the presented data.

3.3 Special Equipment Considerations

Several lessons were learned in developing a test bed to successfully, and reliably, perform combined electrolysis. A brief discussion is mentioned here.

3.3.1 Water Supply

Distilled water was used in early testing for humidification. Scanning electron microscope (SEM) images (see Figure 3-2) and X-ray analyses (see Appendix C.1) of an electrode revealed sodium and silicon contaminants. The silicon was traced back to the humidifier's water supply tubes which were consequently replaced with non-silicon based material such as TYGON flexible tubing. To further eliminate any other sources of

contamination, the water source was changed from distilled to deionized. Subsequent SEM images of the electrodes have been clean and are discussed in section 4.7 of the Experimental Results chapter.

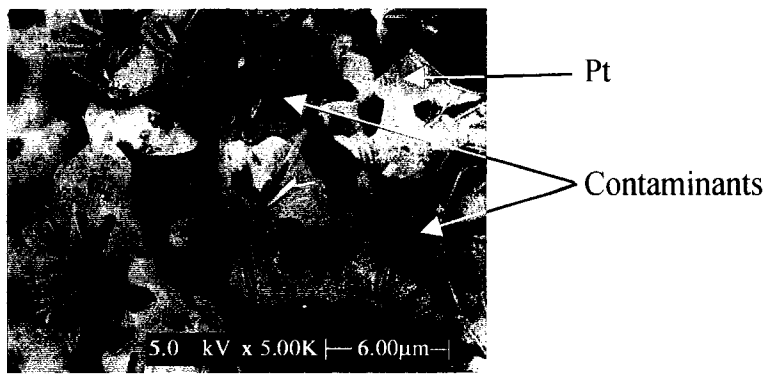

Figure 3-2 SEM image of a platinum electrode shows contamination.

3.3.2 Humidifier

Humidifiers are expensive so one was designed in-house and constructed out of glass by The University of Arizona Chemistry Department Glass Shop. As described in section 3.1, the humidifier is a water filled glass flask that contains a glass frit through which the carrier gas is delivered. To set the humidity, the flask temperature is controlled.

As illustrated in Figure 3-3, the humidifier is topped with a glass stopper that contains the inlet and outlets. At high flow rates, pressure builds inside the flask and gas would escape through the joint between the stopper and flask, reducing the total flow into the cell by an unknown amount. Therefore, the stopper is sealed (Varian Vacuum Technologies "Torr Seal" #9530001) with a material that proved not to contaminate the cell.

All inlets and outlets of the humidifier are made of glass tubes. Stainless steel Swagelok fittings can attach to glass tubes using nylon ferrules allowing connection to stainless steel or copper tubing in the test bed easy. Spacing between the glass tubes had to eventually be adjusted to allow room for these Swagelok fittings. This was done by varying tube heights and/or bending tubes as illustrated in the left of Figure 3-3.

The longer the carrier gas travels through water, the more accurately the gas is humidified. Therefore, the carrier gas is supplied to the bottom of the flask through a tube and then bubbles through a glass frit. Experimentation revealed the frit withstands flow rates up to 1060 standard cubic centimeters per min (sccm, 0°C and 1 atm) of CO_2 without sacrificing target humidity.

The thermocouple should also run the length of the flask because the most consistent humidity control resulted when the thermocouple was always emerged in water. In the design used in this work, the thermocouple and water supply shared the same inlet to save space on top of the stopper. The water supply tube should also submerged in water for "dropping" room temperature water in the heated humidifier sends pressure spikes to the cell and causes the electrolyte to crack.

Though the desired humidity is targeted by controlling the flask temperature, the humidity can drift as water is depleted from the humidifier. For this reason, bigger flasks are better (especially for high H_2O flow rates) because the water level would not lower as quickly and humidity could be better maintained.

Most importantly, the outlet tube should not extend into the humidifier. If it does, experience shows that water condenses inside the tube because it is not directly in contact

with any heating tape. Eventually, the condensation builds up and blocks the outlet tube all together. Pressure inside the flask builds, finally pushing the condensation along the tube out of the humidifier and into the +100°C heated tubes where it vaporizes. Once vaporized, the cell "sees" an instantaneous increase in pressure (pressure spike) causing the electrolyte to crack.

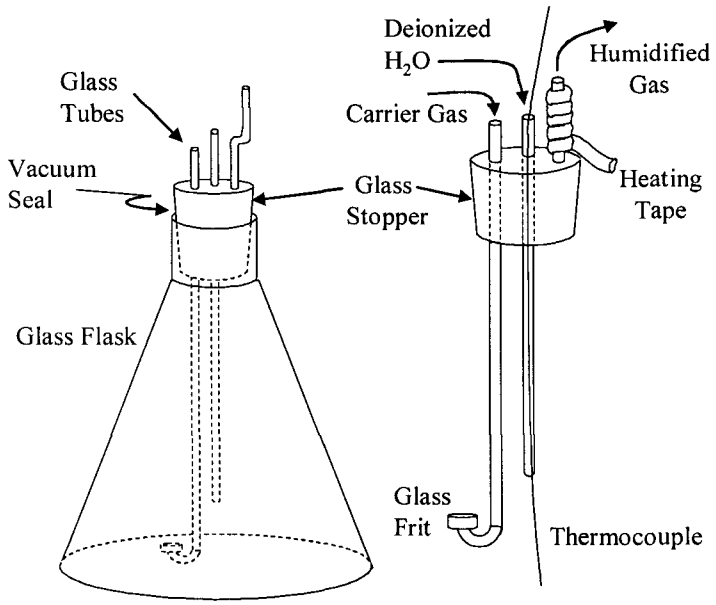

Figure 3-3 Schematic of humidifier.

3.3.3 Gas Chromatography

The gas chromatograph used in this work contains two packed columns: a Hayesep Q 80/100 Mesh (part # 19006-80110) used in detection of CO_2 and a Molecular Sieve 13x 45/60 Mesh (part # 19006-80020) used in detection of CO, CH_4, N_2, O_2 and H_2. For this reason, one sample can not be analyzed in its entirety and instead two samples must be analyzed, one for each column. Sample consistency thus becomes a concern. Experience shows setting the current rather than voltage helps provide this consistency because the same amount of O_2 is always produced for a given input gas. If voltage is

fixed, the oxygen production could (and usually does to some extent) vary. Thus current control is used in collecting GC data.

A single GC analysis (two column passes) can take almost 20 minutes so performing multiple analyses for a given current setting is time intensive. However, at least two consecutive analyses are performed to insure sample consistency. If exhaust uniformity is not observed, another analysis is performed or the GC is re-calibrated. A typical example of sample consistency obtained is shown in Table 3-1.

Table 3-1 Example GC data: alumina cell IAcell06, post IV59, V = 1.09V, I = 0.68A.

Constituent	CO_2	CO	CH_4	N_2	O_2	H_2	Total
1st Sample (% mol)	95.09	0.54	0.00	0.32	0.07	4.38	100.4
2nd Sample (% mol)	95.02	0.51	0.00	0.29	0.06	4.38	100.3

3.3.4 Water Condenser

During combined electrolysis, water can condense in the exhaust plumbing to the fume hood. Pressure inside the cell builds until the water can be moved along the exhaust line. Eventually, the meniscus in the exhaust line is broken and the pressure is released but the water builds up again and the process repeats itself. This obviously causes a fluctuating cell pressure, thus a condenser is used to remove the water prior to exhausting to the fume hood.

More importantly, the gas chromatograph columns described above in section 3.3.3 should not be exposed to water. When testing higher flow rates, condensing the water out of the exhaust becomes difficult. The water contamination causes the GC samples to not add to 100% and eventually de-calibrates the GC all together because of water adsorption on the columns.

A high capacity condenser was built using a two foot long section of spiraled copper tubing, packed in ice and insulted in ¾ inch thick Styrofoam. The Styrofoam enables ice to remain on the coils over night, doubling the maintenance free operation time. Tubing of an outer diameter of ¼ inch works better than ⅛ inch because water can condense without blocking the tube and pressure fluctuations can be avoided.

3.3.5 Carbon Monoxide and Hydrogen Handling

Exhaust from combined electrolysis contains both CO and H_2. CO is an odorless, toxic gas that can be fatal even with adequate oxygen [53]. H_2, being the lightest atom on the periodic chart, can rise in the lab and accumulate in pockets around the ceiling posing a combustion hazard with air. For these reasons, all combined electrolysis exhaust, whether sent through the GC or not, is plumbed to a fume hood that exhausts out of the building.

Additionally, the effects of CO exposure in small amounts can cause headache, nausea, and dizziness. Chronic effects include cardiovascular problems [53]. Therefore, to monitor for leaks a calibrated, quick response CO detector (Industrial Scientific Corporation model 1810-2224) that warns of CO levels exceeding 35 PPM is used at all times.

Finally, when using H_2 as the carrier gas, one must consider the following. 1) Failure to purge lines properly before switching to H_2, 2) leaks in the H_2 line, or 3) cross leaks in the cell (allowing oxygen into the cathode where the H_2 is present) can all cause combustion in the line which can travel back to the H_2 tank. As a result, a flash arrestor is used to shut off gas flow in the event of a flashback.

3.4 SOE Cell Construction

The SOE cells used in the experiments presented here were assembled in-house. The following describes how SOE cells are constructed and the differences between two types of cells tested.

3.4.1 Chromium-alloy Cells

SOE cell components and a fully assembled cell are exemplified in Figure 3-4. The manifolds were originally designed for the Oxygen Generator System (OGS) developed for NASA's 2001 Mars Surveyor Lander to demonstrate oxygen generation on Mars [51]. 50 and 30 mm diameter manifolds are made from an electrically conducting oxide-dispersion-strengthened alloy Cr-5 Fe-1 Y_2O_3 called CRF provided by Plansee, Ltd [37]. Electrical conductivity allows the manifolds to distribute current in addition to gas. The manifolds are then coated with a platinum-based proprietary coating developed by Helicon Research, LCC, to minimize the evaporation of chromium oxide and its subsequent feared contamination of the electrode. Gas is delivered to/from the manifolds via Inconel (NiFeCr) tubes.

Pressed in between the manifolds, the electrolytes are constructed of 8% mol YSZ (Tosoh TZ-8Y) of a thickness 0.25 – 0.37 mm. Typical electrodes are screen-printed on the electrolyte in two layers totaling an electrode thickness of 30 microns (Figure 3-4 a). The first layer applied to the electrolyte is a 50/50 by weight platinum/YSZ mixture [13]. The second layer is pure platinum (Heraeus, Inc., CL11-5100) to better distribute the current delivered to/from the manifolds. The areas are 3.14 and 10 cm^2 for the cells with 30 and 50 mm manifolds, respectively. The electrodes are sintered at 1200°C. The

assembly is finally sealed with a glass glaze [37] under 10.2 kg (22.5 lb) of load (Figure 3-4 b).

Cr-alloy cells with 50 mm manifolds (and electrolytes) are named 50cell## where the ## corresponds to the number of the cell. For instance, the first 50 mm Cr-alloy cell would be called 50cell01.

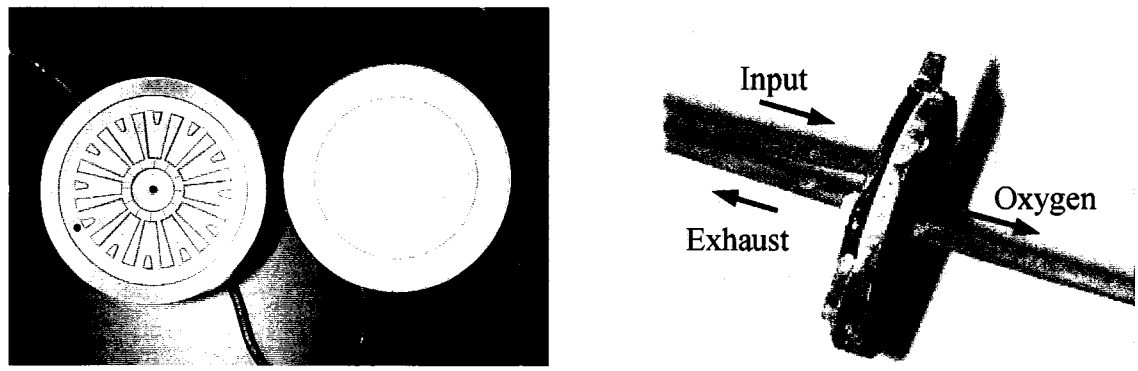

(a) 50 mm manifold & electrolyte/electrode [37] (b) 30 mm assembled cell.

Figure 3-4 Components and assembly of a SOE cell.

3.4.2 Alumina Cells

Cell materials and refurbishment costs are expensive for the Cr-alloy cells. Therefore, a second cell configuration was tested in the interest of cost. Predominately made of aluminum oxide Al_2O_3 (also commonly called alumina), the cells are hence called alumina cells. The electrolyte and electrodes of the alumina cells are of the exact same construction as that used in the Cr-alloy cells, but only 50 mm diameter electrolytes with 10 cm^2 electrodes were used. The fundamental differences between the two cell configurations are in the manifolds/tubing and separate interconnects or current collectors.

The manifolds are made of Bisque Alumina provided by Superior Technical Ceramics Corp. The inlet and outlet tubes are made of alumina as well (CoorsTek AD-998). Alumina is a non-electrically conducting material. Therefore, to deliver current, separate interconnects of Pt gauze (Alfa Aesar, 10283) are placed between the manifolds and electrodes. To apply voltage and carry current to/from the gauze interconnects, 1.0 mm Ni (Alfa Aesar, 14337) leads were initially used but oxidized and could not be recycled for use by subsequent cells. 0.5 mm Ag (Alfa Aesar, 11433) current-carrying leads were then tried but melted during 850°C operation carrying 6.7A. Finally, leads of 0.5 mm Pt (Alfa Aesar, 43288) proved to be successful and recyclable.

Like the Cr-alloy cells, the cathode is sealed with a glass glaze. However, the anode is not sealed. Fort this reason, the anode is flushed with air to guarantee the oxygen partial pressure. Additionally, for the alumina cells a load of only 1.8 kg (4 lb) is sufficient to compressed the manifolds against the gauze interconnects and electrodes.

Alumina cells are named IAcell##. IA stands for Iacomini Alumina because it was built by Christine Iacomini. The ## stands for the number of the cell. For example, the first alumina cell constructed by Iacomini would be called IAcell01.

4 EXPERIMENTAL RESULTS

Between the two cell-types described in section 3.4, twenty cells were tested in all. It is intended that this chapter be used as a reference to general observations with specific examples of phenomena observed. Thorough analyses and interpretations are presented in chapter 5.

4.1 Electrolysis Cell Conditioning

Both types of cells require pre-conditioning to achieve optimal, consistent performance. The conditioning is not to overcome any hysteresis but rather a necessary step to prepare the cell to operate at its maximum performance. Based on observations, if no conditioning is performed, the cell initially performs poorly but over time slowly improves. The rate of this improvement depends upon operating conditions and thus can alter the consistency of a group of experiments. Thus before any investigations are pursued, pre-conditioning is required.

Conditioning appears to be accelerated at higher temperatures and higher voltages. Thus, each new cell is operated at 850°C and 1.8V of applied voltage. Once the cell achieves steady state operation during this process, the cell is considered conditioned and ready for experimental investigations. Such conditioning is exemplified in Figure 4-1 with the current limited to 8A. Figure 4-2 demonstrates consistency in CO_2 electrolysis amongst different cells after conditioning.

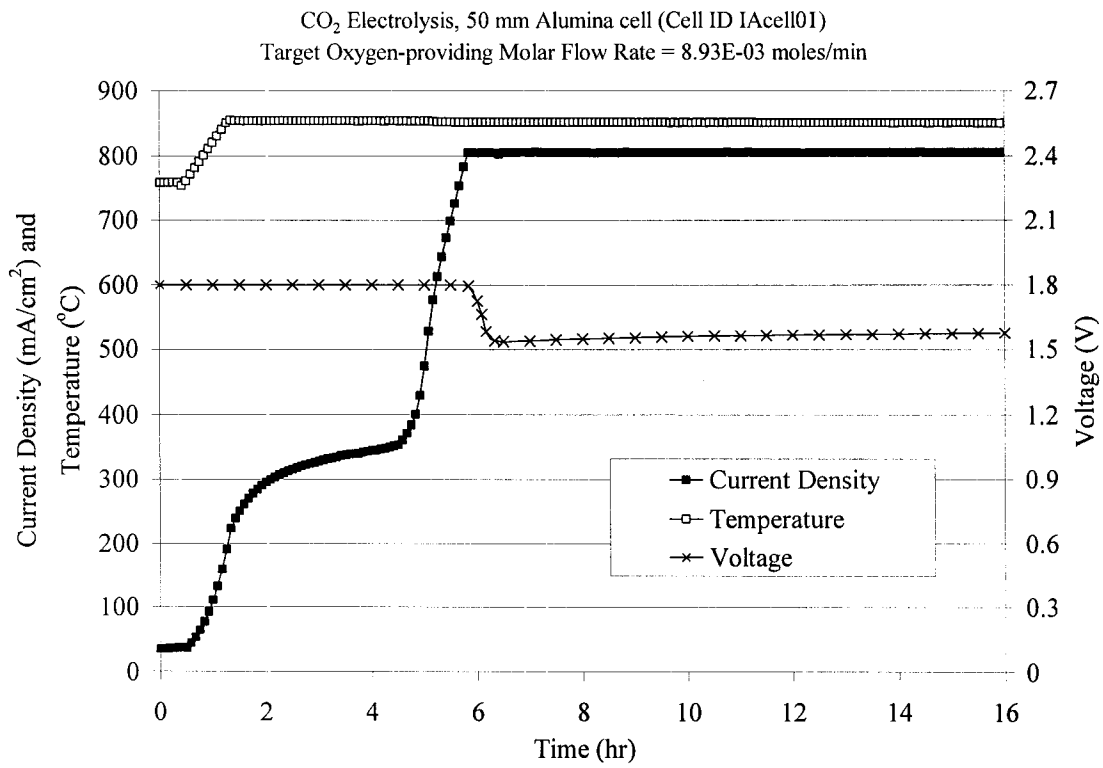

Figure 4-1 Current and voltage during pre-conditioning.

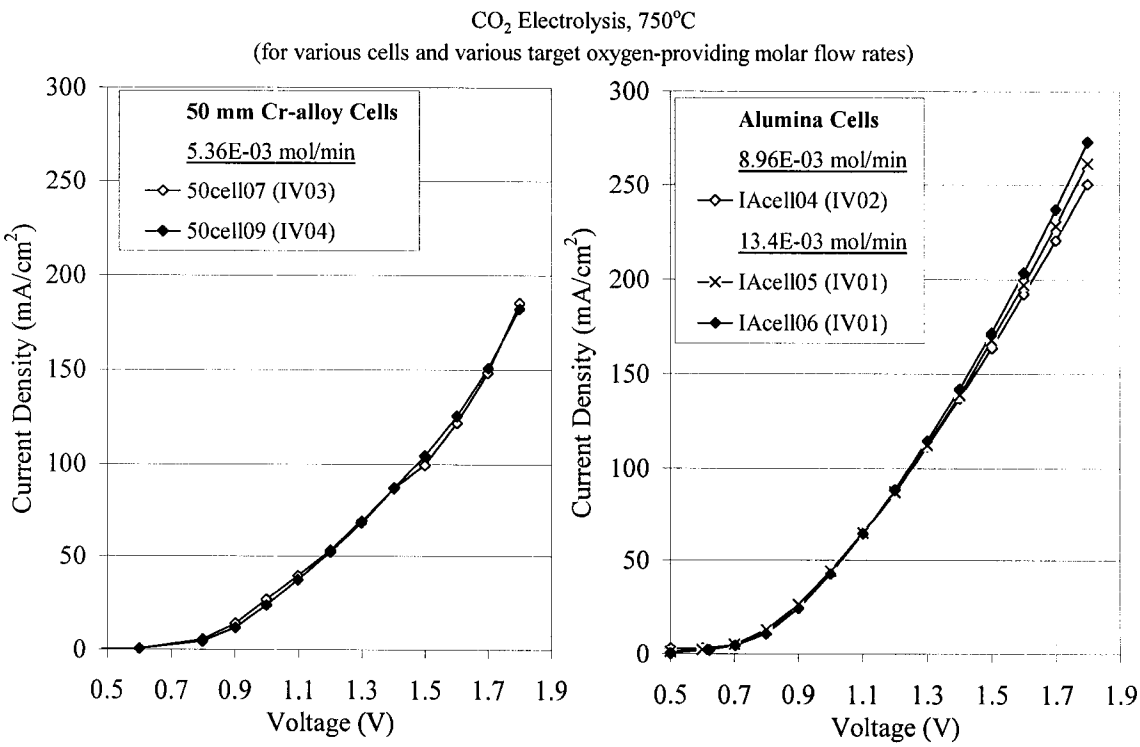

Figure 4-2 Consistency of CO_2 electrolysis from cell to cell.

4.2 Carbon Dioxide Electrolysis Baselines

Throughout an electrolysis cell's life after the initial conditioning has been performed, its CO_2 electrolysis performance slowly degrades. Part of this degradation is due to the stresses of the various investigations. Another cause is due to operational mishaps, such as power outages, input gases depleting or humidifiers running dry. For these reasons, all specific inquires begin with the electrolysis of CO_2 in order to establish a baseline performance. Therefore, any natural cell degradation can be neglected and effects of the particular investigation can be better isolated.

After obtaining experience in testing SOE cells, it was realized that sometimes a cell's performance can drift. Therefore, eventually multiple performance curves (current density versus voltage) were taken in order to not only establish a baseline but a repeatable baseline. This procedure insured any drift seen in subsequent investigations could be attributed to the investigation at hand and not an adjusting cell. Figure 4-3 is an example of establishing a stable baseline. IV66 through IV73 slowly degrade over time. However, IV74 through IV79 are repeatable.

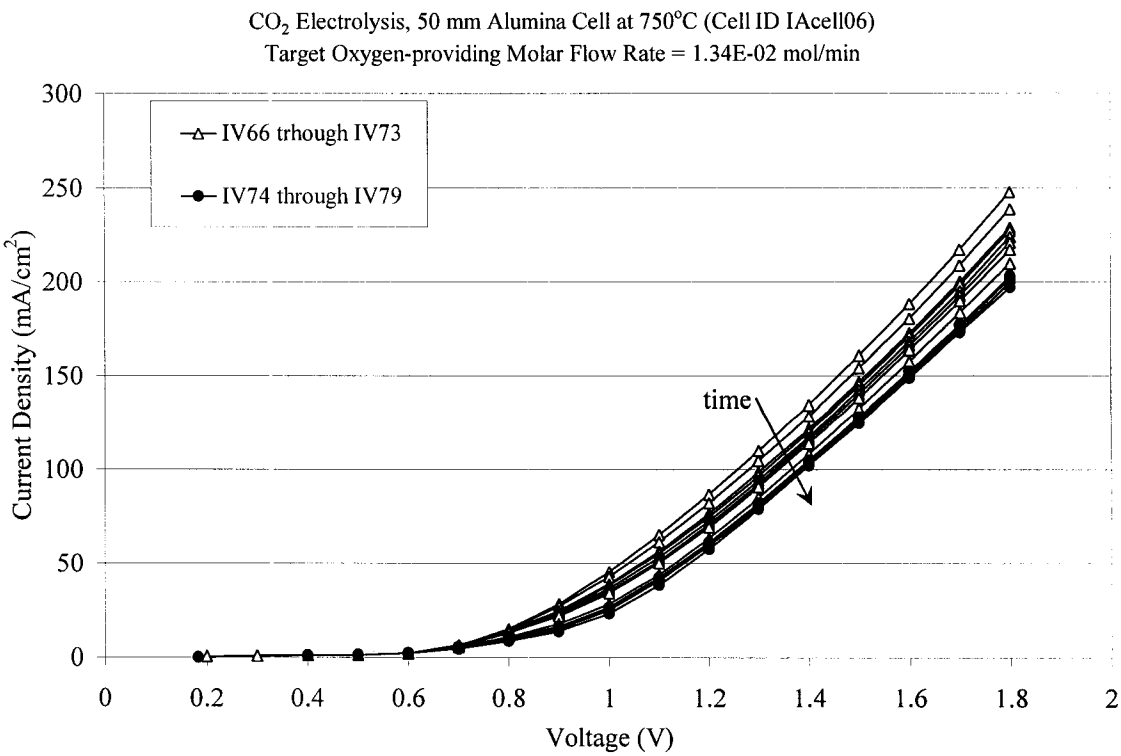

Figure 4-3 Example of establishing a stable CO_2 baseline.

4.3 Mass Limiting Flow Rates

In order to reduce the influence of oxygen-providing molar flow rate on experimental results, tests are carried out above a cell's mass limiting range. The mass limiting flow rate is determined experimentally by monitoring current for a given voltage as the flow rate is increased. Once the performance does not respond to increased flow rate, the cell is operating outside the mass limiting region.

Figure 4-4 shows the results from mass limiting investigations using CO_2 as the oxygen-providing gas. For 50 mm Cr-alloy cells, operating out of the mass limiting range requires oxygen-providing molar flow rates above 6.25E-03 mol/min. For 50 mm alumina cells, molar flow rates of at least 8.12-E03 mol/min should be set. Therefore,

subsequent tests are run at flow rates higher than these such that the influence due to fluctuations in the number of oxygen-providing molecules will be minimized.

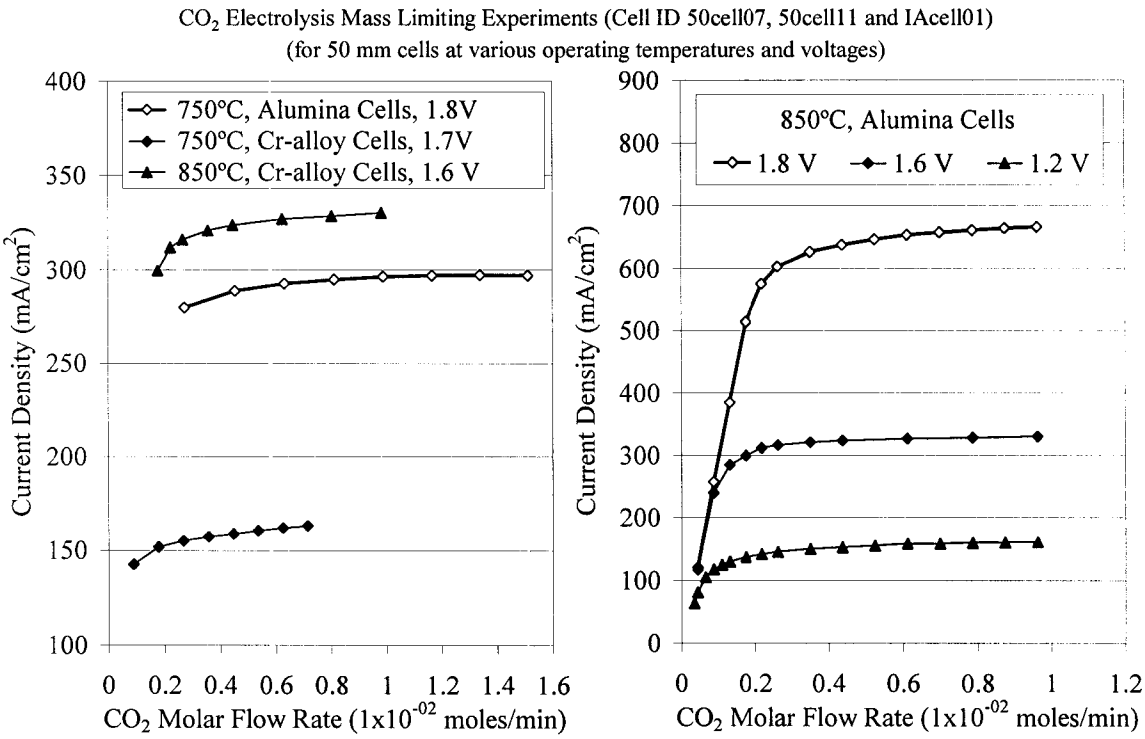

Figure 4-4 Mass limiting experiments for CO_2 electrolysis.

4.4 Chromium-alloy Cells

Fourteen Cr-alloy cells were tested at 750 and 850°C. Mixtures are reported in percentage by volume. Two 50 mm cells were consistently tested providing over 20 runs of the following inputs: 100% CO_2; 41 – 45% H_2O in He; and 30 – 58% H_2O in CO_2. As a reminder, usually 50 mm diameter Cr-alloy cells are designated as 50cell##, where the ## stands for cell number 01, 02, etc. In general, differences between the different input gas mixtures tested in Cr-alloy cells are sometimes difficult to distinguish. To aid in comparisons of the many tests, all Cr-alloy cell data will also be presented normalized by

IV03 of cell 50cell07 (refer to Figure 4-2). The experimental results obtained are summarized in the following sections.

4.4.1 Effects of Humidified Mixtures on Cell Health

Initially both H_2O electrolysis and combined electrolysis appear to degrade the performance of CO_2 electrolysis. However, the degradation is recoverable during pure CO_2 electrolysis. Usually the recovery time was accomplished over the course of a performance test, which can take anywhere from 3 to 6 hours. For H_2O electrolysis, all subsequent H_2O electrolysis tests after the initial CO_2 recovery cause no degradation. Not enough data has been collected to make the same assessment for after combined electrolysis. Detailed examples of these statements follow.

First, H_2O electrolysis is considered. Figure 4-5 and Figure 4-6 show data from cell 50cell07. Figure 4-5 shows that after the first H_2O run, up to 36% degradation (at 1.1V) in CO_2 performance is observed but by the end of the IV test, recovery is accomplished to within 5% (at 1.8V) of the initial CO_2 performance. A subsequent CO_2 run (IV06) demonstrates full recovery.

Then two additional H_2O electrolysis runs were again followed by CO_2 electrolysis. Figure 4-6 shows that the following CO_2 electrolysis performance (during a mass limiting experiment) showed no degradation this time but accomplished an 8% (at 1.7V) increase over initial and recovered CO_2 runs.

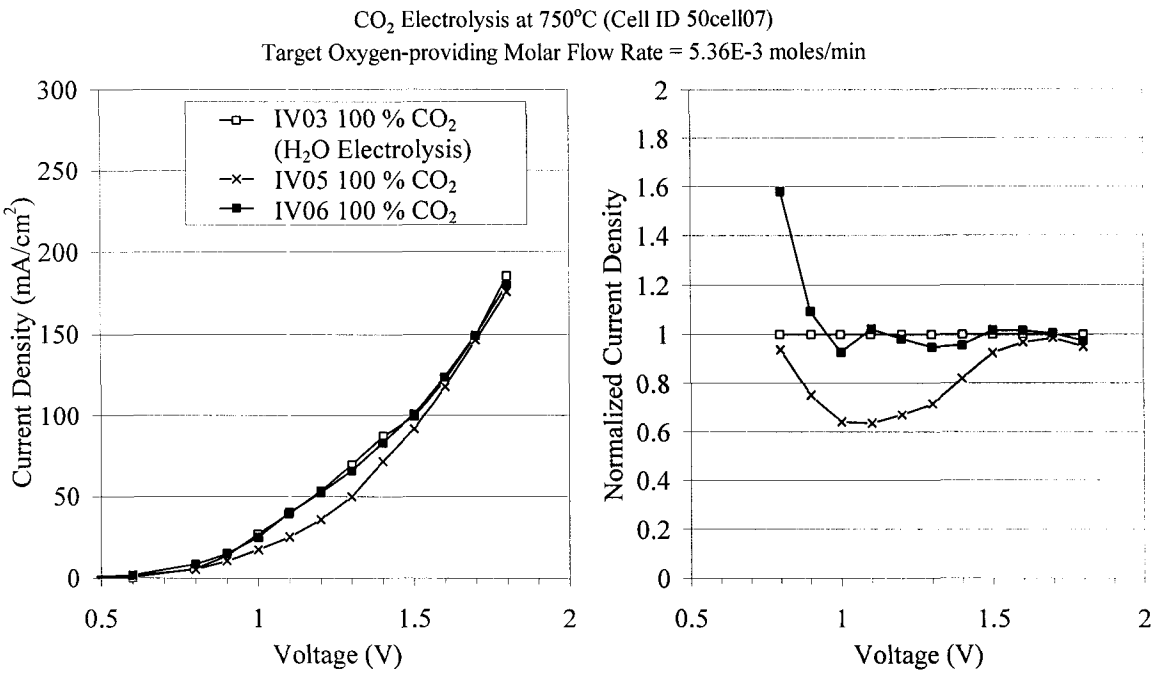

Figure 4-5 CO_2 electrolysis degradation and recovery after initial H_2O electrolysis.

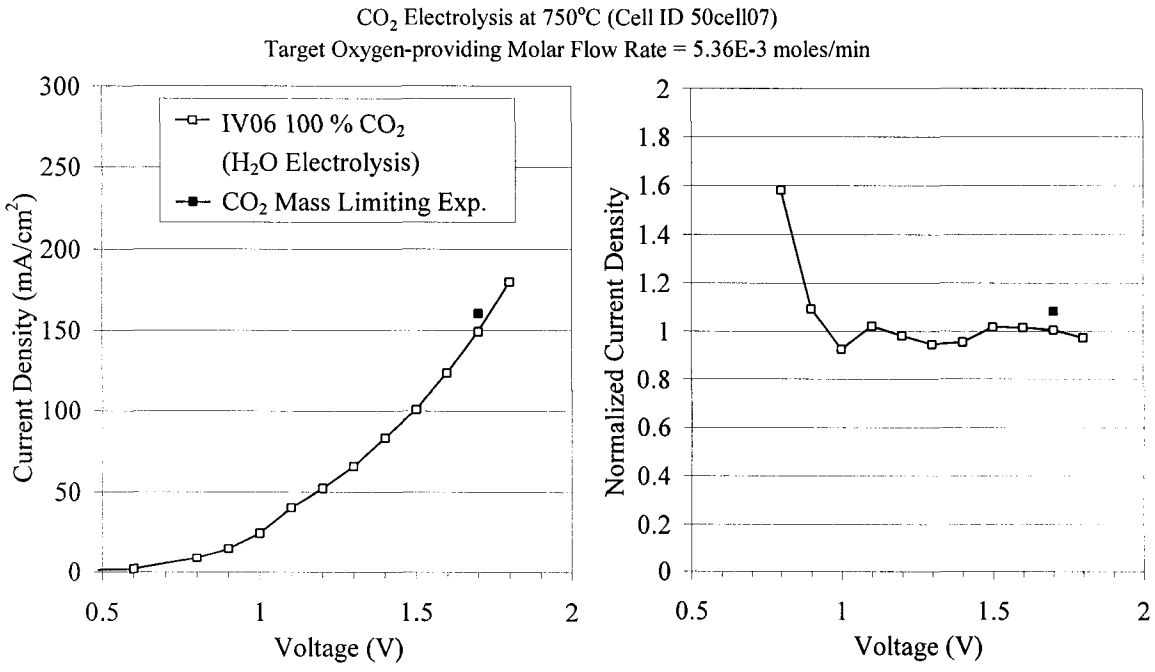

Figure 4-6 No CO_2 performance degradation after recovery and additional H_2O exposure.

Next an example of CO_2 degradation after initial combined electrolysis runs is shown in Figure 4-7 for a different cell, 50cell09. A CO_2 run was performed after five combined electrolysis runs. CO_2 electrolysis initially shows a degradation of up to 35% (at 1.0V) from the first CO_2 electrolysis run but is observed to recover to within 3% (1.8V) by the end of the run. A cross leak developed, as described in section 4.6, preventing further investigation of the stability of the cell after combined electrolysis exposure.

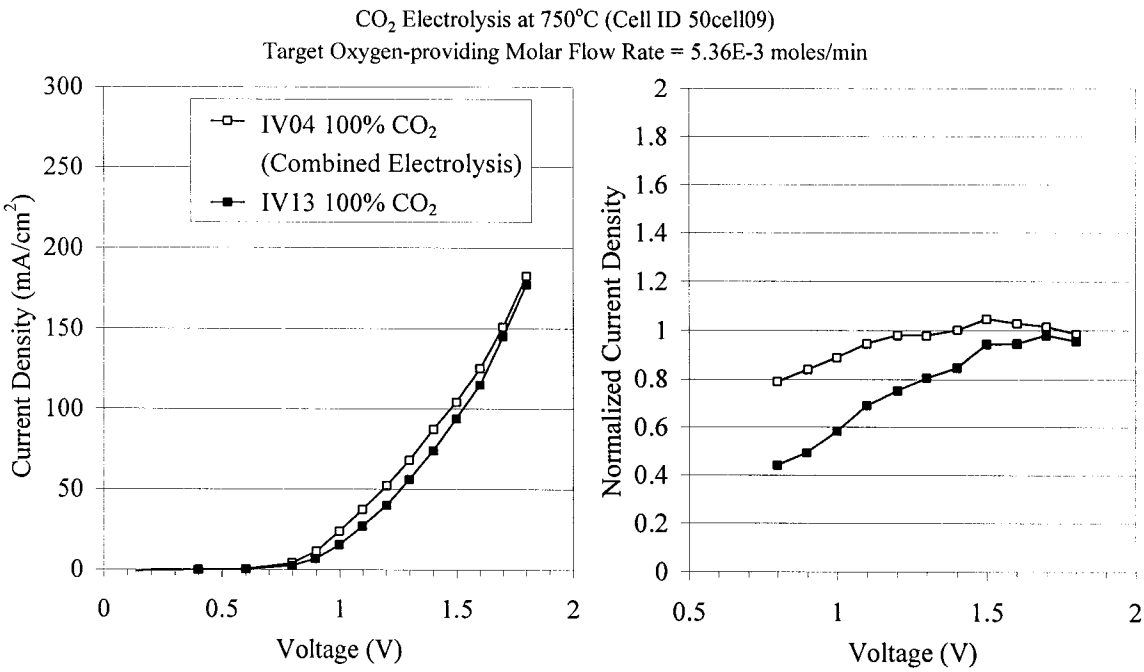

Figure 4-7 CO_2 electrolysis degradation & recovery after combined electrolysis.

4.4.2 Water Electrolysis Performance

Water electrolysis of humidity from 41 – 45% (50% was targeted), outperforms CO_2 electrolysis. Eventually, over a 50% improvement in performance is observed. For

example, Figure 4-8 shows that the last H_2O electrolysis run of 45% humidity performs better than CO_2 by 53% (at 1.5V).

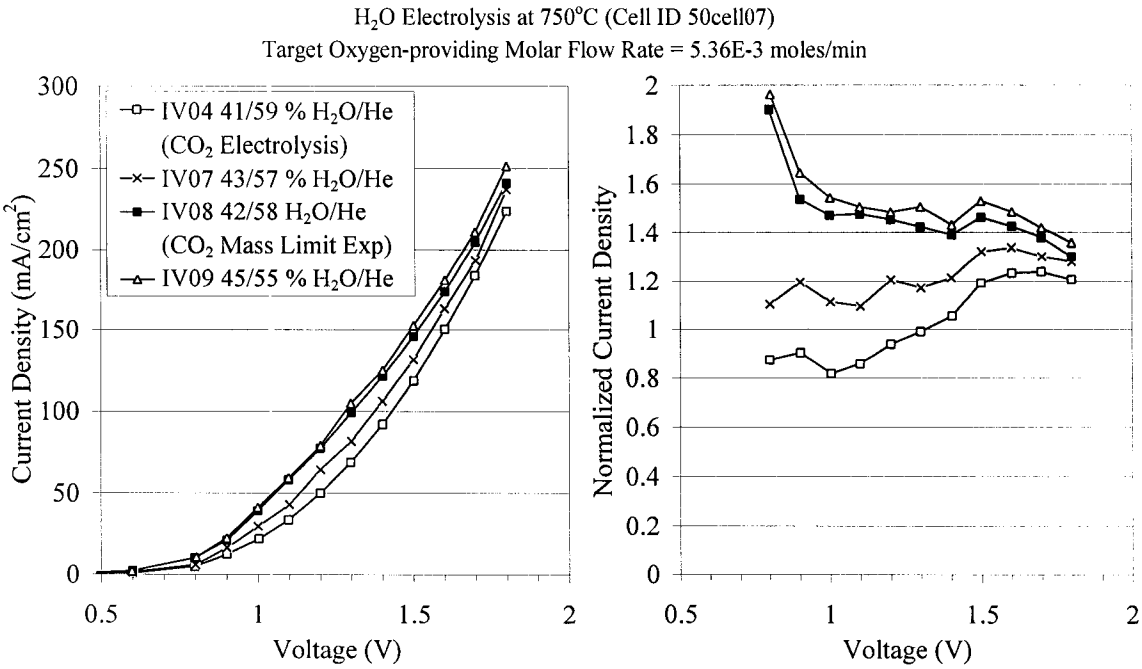

Figure 4-8 H_2O electrolysis versus CO_2 electrolysis.

Cr-alloy cells could require additional conditioning prior to H_2O electrolysis because initially the first H_2O electrolysis test underperforms CO_2 electrolysis performance. However, during the test it improves such that it and subsequent H_2O electrolysis tests of similar humidity exceed that of CO_2 electrolysis. For example, Figure 4-8 shows the first H_2O run of cell 50cell07 (IV04) slightly under performs CO_2 electrolysis at voltage below 1.3 by up to 18% (at 1.0V). However, the cell could be "conditioning" during the performance test because at higher voltage, H_2O electrolysis out performs CO_2 electrolysis by up to 24% (at 1.7V).

4.4.3 Combined Electrolysis Performance

Combined electrolysis outperforms CO_2 electrolysis as well. Unlike H_2O electrolysis, combined electrolysis may not require conditioning. During testing of another cell, 50cell09, all tests outperform CO_2 and do so consistently. Humidity content could directly influence the improvement in performance. For example, Figure 4-9 shows the first combined electrolysis run (IV05) of 51/49% H_2O/CO_2 outperforms CO_2 electrolysis by up to 30% (at 1.5V). A lower humidity mixture of 31/69% H_2O/CO_2 outperforms CO_2 by only 21% (at 1.5V). A second run of the same mixture provided repeatable results.

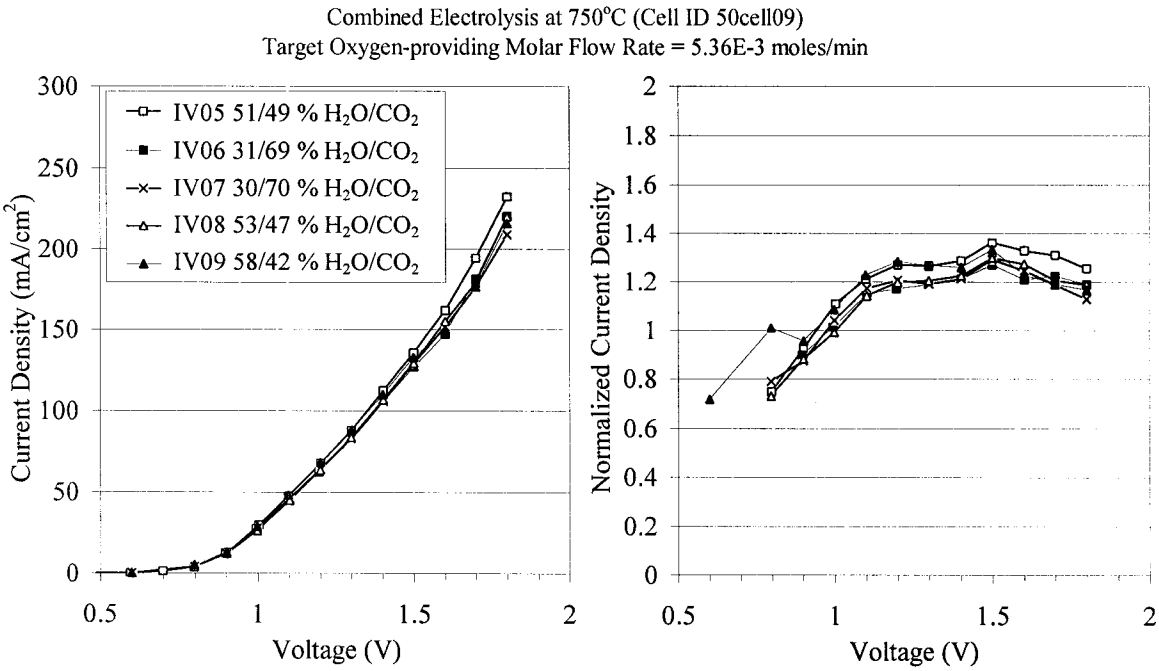

Figure 4-9 Combined electrolysis outperforms CO_2 electrolysis.

However, subsequent combined electrolysis runs shows that raising the humidity to 53% or even 58% only incurs a 5% increase (at 1.8V) over the previous 30/70% test. This is up to 8% below (at 1.7V) the results of the first combined electrolysis test of 51%

humidity. It could be that combined electrolysis requires time to stabilize and that there is little dependence upon humidity. More testing is required before solid conclusions can be drawn.

How does combined electrolysis compare to H_2O electrolysis? During testing of cell 50cell07, Figure 4-10 shows that 55/45% H_2O/CO_2 combined electrolysis outperforms CO_2 electrolysis by up to 64% (at 1.5V) and 45/55% H_2O electrolysis by up to 7% (at 1.5V). However, it is noteworthy that in comparing Figure 4-7 to Figure 4-8, H_2O electrolysis of 50cell07 outperforms combined electrolysis of cell 50cell09 even though they exhibit the same CO_2 performance.

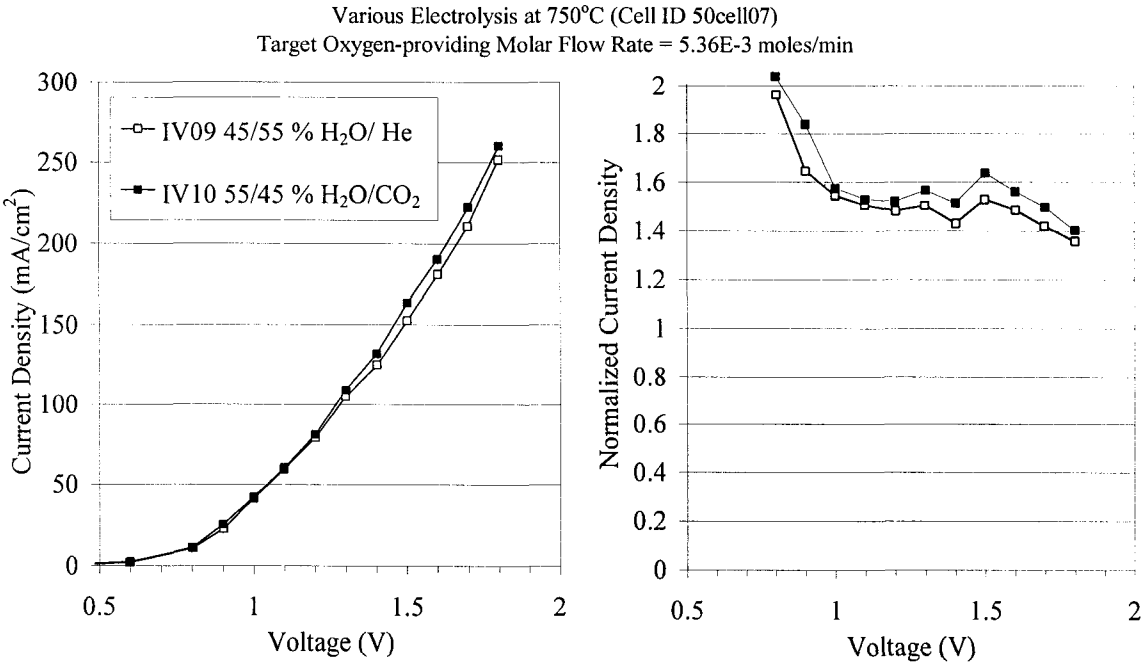

Figure 4-10 Combined electrolysis versus H_2O electrolysis.

Unfortunately, a cross leak developed in 50cell07 so further combined electrolysis runs could not be performed to assess combined electrolysis stability after H_2O electrolysis. It should be remembered that the H_2O runs improved over time and that

could possibly condition the cell to perform combined electrolysis well. Whether better combined electrolysis performance could be maintained is unverified.

4.4.4 Effects of Low Flow Rates

As discussed in section 1.2, lowering the flow rate for a given operating temperature and voltage setting increases utilization. Figure 4-11 exemplifies typical utilization as a function of flow rate for CO_2 electrolysis at 850°C. Operating at higher utilization is desirable when recycle costs are high. To achieve very high utilization, a cell must be operated in its mass limiting region. Electrolysis data show that performance is relatively insensitive to input gas mixture when operated below the mass limiting flow rate. Details follow.

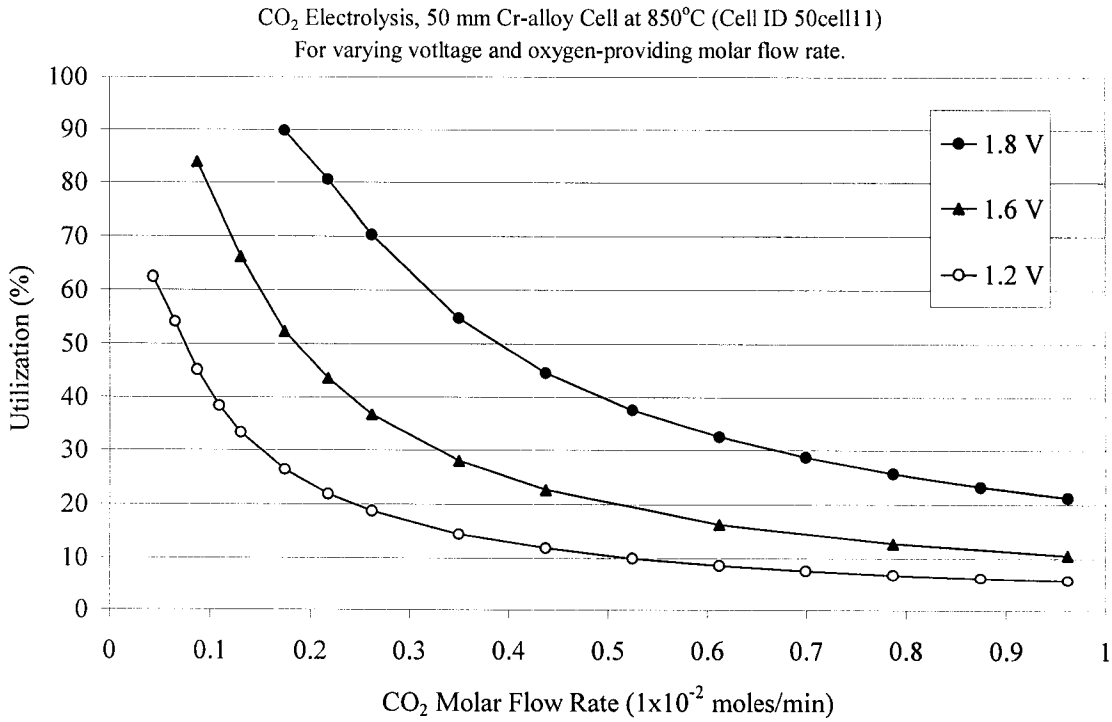

Figure 4-11 Electrolysis utilization versus input flow rate.

Experiments were carried out on a 30 mm retired cell from the OGS program. Its electrodes were made with only one layer of pure Pt. A Pt gauze served as the interconnect so in essence the cell was sort of a combination design of the Cr-alloy cell and the alumina cell described in section 3.4.

CO_2 electrolysis input flow rates were 4.47E-04 moles/min (10 sccm, 0°C, 1 atm). For humidified runs, the carrier gas (He in the case of pure H_2O electrolysis and CO_2 for combined electrolysis) was always set to 4.47E-04 moles/min as well. Humidity was adjusted by increasing the temperature of the humidifier. Initial results suggested that H_2O strongly increased performance: the higher the humidity, the better the performance. However, by keeping the carrier gas flow rate constant, increasing the humidity meant adding H_2O to the flow, or more explicitly put, giving the cell more oxygen-providing molecules to electrolyze.

A second set of tests was performed with the same 30 mm cell matching the oxygen-providing molar flow rate of the previous runs. An example of the data from both sets of tests is presented in Figure 4-12 and suggests performance is strongly dependent on oxygen-providing molar flow rate yet relatively insensitive to the input gas.

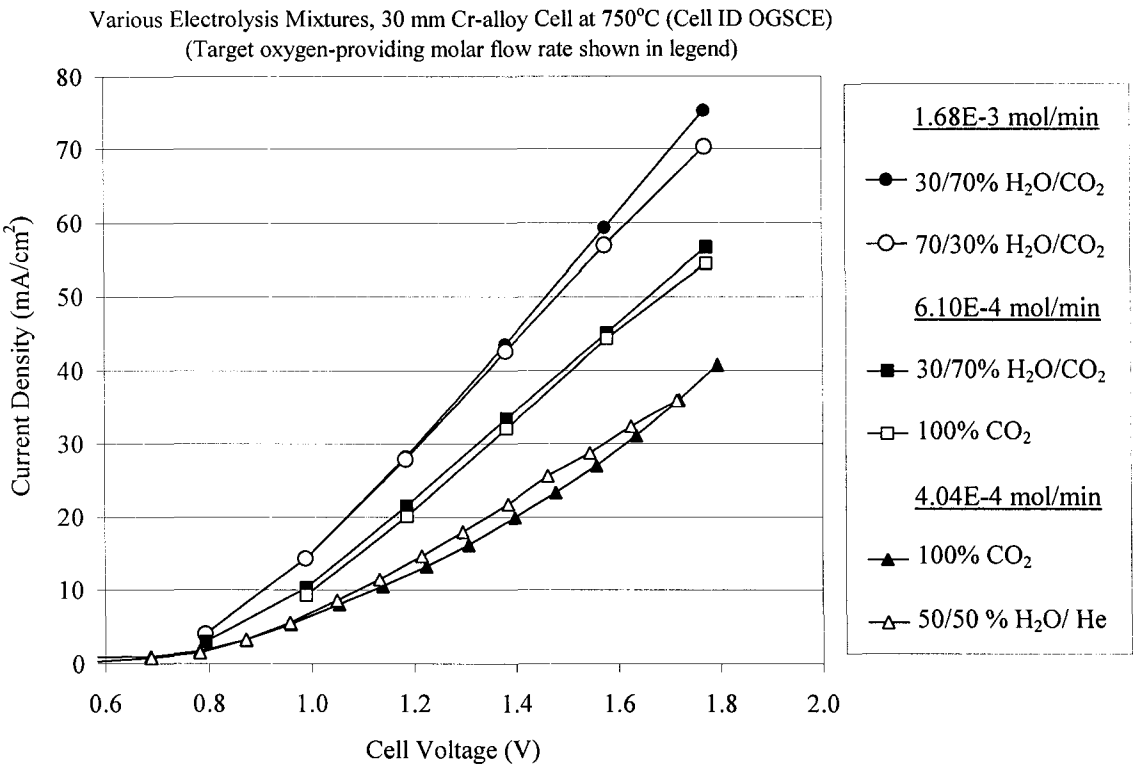

Figure 4-12 Electrolysis performance for low oxygen-providing molar flow rates.

4.4.5 Performance Dependence on Humidity

For investigations performed at flow rates above the mass limiting range (as determined during CO_2 electrolysis), close inspection of the performance curves suggest that increasing H_2O content in the inlet mixture (absolute humidity) could encourage better performance for both H_2O electrolysis and combined electrolysis. Figure 4-13 demonstrates that Cr-alloy H_2O electrolysis data suggest that H_2O electrolysis is sensitive to the level of humidity. Unfortunately, only 41– 45% humidification of He was targeted and not sequentially to specifically investigate the effects of H_2O concentration. Could the He be acting as a diffusion barrier, increasing concentration overpotential? If this is

true, it could be possible that 100% H_2O electrolysis performs as well as combined electrolysis.

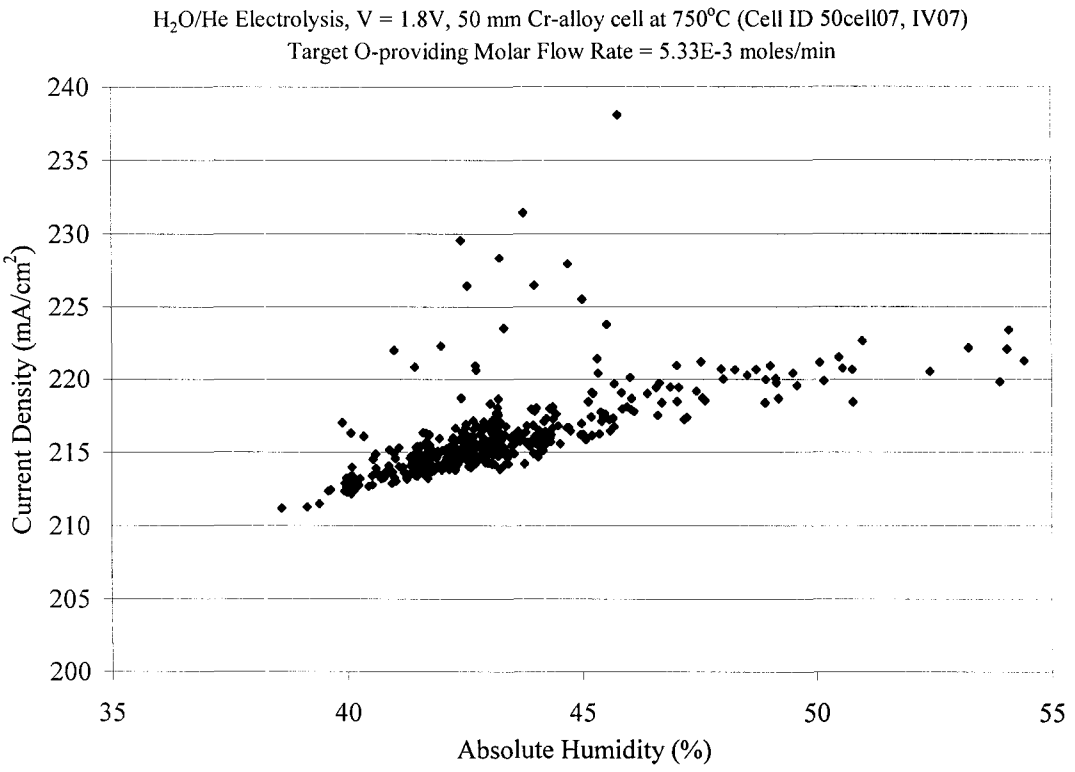

Figure 4-13 Cr-alloy cell performance exhibits sensitivity to humidity level.

4.4.6 Combined Electrolysis Preference to Water or Carbon Dioxide

Knowledge regarding how combined electrolysis utilizes the H_2O/CO_2 mixture is imperative to implementing the technology effectively. Therefore, the exhaust of the cell is analyzed to quantify the composition of H_2 and CO providing a direct correlation to whether H_2O or CO_2 is preferentially electrolyzed.

The exhaust of a Cr-alloy cell is carried via a tube made out of Inconel (NiCrFe) while being cooled. As described in section 3.3.4, when testing combined electrolysis the exhaust is then fed through a condenser where left over H_2O is removed. For several

tests, GC analyses were then conducted on the remaining exhaust. All constituents detected summed on average to 99.97% (σ_m = 0.06%, 21 samples) indicating no unknown compounds, such as hydrocarbons, survive the cell exhaust. Not once was CH_4 detected. That is not to say hydrocarbons at one time did not exist. Because Inconel contains metal catalysts, hydrocarbons could be converted to CO, CO_2, H_2, and/or H_2O while cooling along the tubes.

GC results indicate that there could be a slight preference to H_2O electrolysis over CO_2. The GC detected greater levels of H_2 than CO. For example, Figure 4-14 plots the percentage of electrolyzed molecules that is H_2 versus the H_2O concentration contained in the input. Data points above the dashed line indicate a preference to H_2O. Data points below the dashed line indicate a preference to CO_2.

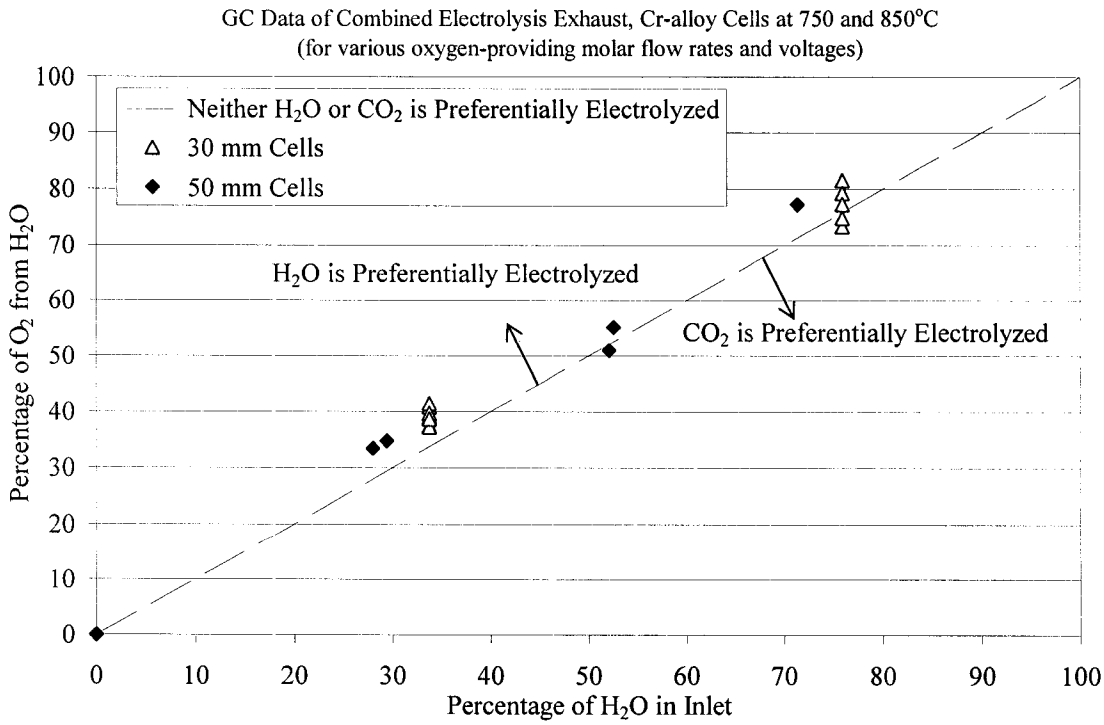

Figure 4-14 Cr-alloy GC results suggest slight H_2O to CO_2 preference.

4.5 Alumina Cells

Cr-alloy cell testing was followed by alumina cell testing. Six alumina cells were tested at 750°C after initial conditioning at 850°C. As a reminder, designators are IAcell##, where ## stands for cell number 01, 02, etc. The first three were mostly used in perfecting cell construction and verifying testing procedures. The last three were the work horses of electrolysis investigations. Like Cr-alloy data, humidified mixtures are reported in percentage by volume. However, additional gas mixtures were tested to investigate some questions raised during Cr-alloy cell testing. Over 140 tests were executed of the following inputs: 100% CO_2; 55 – 91% CO_2 in N_2; 77 – 95% CO_2 in He; 20 – 92% H_2O in He; and 6 – 75% H_2O in CO_2. The experimental results obtained are summarized in the following sections.

4.5.1 Hydrogen Effects on Carbon Dioxide Electrolysis

As shown in section 4.4.2, combined electrolysis slightly outperforms that of H_2O. One explanation could be that CH_4 is forming via one or both of the following Sabatier reactions:

$$CO_2 + 4H_2 \rightarrow CH_4 + 2H_2O \quad (4.1)$$

$$CO + 3H_2 \rightarrow CH_4 + H_2O \quad (4.2)$$

If either of these is occurring, then CO and/or H_2 are being consumed which would push the electrolysis reactions (equations (1.4) and (1.5)) to the right. For instance, extracting H_2 from the electrolysis atmosphere via reaction (4.1) would push the reaction quotient for H_2O electrolysis below its equilibrium constant and thus encourage more H_2O

electrolysis (see text near Figure 5-25 for a discussion on reaction quotient versus equilibrium constant).

Three tests were executed in order to investigate the performance of CO_2 electrolysis solely in the presence of H_2. Such results will test the validity of reactions (4.1) and (4.2) if CH_4 is detected in the cell exhaust. The results are presented in Figure 4-15 and Table 4-1. In summary, a small amount of H_2 appears to induce performance enhancement though this may only be a temporary effect. The enhancement does not seem to be directly proportional to the amount of H_2 added. In fact, there appears to be a point at which adding more has no long term effect on performance. The entire removal of H_2 reduces performance below the original baseline. The dynamic responses amongst the tests are not consistent. Regardless, no CH_4 is detected in the exhaust. Thus reactions (4.1) and (4.2) are unlikely occurring. Details follow.

CO_2 electrolysis is first established at 1.8V. Then H_2 is added via a separate mass flow controller and line that tees into the main inlet line. This mass flow controller and line are also used for He and N_2 dilution experiments described in section 4.5.2. Switching the gas supply from He or N_2 to H_2 may induce air in the line. It is believed that this air contamination causes a huge increase in performance when H_2 is originally added in the first two tests shown in Figure 4-15 (a) and (b). The third test shown in Figure 4-15 (b) was performed without having to expose the line to ambient; therefore, a huge performance spike upon original H_2 addition is not observed.

The first test was performed at a CO_2 molar flow rate of 8.93E-03 mol/min. The CO_2 baseline performance is on average 217mA at 1.8V. The original concentration of

H_2 added is 4.7% by mol. Once the contamination O_2 is electrolyzed, Figure 4-15 (a) shows 95.3/4.7% CO_2/H_2 electrolysis performance dips below the 100% CO_2 by about 2%. Shutting off the H_2 flow causes the performance to drop further for a total 3.2% deterioration. Doubling the H_2 addition over the last exposure for a concentration of 9%, induces an immediate 3% performance increase that eventually rises to almost 1% above the original 100% CO_2 performance. Interestingly, adding more H_2 does not necessarily result in more performance. When the H_2 concentration is increased to 16.6%, the response is an immediate 1.5% decline and then growth to within 0.03% of the previous 81/9% CO_2/H_2 mixture. When the extra H_2 is then removed, the response is an immediate 1.6% increase with a slow decline that settles to 0.3% above the performance of the previous 81/9% CO_2/H_2 mixture. When the H_2 content is totally removed, the response is again an immediate increase followed by a decline where the 100% CO_2 performance settles on average about 0.7% below the original baseline.

The second test was conducted at the same flow rate. As shown in Figure 4-15 (b), the baseline CO_2 performance at 1.8V is 212mA. Initial H_2 addition is doubled. Once the contamination O_2 is electrolyzed the 81/9% CO_2/H_2 mixture does not dip below the CO_2 baseline but settles at it and then slowly rises for a 1% increase before the H_2 is removed. Upon the complete removal of H_2 from the inlet stream, the performance immediately drops to an average 1.2% below the baseline. Reintroducing H_2 in a smaller concentration (2.4%) induces an immediate 2.4% increase followed by an immediate and rapid decline in performance. Further increasing the H_2 concentration back up to 9% increases the rate of deterioration even more. The performance of the 81/9% CO_2/H_2

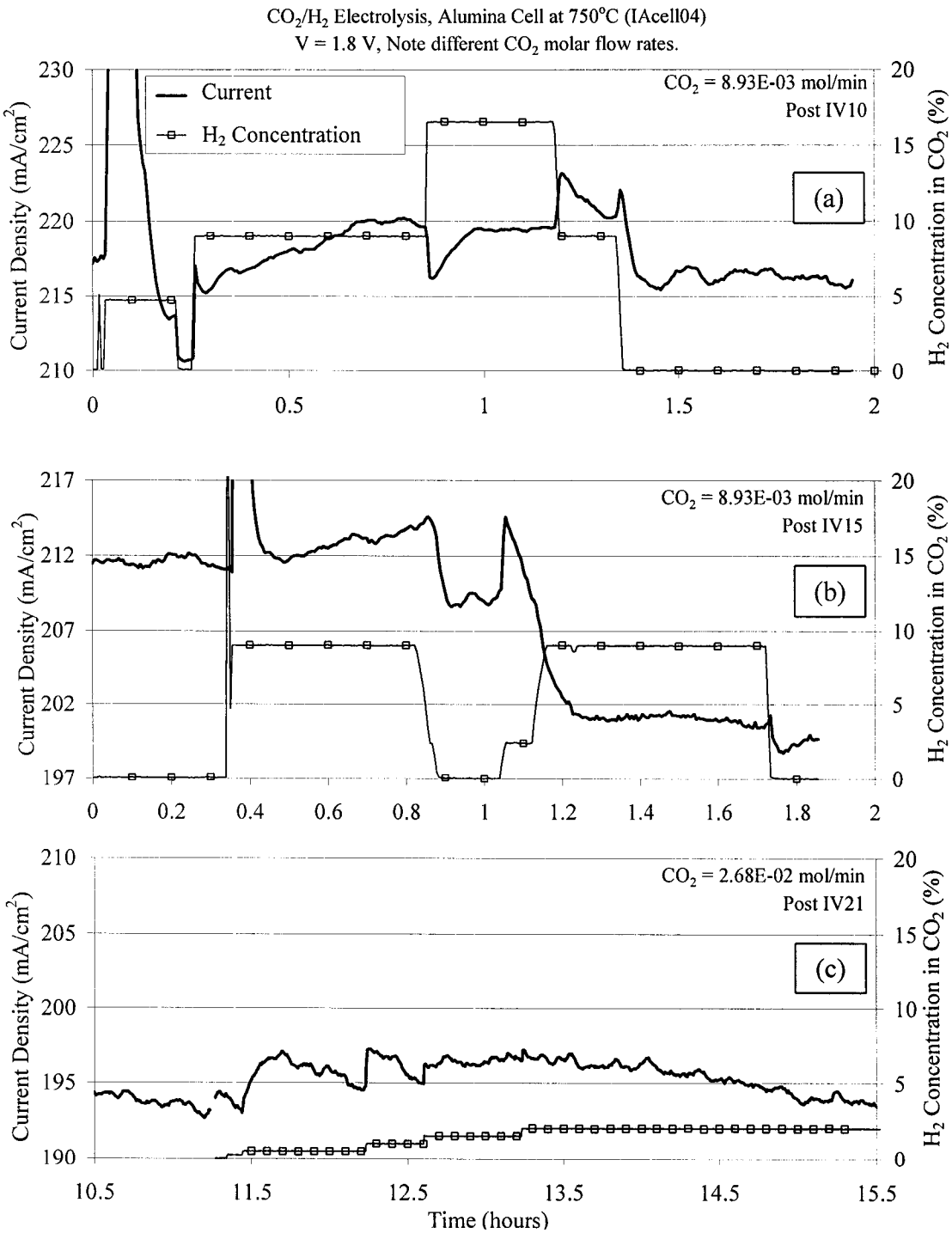

Figure 4-15 CO_2 electrolysis with the addition of H_2.

mixture achieves steady state at 5% below the baseline. Removing the H_2 all together causes another immediate decline with the performance eventually settling at 5.4% below the baseline.

To remove possible dynamics in cell response invoked by suddenly adding large quantities of H_2 to the inlet stream, a third test was performed at double the CO_2 flow rate and with much smaller concentrations of H_2 beginning with only 0.5%. Figure 4-15 (c) shows that the CO_2 performance before any H_2 addition is on average about 193mA with a steady decay of approximately 0.03 mA/cm^2-min. The addition of 0.5% H_2 induces a 1.9% increase. Doubling the H_2 addition to 1% induces an immediate 1.4% increase, followed by a 0.12 mA/cm^2-min decay. Further increasing the H_2 addition to 1.5% still induces an immediate increase in performance, but not as dramatically at only 0.6%. However, steady state appears to be achieved with a performance increase of 1.9% over the CO_2 baseline. A final H_2 increase to 2% only induces 0.3% increase which is followed by a 0.03 mA/cm^2-min decay matching that of the previous CO_2 baseline. With the decay, the final performance at 98.5/1.5% CO_2/H_2 matches that of the CO_2 baseline.

GC analyses were performed during the first and second tests shown in Figure 4-15 (a) and (b). The principle objective was to search for CH_4 so only the Molecular Sieve column, as described in section 3.3.3, was used. No CH_4 was detected. Constituents that were detected are listed in Table 4-1.

Table 4-1 GC results of CO_2/H_2 electrolysis runs.

Test	Figure 4-15 (a)				Figure 4-15 (b)	
Sample	1	2	3	4	3	4
H_2 Concentration in Inlet (%)	9.07	9.07	16.62	16.62	9.01	9.02
GC Detected Constituents:						
H_2 (% mol)	5.31	6.02	9.79	12.35	3.00	4.19
O_2 (% mol)	0.36	0.37	0.26	0.25	0.30	0.29
N_2 (% mol)	1.48	1.16	0.94	0.85	1.44	1.23
CO (% mol)	7.97	8.29	8.32	9.69	7.83	8.42

4.5.2 Electrolysis Performance of Diluted Carbon Dioxide

Water electrolysis is performed to ascertain if increased performance in combined electrolysis is due to the combination of CO_2 and H_2O or just H_2O itself. As was shown in section 4.4.2, only 40-50% humidified He was tested but closer inspection revealed a possible sensitivity to absolute humidity. Could the presence of He act as a diffusion barrier? Such a dilution effect could skew the interpretation of combined electrolysis performance versus H_2O performance.

To further investigate the effect of dilute gases, several experiments using cell IAcell04, tabulated in Table 4-2, were run at a constant oxygen-providing molar flow rate of CO_2 and 1.8V. Then He was added to simulate different levels of "humidification": 55, 70, 85, and 90 % by mol CO_2 in He. All results show that performance decreased when He was added and performance recovered when He was removed.

Table 4-2 Effects of diluent in CO_2 electrolysis for fixed voltage.

Cell	IAcell04			IAcell04			IAcell04	
Test	Post IV11 July 16 2003			Post IV20 24 July 2003			Post IV21 25 July 2003	
Voltage	1.8			1.8			1.8	
Dilute Gas	He			He			N_2	
CO_2/Dilute Gas (% mol)	91/9	87/13	83/17	85/15	70/30	55/45	85/15	77/23
CO_2 flow rate (mol/min)	8.93E-03			9.750E-03			17.85E-03	
Effect increase (%)	1.6	0.5 further	0.5 further	1.3	1.2 further	2.2 further	2.3	1.7 further
Recovery when dilute was removed?	N/A	N/A	Yes	N/A	NA	Yes	N/A	Yes

N_2 was used as a diluent as well to insure the He observations were not caused by He cooling. The thermal conductivity of He is larger than N_2 however N_2 is about the same as CO_2 (see Table 4-3). However, the N_2 had the same general effect as He.

Table 4-3 Thermal conductivities of various gases

Gas	**k x 10^3, W/m-K [33]**	**T, °C (K)**
H_2	448	727 (1000)
He	345	727 (1000)
N_2	64.7	727 (1000)
N_2	54.8	527 (800)
CO_2	55.1	527 (800)

These results show that CO_2 diluted with He or N_2 causes electrolysis performance to diminish. However, the tests were performed by adding the diluent and then watching the performance react. This method of testing was difficult to ascertain any effect due to the type of diluent used. Therefore, CO_2 baseline IVs were performed followed by a diluted CO_2 IV. Then the diluted run was followed by a 100% CO_2 run to assess the level of recoverability. This was performed twice, once for N_2 and another for He.

Overall the difference between the two diluents was negligible and subsequent CO_2 electrolysis obtained absolute full recovery. Details are as follows. Figure 4-16 shows CO_2 diluted with 5% of N_2 and then 5% of He underperforms 100% CO_2 by 1.9% and 2.3% at 1.8V, respectively, and by 11.5% and 5.9% at 1.1V.

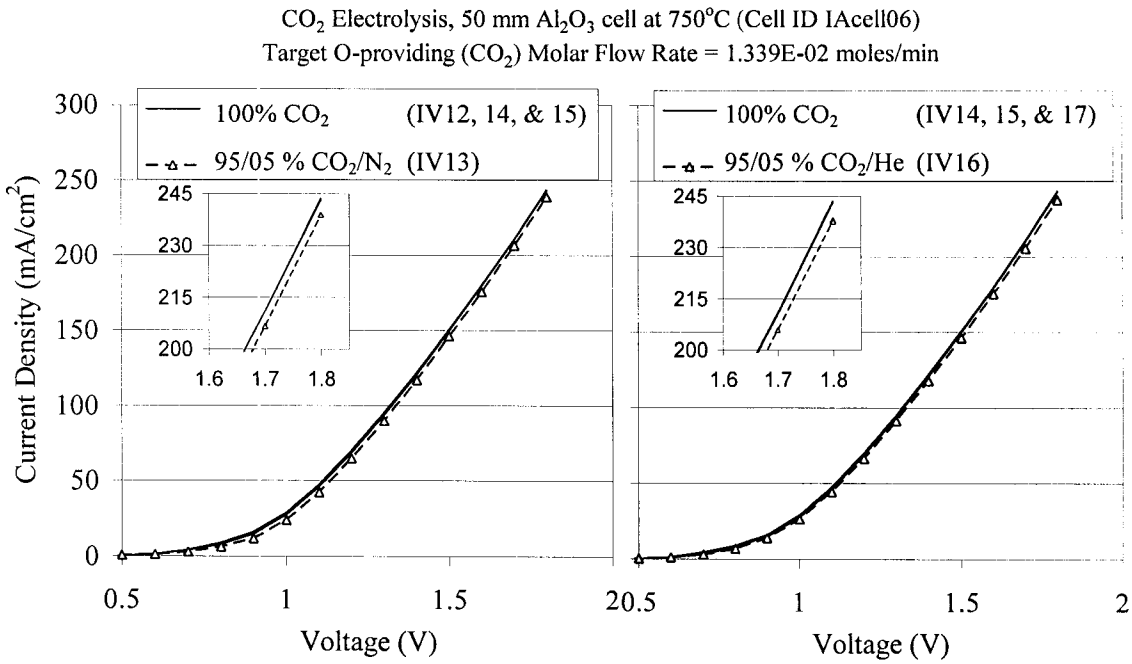

Figure 4-16 The effects of diluting CO_2 with (a) N_2 and (b) He for various voltages.

In summary, He in CO_2 electrolysis is acting as a diffusive barrier, not a coolant. These results suggest H_2O/He electrolysis would perform better if the He concentration was reduced (humidity increased). If this is true, the next question to ask in understanding combined electrolysis is could 100% H_2O perform as well as combined electrolysis?

4.5.3 Water Electrolysis Dependence on Humidity

As explained in the previous section, experiments are suggesting H_2O/He electrolysis would perform better if the humidity content were raised. Experiments were conducted by fixing He input flow rate while increasing absolute humidity from values of 20% to 90%. A voltage of either 1.8V or 1.3V was maintained and current was recorded. Results show that cell performance is directly proportional to humidity. An example is given in Figure 4-17.

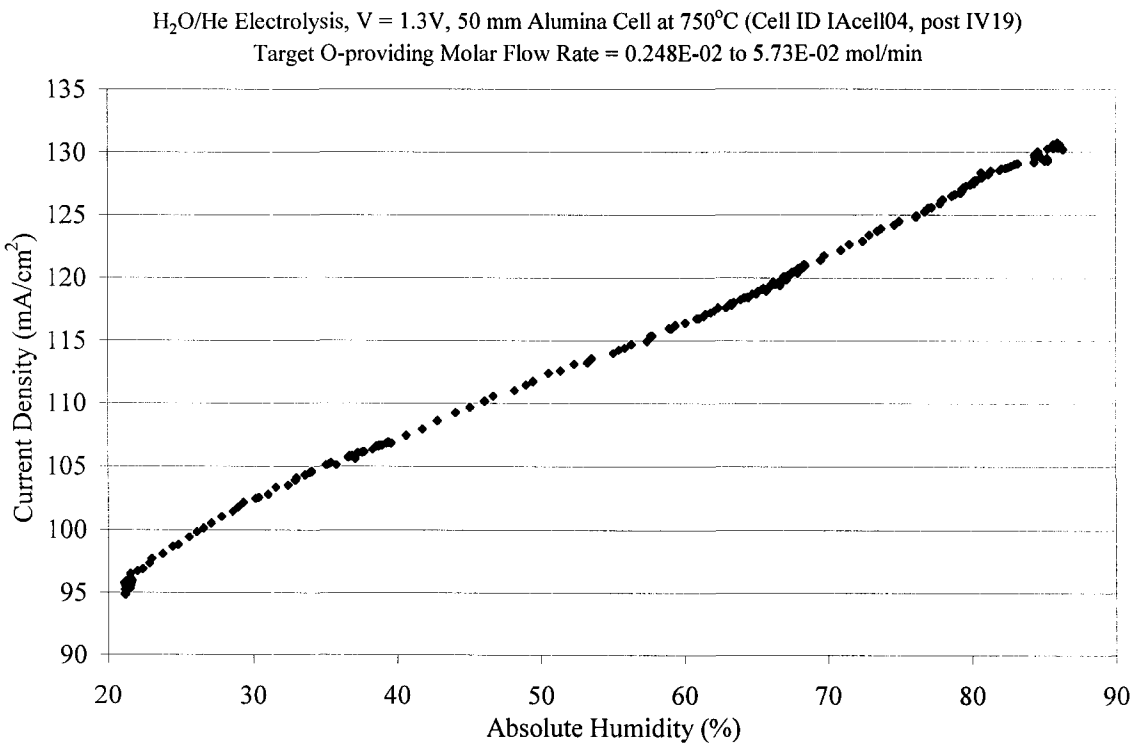

Figure 4-17 H_2O electrolysis performance vs. absolute humidity.

The question must be asked, is the increase in performance due to the decrease in the percentage of the mixture that acts as a He diffusion barrier? Or is it due to the increase in oxygen-providing molar flow rate by fixing the He flow rate and raising humidity? If the

cell is operating in its mass limiting range, the latter could be true. This is why the test shown in Figure 4-17 was operated at a reduced voltage of 1.3V. As shown in Figure 4-4, lower voltages consume less oxygen-providing molecules and the mass limiting range lowers. However, to be sure, another quick test followed.

Just after the test shown in Figure 4-17, while the humidity was still 85.7%, the He input flow rate was decreased to accomplish a 20% decrease in the oxygen-providing molar flow rate. The performance was observed to decrease by only 0.8%. Had the cell been in its mass limiting range, the decrease in performance would have been more substantial. Furthermore, according to data presented in Figure 4-17, invoking a 20% decrease in oxygen-providing molar flow rate through a humidity decrease from 85.7% to 68.6% causes over a 7% decrease in performance. Therefore, it is concluded that H_2O electrolysis is indeed dependent upon absolute humidity. Thus, comparing combined electrolysis to 50% (or less) humidified He is not a true comparison to the full performance capability of H_2O electrolysis.

4.5.4 Water Electrolysis Mass Limiting Flow Rate

H_2O electrolysis experiments conducted at oxygen-providing molar flow rates determined by CO_2 mass limiting experiments have trouble achieving stable performance. For example, at these flow rates 50% H_2O electrolysis exhibits degradation rates during automated performance tests (IV curves) between -0.1 to -0.3 mA/cm^2-min. Performance consequently declines over consecutive tests and in fact, as shown in Figure 4-18, begins to flatten out after 1.3 to 1.4 V. This flattening suggests a mass limiting

phenomenon. This could be from H_2O not being supplied to reaction sites quickly enough or adsorption of H_2 plugging reaction cites.

The first indication of non-deteriorating H_2O electrolysis performance was observed during the humidity-dependency test (described in the previous section) while increasing the humidity from 50% to 74% raising the oxygen-providing molar flow rate from 8.93E-03 a 2.69E-02 mol/min. To insure stability could be maintained and at higher voltages (the previous test was conducted at 1.3V), an abbreviated performance test was conducted at 4.32E-02 mol/min (83% humidity). Figure 4-18 shows a strong performance curve with no flattening of its slope.

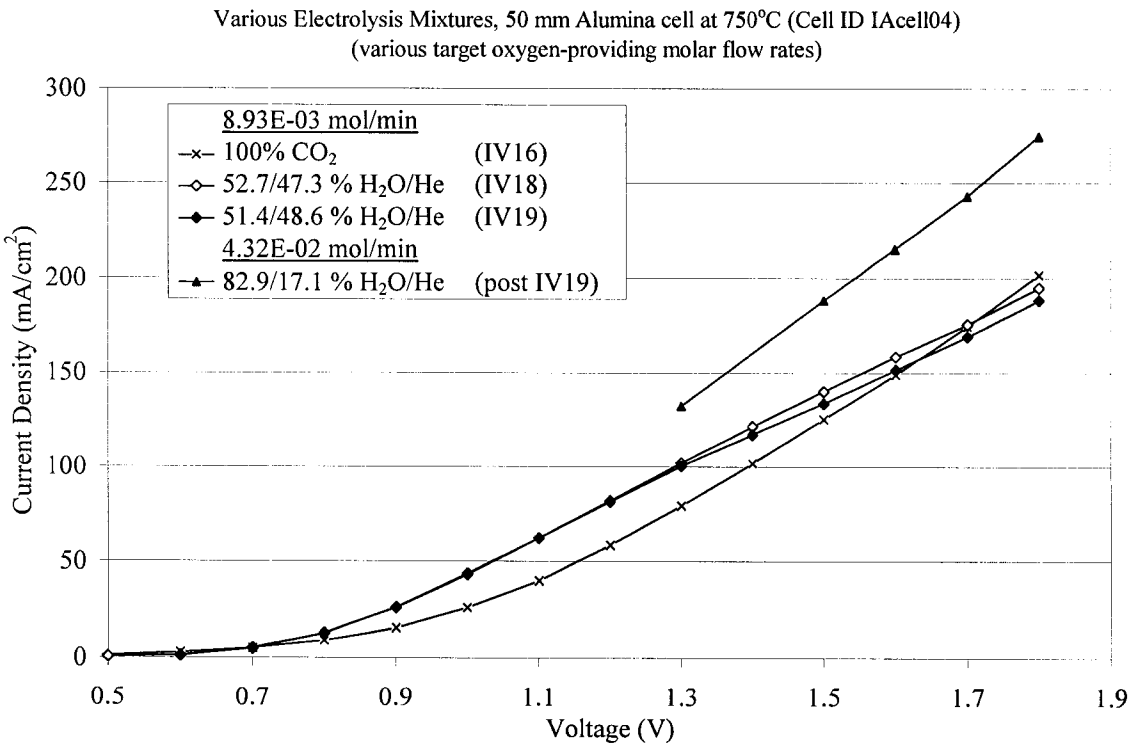

Figure 4-18 Alumina cells: H_2O electrolysis performance for different flow rates.

An increase in humidity (decrease in a He diffusion barrier), could be the cause for improved performance. However, Cr-alloy cells show no deterioration during H_2O electrolysis at 50% as well as 30% humidity. Thus it is more likely that to achieve stable H_2O electrolysis in alumina cells, oxygen-providing molar flow rates have to be increased above that needed for CO_2 electrolysis.

As suggested in section 4.5.3, H_2O electrolysis should be tested at the highest humidity possible to fairly compare to combined electrolysis. Thus, subsequent H_2O electrolysis tests were successfully run at He carrier gas flow rates of 200 sccm (0°C, 1 atm), and humidity above 88% which establishes an oxygen-providing molar flow rate above 6.0E-2 mol/min.

4.5.5 Water Electrolysis versus Carbon Dioxide Electrolysis

The high flow rate H_2O experiment presented in the previous section suggests that up to 85% (at 1.5V) performance improvement can be gained by 83% humidity H_2O electrolysis over CO_2 electrolysis (see Figure 4-18). Higher humidity was tested for a full performance curve to better quantify the relative performance. Details follow.

Two tests were performed with a new cell, one at the onset of testing and another after 20 days of intense testing of various mixtures. In both cases, CO_2 performance baselines were performed first. Figure 4-19 shows that both H_2O electrolysis tests outperform CO_2. Over the twenty days that passed between the tests, the CO_2 baseline declines between 40 to 19% over voltage 1 to 1.8V, respectively. Regardless, if each H_2O electrolysis run is normalized by its respective baseline, Figure 4-20 shows H_2O electrolysis outperforms CO_2 by a minimum of 17% for both cases (at 1.8V).

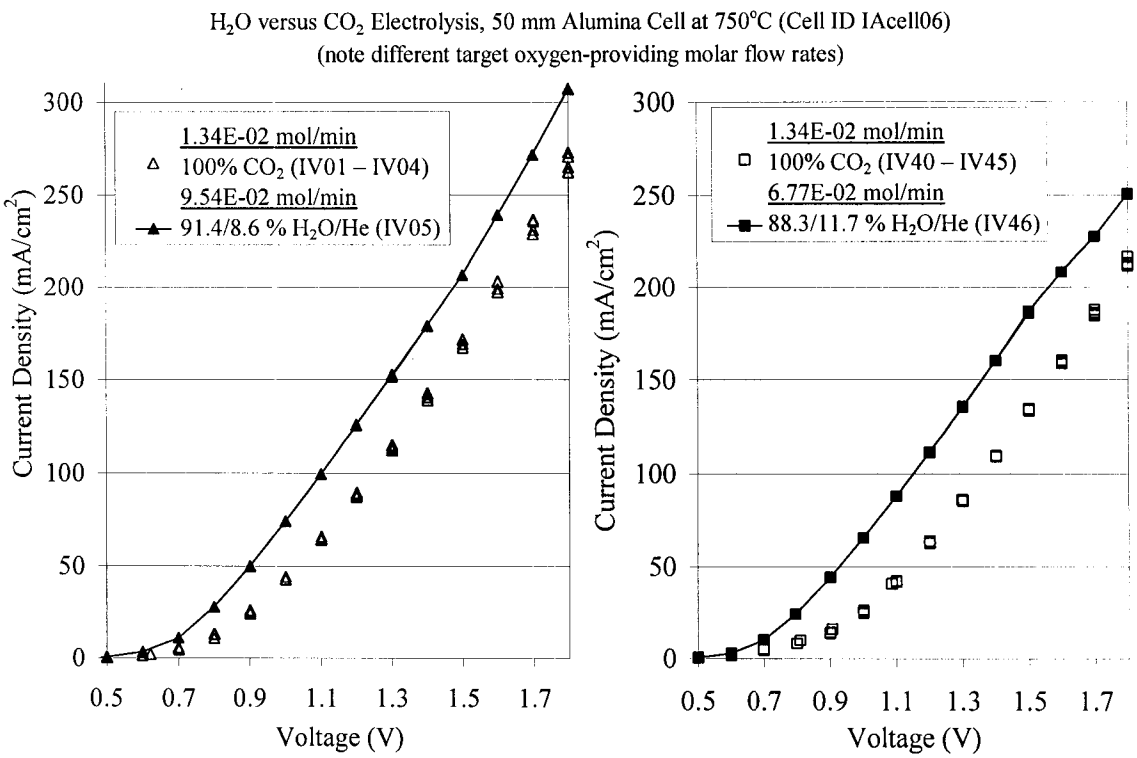

Figure 4-19 Alumina cells: H_2O electrolysis versus CO_2 electrolysis.

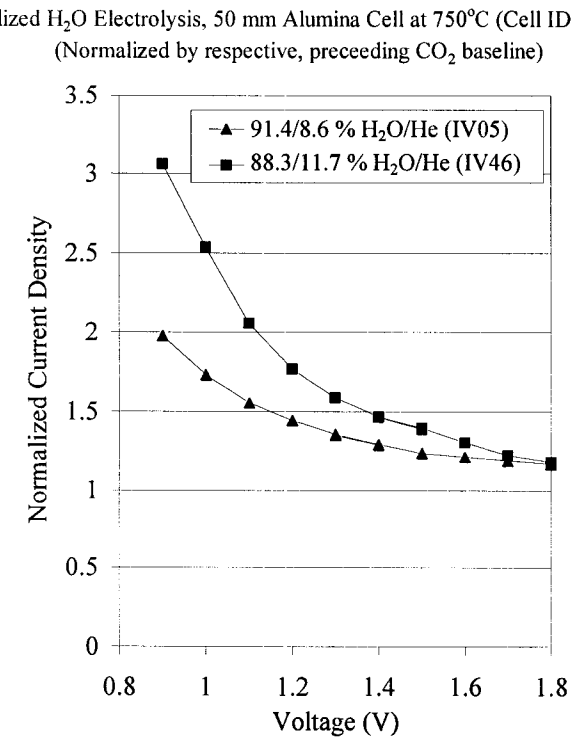

Figure 4-20 Normalized (as compared to CO_2 baselines) H_2O electrolysis versus voltage.

4.5.6 Effects of Humidified Mixtures on Cell Health

Initially, H_2O electrolysis appears to weaken the cell's capability to produce oxygen from CO_2. CO_2 electrolysis following a cell's initial H_2O electrolysis run underperforms the CO_2 electrolysis baseline, as exemplified in Figure 4-21. Recovery is observed during the next CO_2 test, though never fully. As with the Cr-alloy cells, this only appears after initial exposure to humidity because CO_2 tests following the subsequent H_2O electrolysis tests obtain full recovery. Thus, if alumina cells are to be used for pure H_2O electrolysis in addition to CO_2 electrolysis, they may require a single period of H_2O conditioning before a cell's ability can be accurately determined.

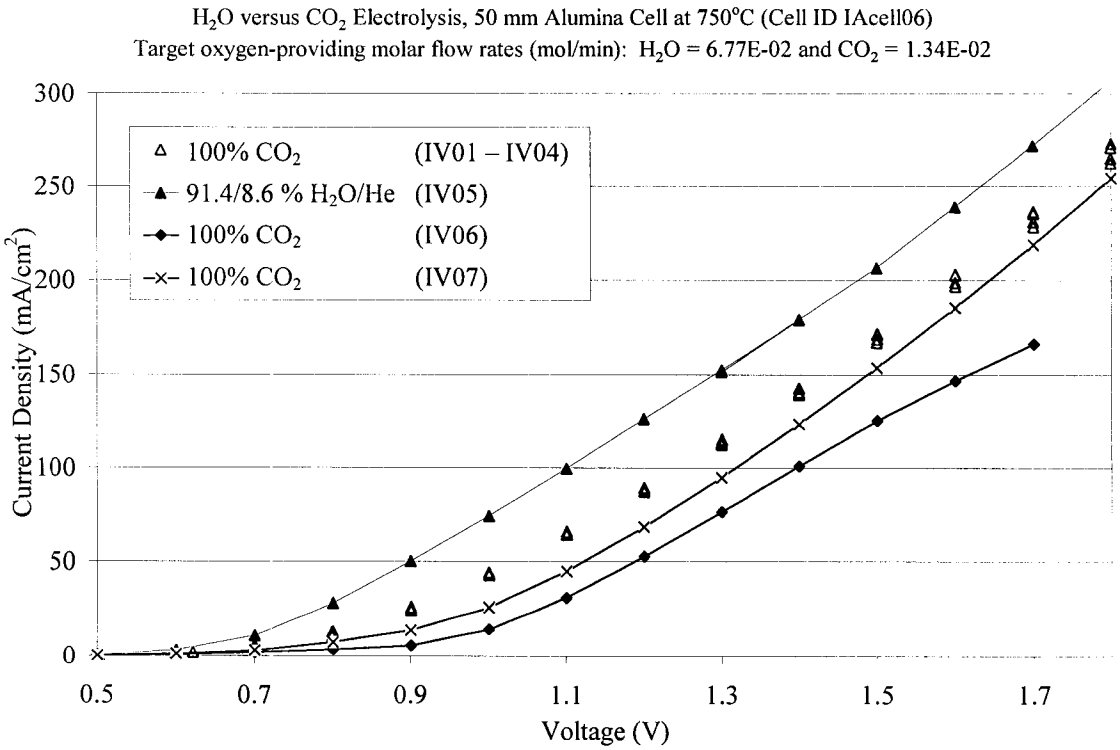

Figure 4-21 Initial H_2O electrolysis appears to deteriorate alumina cell performance.

Combined electrolysis definitely weakens the cell ability to immediately produce O_2 via CO_2 electrolysis. Several mixture ratios were tested and subsequent CO_2 electrolysis is shown to degrade by at least 20% in each case. As in H_2O electrolysis, CO_2 electrolysis recovery is usually observed to within 5% of the original performance. However, in one instance recovery is extremely slow. Details follow.

Figure 4-22 shows a progression of tests where CO_2 baselines were first established before testing combined electrolysis. All combined electrolysis tests were then followed by CO_2 electrolysis to assess the effect of combined electrolysis on the cell's health. Because the combined electrolysis input contains 100% oxygen-providing molecules of which some portion is CO_2, a flow rate equivalent to that needed for eluding the mass limiting range of CO_2 electrolysis was first used (1.34E-02 moles/min).

Figure 4-22 (a) shows that 10/90% H_2O/CO_2 barely outperforms CO_2 with a slope different than that of CO_2 electrolysis. Follow-up CO_2 electrolysis shows at least a 21% decrease (at 1.8V) from the previous baseline. Air electrolysis was used to achieve recovery to within 5% (at 1.8V) of the previous baseline.

Figure 4-22 (b) shows that a higher humidity of 31/69% H_2O/CO_2 faired worse with performance quickly dipping below CO_2 at 1.5V. In fear of destroying the cell the performance test was halted. Follow-up CO_2 electrolysis demonstrated at least a 25% (at 1.8V) decrease in CO_2 electrolysis. Fortunately, recovery was established to within 4% (at 1.8V) by simply using CO_2 electrolysis.

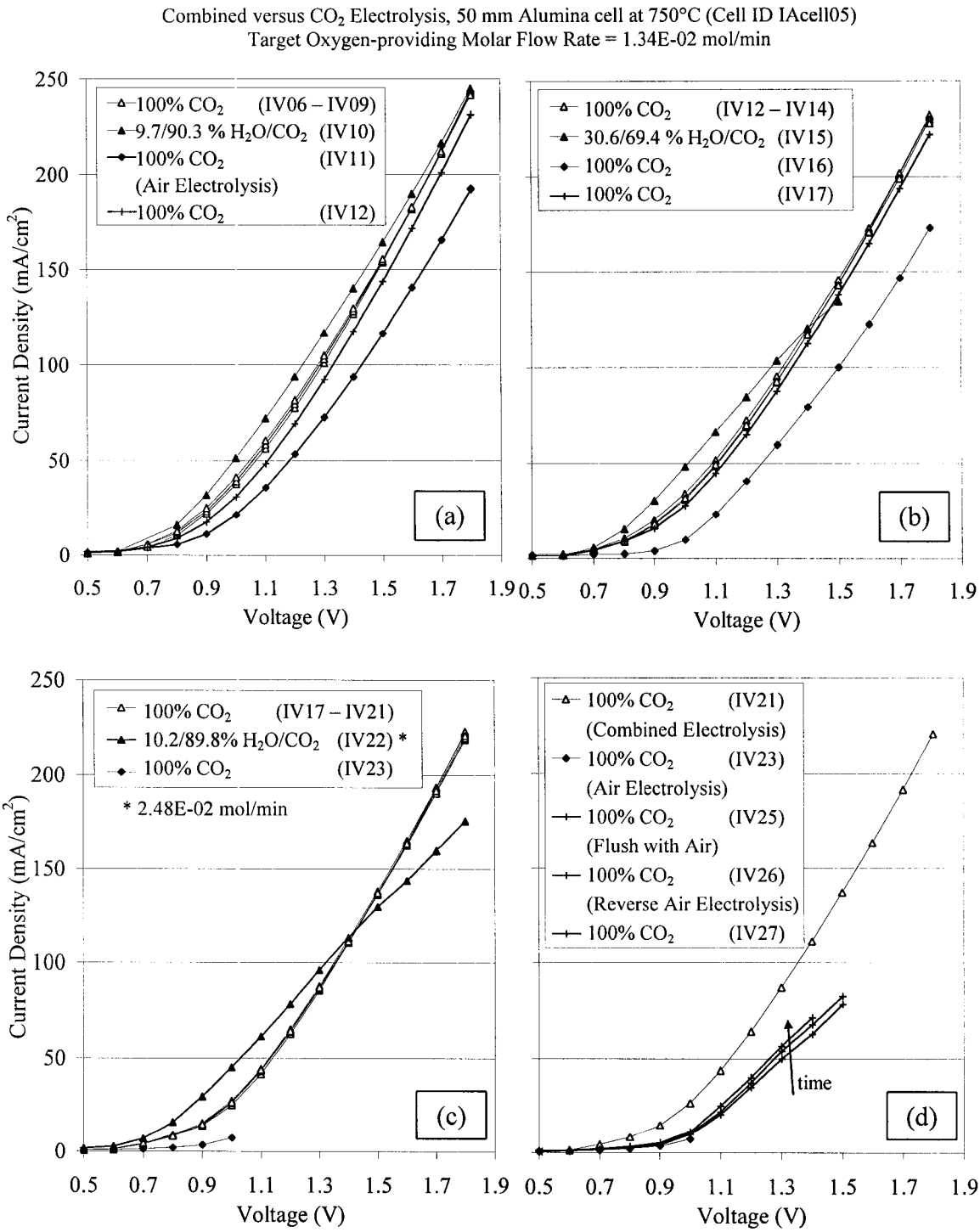

Figure 4-22 (a) – (d) Initial combined electrolysis for alumina cells.

The change in slope of the last combined electrolysis test (IV15 of Figure 4-22 (b)) suggests a mass limiting problem. Thus the flow rate was almost doubled for the next combined electrolysis test and a mixture of 10/90% H_2O/CO_2 was tested again. Comparing Figure 4-22 (b) to Figure 4-22 (c), the performance of 10/90% H_2O/CO_2 degraded by up to 28% (at 1.8V). Either the cell is experiencing a conditioning for combined electrolysis or higher flow rates actually hurt combined electrolysis performance.

Follow-up CO_2 electrolysis had an extremely difficult time recovering. Usually the recovery process occurs during the follow-up CO_2 electrolysis test, which can take over several hours. However, over four days, several techniques of "rejuvenating" the cell were attempted and are listed in Figure 4-22 (d). Slight recovery is observed but not fully before a crack in the electrolyte developed.

Cooling down the cell and opening the furnace revealed the cell had shifted disturbing the cell alignment. This could be attributed to the recovery troubles. Postmortem inspection of the cell IVcell05 revealed seemingly intact and clean electrodes. No SEM analyses were performed.

4.5.7 Conditioning Required for Combined Electrolysis

As it may have been evident in the previous section, the first test of combined electrolysis performed in an alumina cell is not stable. In pursuing stable combined electrolysis, it was discovered that alumina cells require a significant period of operation before repeatable performance can be accomplished. Suspecting a mass limiting

problem, increased flow rates were tested but the performance still did not stabilize and in fact, displayed increased degradation rates. Details of these results follow.

Stable combined electrolysis was attempted by repeating tests of a given mixture ratio. Figure 4-23 shows that over seven tests were conducted during three days of testing at a mixture of 7/93% H_2O/CO_2. Repeatable combined electrolysis does not occur. After the fourth performance test (IV24), the flow rate was almost tripled. As shown before in Figure 4-22 (c), the increased flow rate causes the performance to decrease even more with an inflection point occurring at 1.3 – 1.4V.

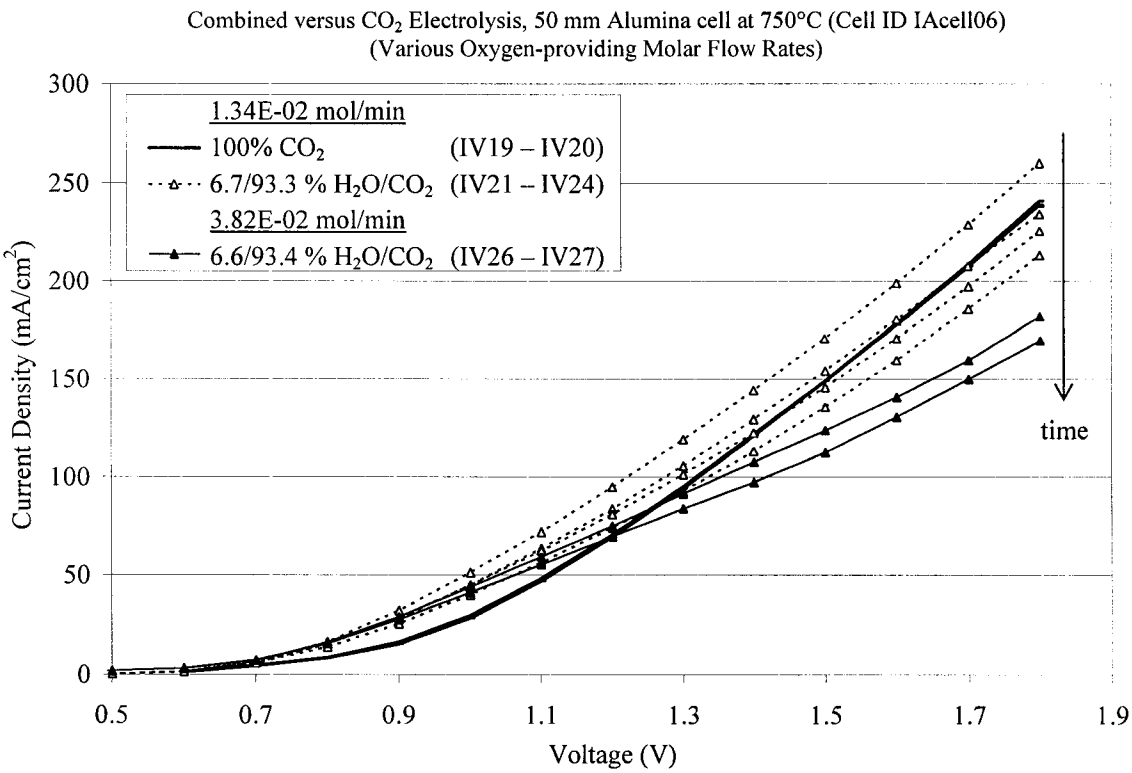

Figure 4-23 Combined electrolysis requires many days to stabilize.

Follow-up CO_2 electrolysis again was diminished, this time by at least 45% (at 1.8V). Interestingly, during CO_2 electrolysis, full recovery was achieved at 1.8V with performance exceeding the previous baseline at lower voltages (up to 19% at 1.0V). However, over the next ten days, as exemplified in Figure 4-3 of section 4.2, the CO_2 performance slowly settled at a new baseline underperforming the previous by up to 11% (at 1.8V).

4.5.8 Combined Electrolysis versus Carbon Dioxide Electrolysis

Repeatable combined electrolysis was finally established after several more runs were performed at a constant inlet mixture. Figure 4-24 shows two cases of different humidity. Figure 4-24 (a) shows that repeatable performance is established for 30/70% H_2O/CO_2 (σ_m = 0.2%). The combined electrolysis run outperforms CO_2 at low voltages by up to 19% (at 0.9V) but then under performs by up to 45% (at 1.7V). Unlike the trends exhibited by the H_2O or CO_2 electrolysis, an inflection point is observed in the combined electrolysis performance around 1.3V.

As the humidity in the mixture is increased, the alumina cell requires a few more runs to re-establish repeatable performance. As Figure 4-24 (b) shows, the inflection point disappears and the higher humidity mixture completely outperforms CO_2 from at least 5% (at 1.8V) up to as much as 123% (at 0.9V).

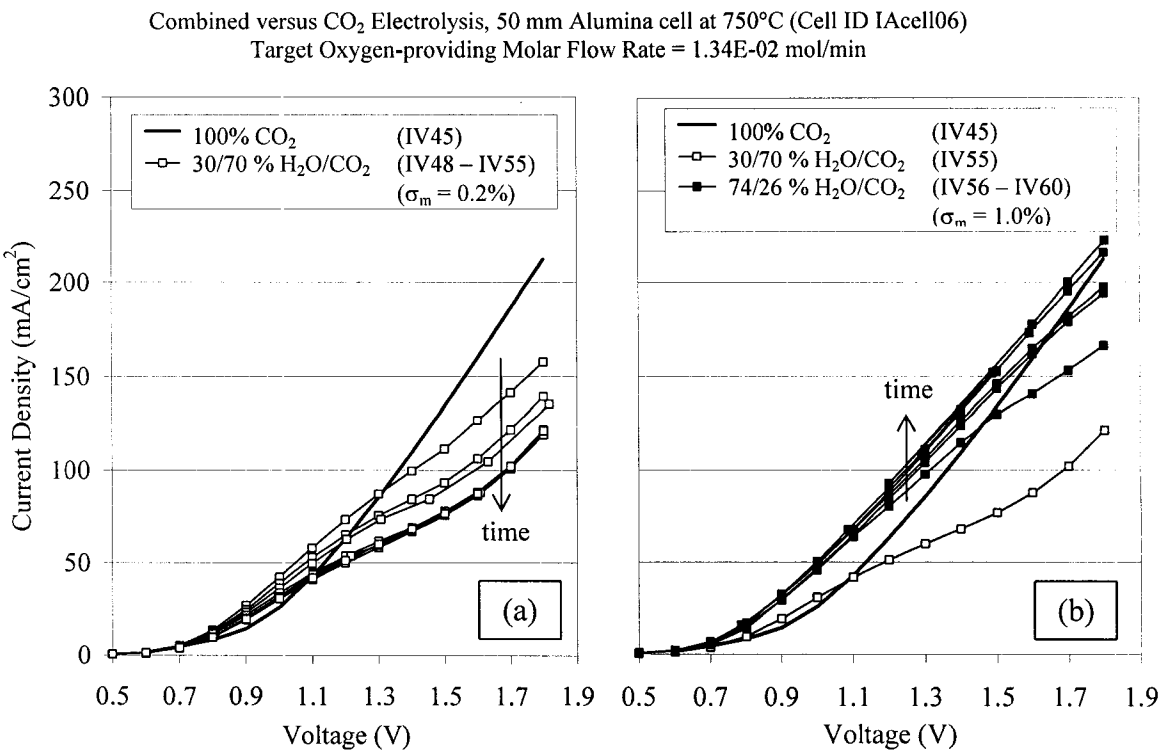

Figure 4-24 Alumina cell exhibits repeatable performance for combined electrolysis of (a) 30/70% and (b) 74/26% H_2O/CO_2.

4.5.9 Effects of Higher Flow Rates on Combined Electrolysis

As discussed in sections 4.5.6 and 4.5.7, the oxygen-providing molar flow rate was increased during two different testing sequences. Both times the increase in flow rate caused the performance to worsen. As was shown later, combined electrolysis requires a period of conditioning. What if the increased molar flow rate was accelerating this conditioning much like increasing temperature and voltage does for CO_2 electrolysis conditioning? An idea pursued was to increase the flow rate once stable combined electrolysis was achieved for a given input gas mixture ratio. If a performance increase is observed, the cell is operating in a mass limiting range. If an immediate decrease in performance is observed, the higher flow rate could be cooling cell. If a gradual decrease

in performance is observed, then somehow higher flow rates disturb the steady state operation of the cell. As it turns out, a gradual decrease in performance was observed when the oxygen-providing molar flow rate was increased. Details of the investigation follow.

Combined electrolysis was established for an input mixture of 74/26% H_2O/CO_2. Then the flow rate was increased by almost three and a half times to 4.64E-02 mol/min. Initially, Figure 4-25 (a) shows the performance appears stable and improves but subsequent performance curves decline. Repeatable performance at the higher flow rate was not pursued. CO_2 electrolysis immediately-following combined electrolysis performs a devastating 73% below the previous baseline (at 1.8V). However, a remarkable recovery is made by the very next test with performance surpassing the baseline by at least 16% (at 1.8V). The cell stabilizes over the next 10 days of CO_2 electrolysis when eventually the performance becomes repeatable. The performance of the new baseline is only 11% (at 1.2 V) to 5% (at 1.8V) less than the previous baseline.

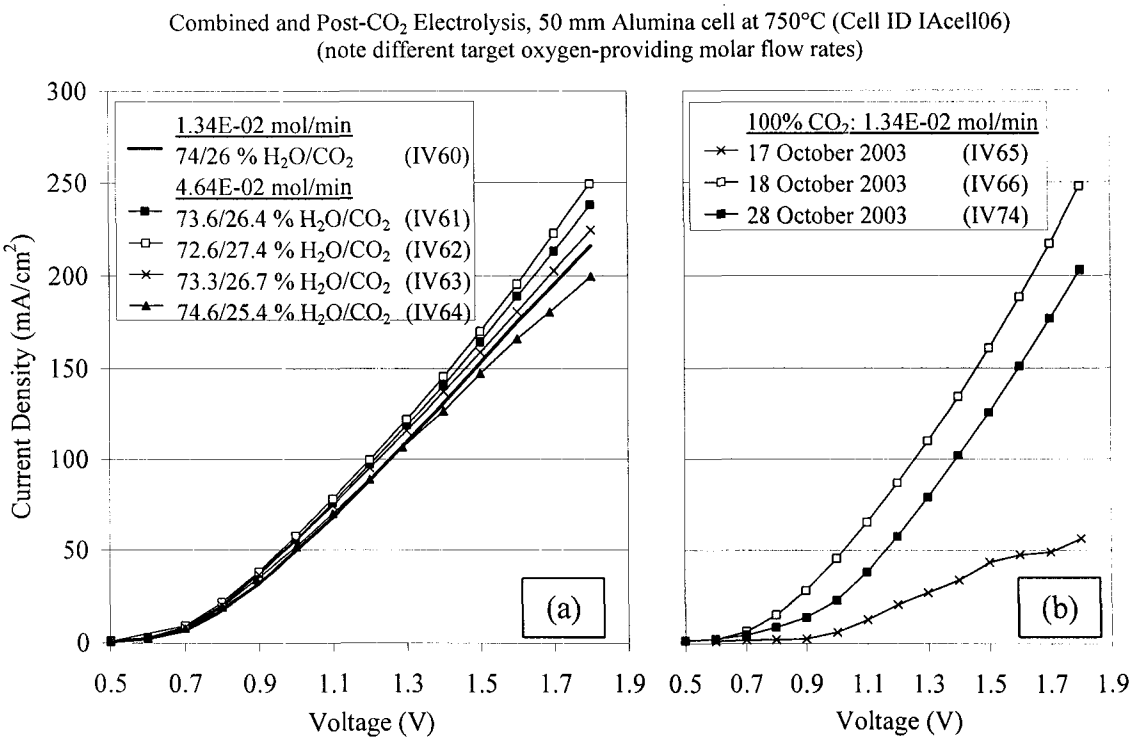

Figure 4-25 (a) Combined electrolysis at higher flow rates and (b) post CO_2 electrolysis performance.

4.5.10 Combined Electrolysis Preference to Water or Carbon Dioxide

With such different combined electrolysis performance exhibited between the alumina and Cr-alloy cells, more GC analyses were conducted on the exhaust of several combined electrolysis tests. The results are very different than that presented for Cr-alloy cells in section 4.4.6. Details follow.

The exhaust of an alumina cell is carried via a tube made out of alumina. As described in section 3.3.4, when testing combined electrolysis the exhaust is then fed through a condenser where left over H_2O is removed. For several tests, GC analyses were then conducted on the remaining exhaust. All constituents detected summed on

average to 99.7% (σ_m = 0.18%, 25 samples) indicating no unknown compounds, such as hydrocarbons, survive the cell exit. Not once was CH_4 detected.

Unlike Cr-alloy cells, GC results indicate that there is a significant preference to H_2O electrolysis over CO_2. The GC detected greater levels of H_2 than CO, as indicated in Figure 4-26. There appears to be no dependence regarding inlet pressure or inlet flow rate. However, the amount of H_2 produced is directly proportional to the absolute humidity as well as the oxygen production, as shown in Figure 4-27.

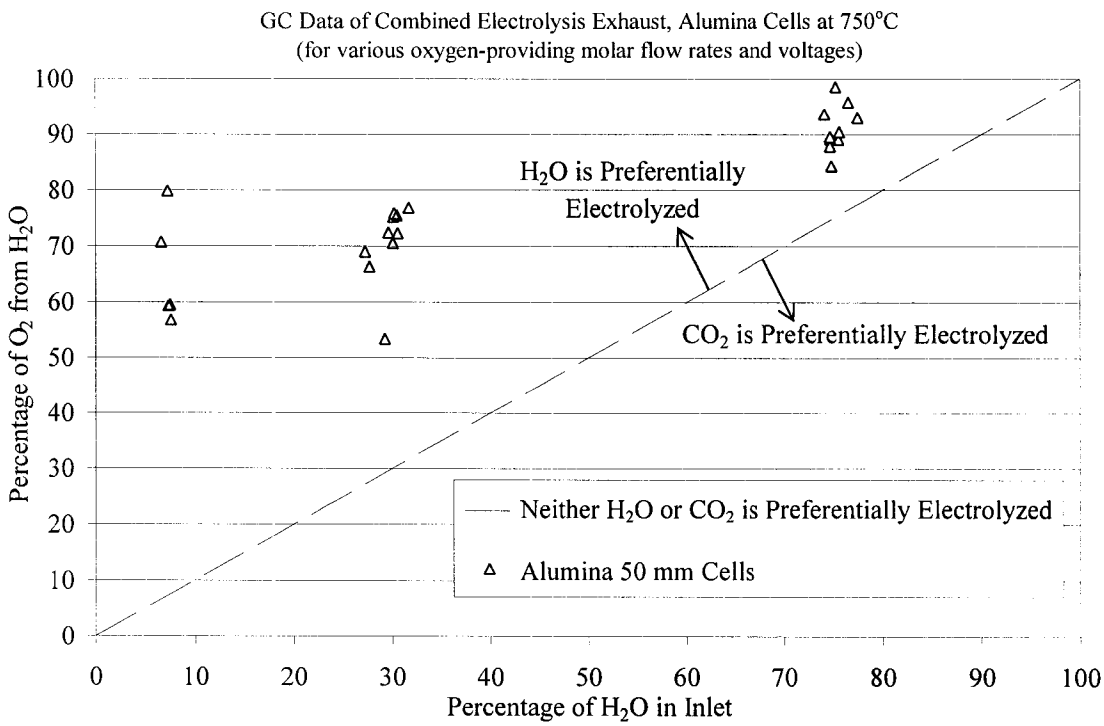

Figure 4-26 Alumina cell GC results suggest significant H_2O to CO_2 preference.

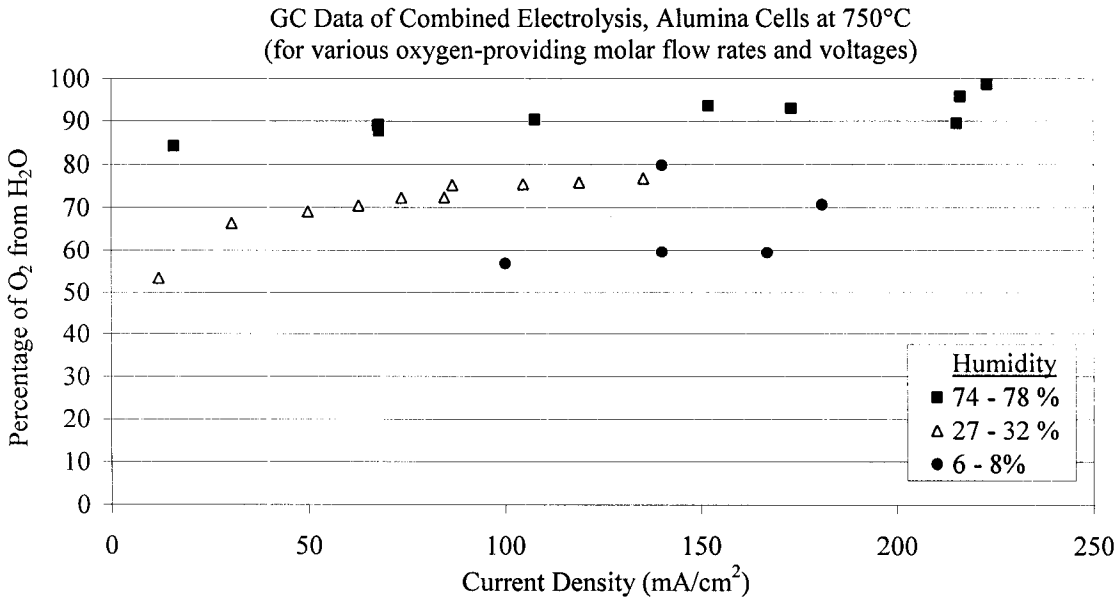

Figure 4-27 H_2O electrolysis is directly proportional to humidity and current density.

4.6 Termination of Experiments

Not one cell was terminated due to a failure in performance. Only one alumina cell seemed to significantly suffer from exposure to combined electrolysis requiring an unusually long time to recover, as described in section 4.5.6. However, it had to be terminated due to a bad seal developing after a shift in the test bed had occurred. The shift could have also affected the electrical contact inside the cell which could significantly diminish performance. Consequently, it is difficult to make any conclusions regarding cell health with that cell.

50% of the terminations occurred when leaks developed across the electrolyte, termed "cross leaks". Cross leaks contaminate the inlet with oxygen, falsely boosting performance and altering the exhaust composition. Cross leaks also allow for cell exhaust to escape to the anode corrupting the oxygen production reading. Evidence

shows a majority of the cross leaks was from pressure spikes caused by the humidifier system. Over time the humidifier system was improved (see section 3.3.2) and thicker electrolytes were employed. Increasing the strength of the electrolytes by increasing the thickness from 0.269 to 0.315 mm (0.0106 to 0.0124 inches) made the cell more resilient against pressure spikes caused by condensation in the lines. A brief account of the reasons for each cell's termination is summarized in Table 4-4.

Table 4-4 Reason for terminating testing of each SOE cell.

Cell ID	**Reason for Termination**	**Time at Temp (~ days)**	**Time[1] of Operation (~ hr)**	**# of IV Tests**	**# of H_2O & H_2O/CO_2 Runs**
50cell05	leak developed in cell's seal	1	10	1	0
50cell06	anode tube fell off	26	195	13	4
50cell07	cross leak occurred during water addition to humidifier	10	225	10	7
50cell09	cross leak during humidified runs; no specific event cited as cause	71	470	21	9
50cell11	furnace failure	35	440	16	5
IAcell01	cross leak[2] from humidifier pressure spike	6	55	6	1
IAcell04	cross leak[3]; no specific event cited as cause	18	390	22	7
IAcell05	jarred seal due to shift in test bed[4]	19	290	28	3
IAcell06	(5)	73	750	80	29

(1) Not necessarily continuous.

(2) Last 0.00106" thick electrolyte. All previous cells were also 0.00106". The last three used at least 0.00124" thick electrolytes.

(3) Endured several humidity spikes before eventual small cross leak occurred.

(4) Never fully recovered from last combined electrolysis runs.

(5) As of November 3rd, 2003. Three months later the cell was still performing CO_2 electrolysis at same level as IV68 (see Figure 4-3). To date, still in test bed at operating temperature.

4.7 Postmortem Inspections

Earlier testing of Cr-alloy cells with different seal materials [37] contained elements that caused electrode deterioration. The electrodes would turn from silver to brown and become powdery being easily scraped off the electrolyte. Postmortem inspection of the electrodes used in the results presented here only sometimes exhibits a slight discoloration. However, one of the two electrodes separated on every Cr-alloy cell except 50cell05, which only operated for a half a day. Unfortunately, careful note of whether this separation occurred on the anode or cathode was not taken. Notes suggest that separation occurred twice on the anode and twice on the cathode.

Because of the load on the cells, it is believed any separation had no ill effects on performance. Visual inspection suggests the separation occurred between the pure Pt layer and the Pt/YSZ layer. SEM analyses, which are summarized below, also support this observation. The Pt layer peals off the electrolyte like foil. An example of both electrodes from a single cell is shown in Figure 4-28 (a).

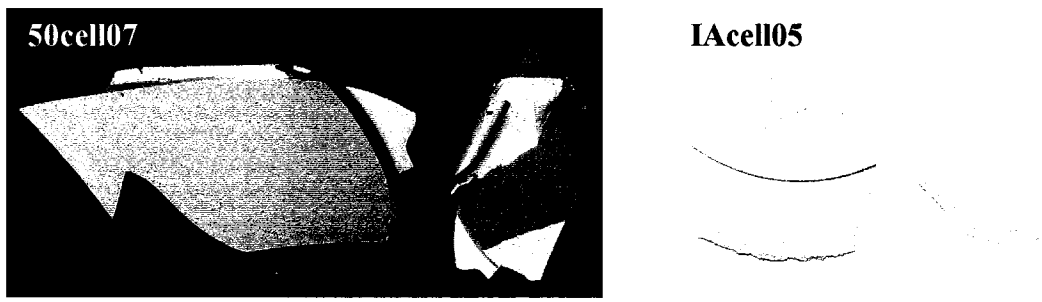

(a) Cr-alloy electrodes (b) Alumina anode and cathode

Figure 4-28 Postmortem inspection of electrodes.

The alumina cells, on the other hand, survived beautifully, as shown in Figure 4-28 (b). Visually it is difficult to tell the difference between a new printed electrolyte (called

a PEN for Positive electrode/Electrolyte/Negative electrode) and a used alumina PEN. However, SEM analyses reveal differences.

Imaging of the electrode structures were taken with a field-emission scanning electron microscope (Hitachi S-4500/Thermo-Noran Digital Imaging/EDS). To aid in comparison, the cells were compared to a new, unused PEN. SEM images were taken of an unused PEN, a Cr-alloy PEN (50cell09), and an alumina PEN (IAcell04). All PENs were originally created with the same approach which is summarized in Appendix C. No coatings or epoxies were used in preparing the samples for imaging.

Figure 4-29 shows cross sections of the entire electrode assembly on top of the electrolyte. Figure 4-29 (a) is the new unused PEN for comparison. Three distinct layers can be seen: top) the pure platinum layer; middle) the 50/50 % by wt. Pt/YSZ layer, and bottom) the electrolyte. All three layers are recognizable in the Cr-alloy and alumina cross sections shown in Figure 4-29 (b) through (e). As alluded to above, Figure 4-29 (c) shows that the platinum layer of one of the Cr-alloy electrodes separates from the Pt/YSZ layer. All layers of the other electrodes remain intact.

The other prominent difference amongst the images is of the alumina anode's pure Pt layer shown in Figure 4-29 (d). Closer inspection of the Pt layers is presented in Figure 4-30. All the other Pt layers look similar to the new PEN in Figure 4-30 (a), but the alumina anode Pt layer in Figure 4-30 (d) looks like it has sintered at a higher temperature. Close inspection of the mixed layer of the electrodes suggest that alumina cells could be achieving higher temperatures at the cathode as well. Figure 4-31 shows

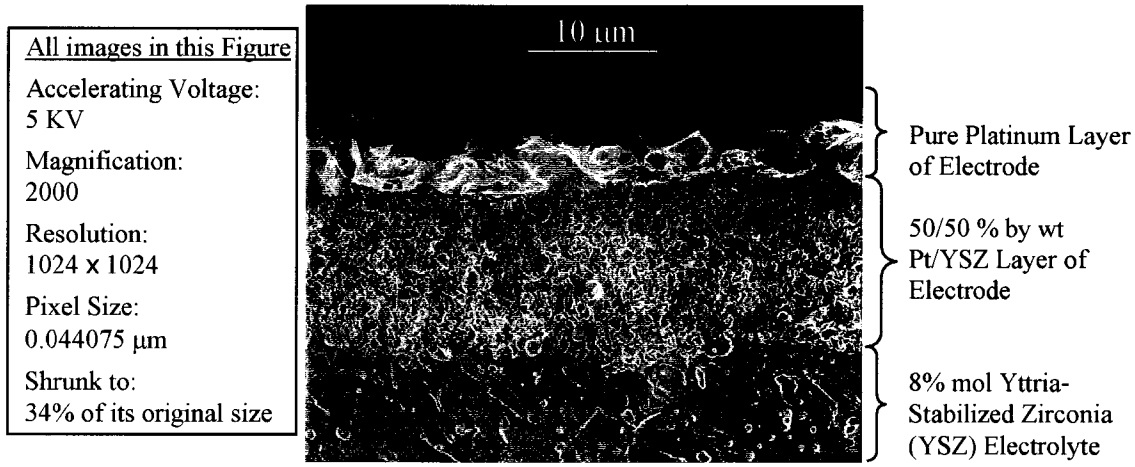

(a) Unused PEN

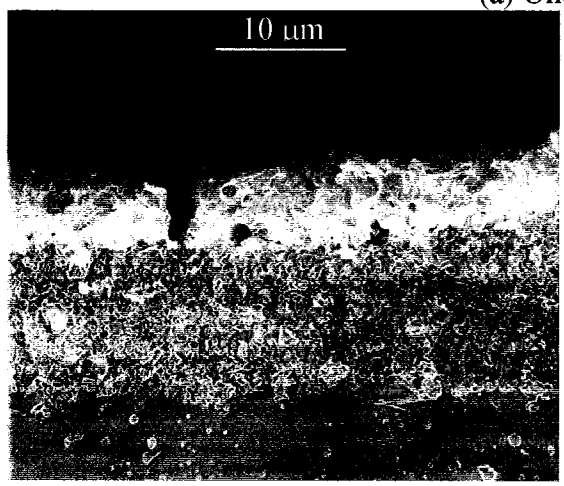

(b) Cr-alloy system electrode 1

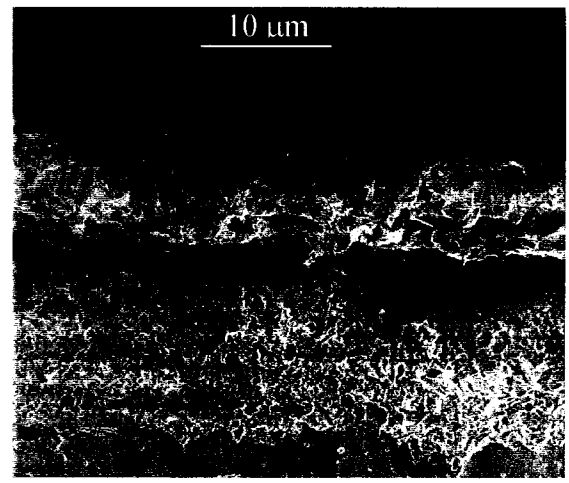

(c) Cr-alloy system electrode 2

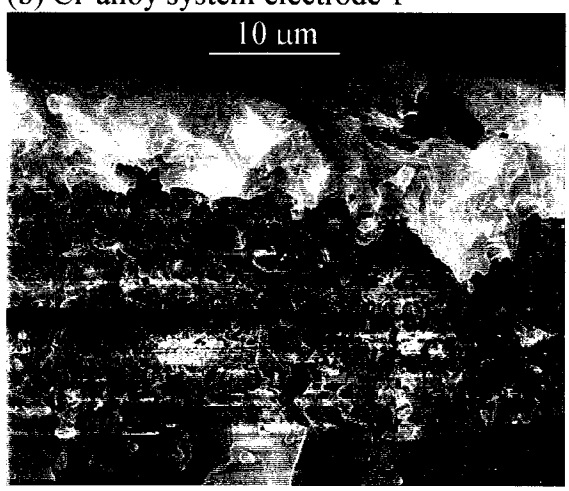

(d) Alumina system anode

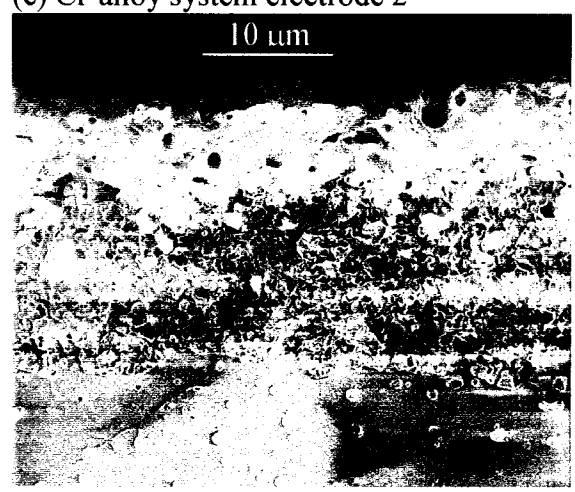

(e) Alumina system cathode

Figure 4-29 SEM Images: Cross sections of electrolyte and electrodes.

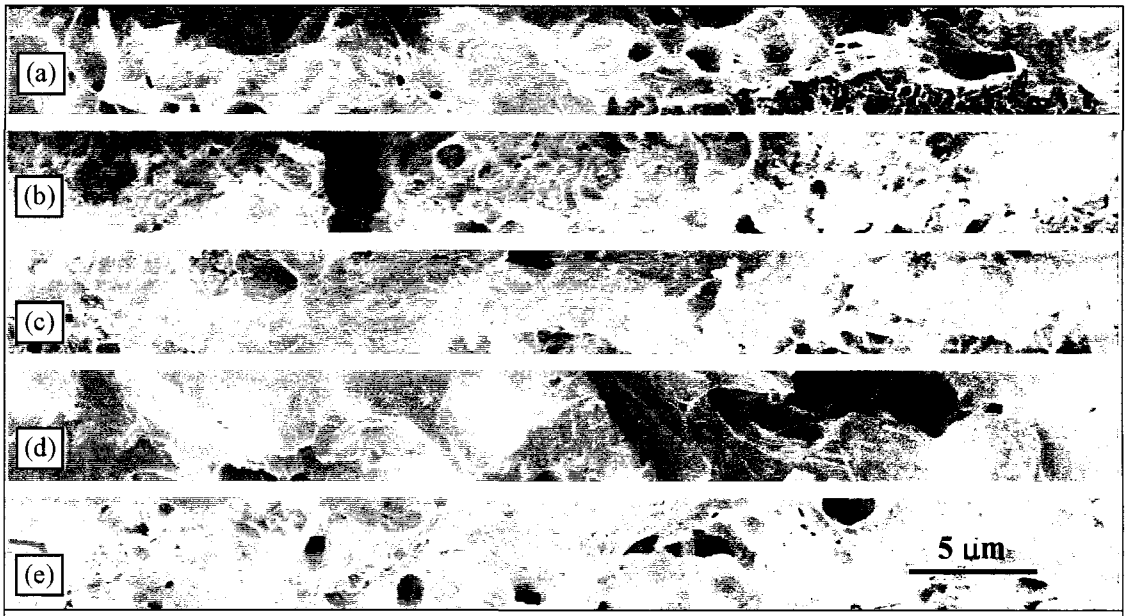

(a) Unused PEN, (b) Cr-alloy system electrode 1, (c) Cr-alloy system electrode 2, (d) alumina system anode, and (e) alumina system cathode

Figure 4-30 SEM Images: Cross sections of Pt layer of electrode.

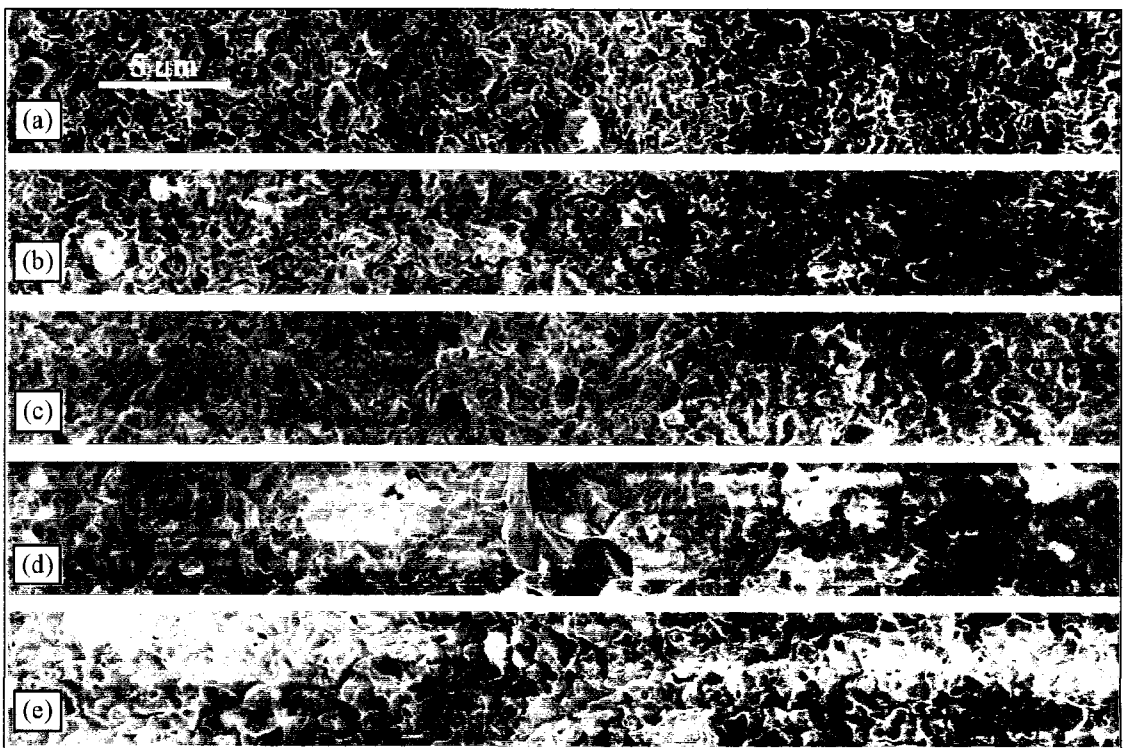

(a) Unused PEN, (b) Cr-alloy system electrode 1, (c) Cr-alloy system electrode 2, (d) alumina system anode, and (e) alumina system cathode

Figure 4-31 SEM Images: Cross sections of Pt/YSZ layer of electrode.

that as compared to the new electrode (a), both the alumina anode (d) and cathode (e) appear to have coagulated more. This is not entirely implausible.

First, at the anode, the recombination of oxygen atoms into diatomic oxygen is an exothermic reaction. The alumina cell, with a lower thermal conductivity manifold than that of the Cr-alloy manifolds, could be higher in temperature. On the cathode, localized current could be heating the cell. Post-mortem analysis of 50cell05 revealed that the electrode had melted and acted as "glue" between the manifold and electrolyte. Figure 4-32 shows that the adhesion was so great, the electrolyte chipped during disassembly and remained stuck to the manifold.

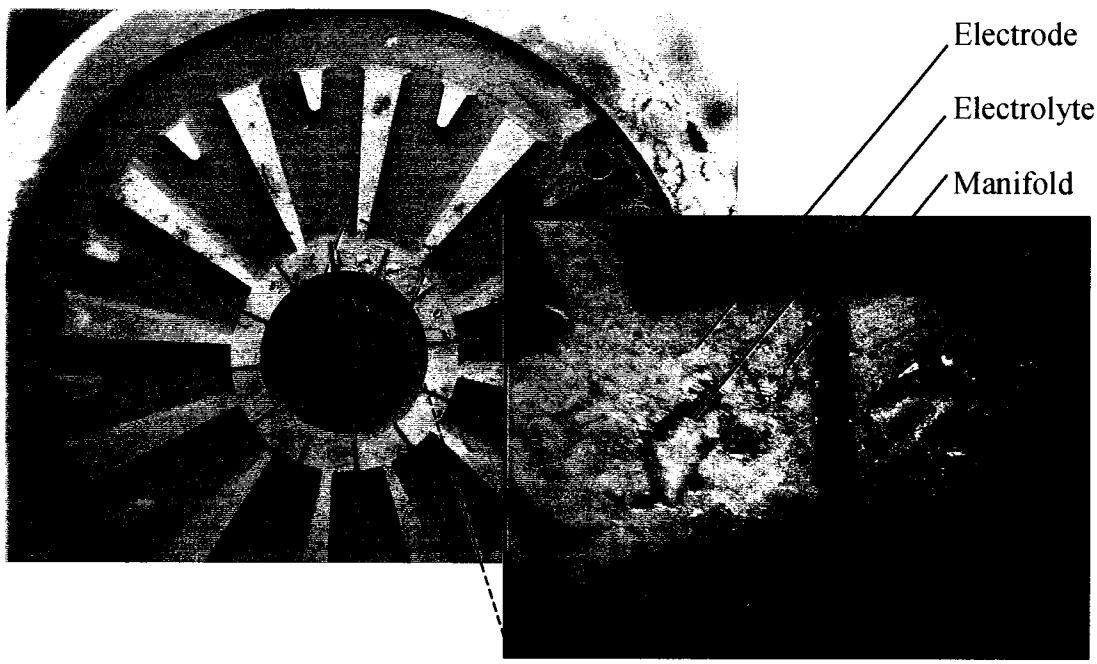

Figure 4-32 Electrolyte adhesion on a Cr-alloy manifold.

5 ANALYSIS AND DISCUSSION

Several observations are presented in chapter 4. This chapter is dedicated to explaining the observations via further data analyses and theoretical modeling. A road map is provided here to motivate the discussion and presentation of ideas.

As a sanity check, Section 5.1 compares the experimental results collected in this work to electrolysis results published in the literature. Section 5.2 summarizes for both cells the electrolysis performance of H_2O versus CO_2. The nature of electrolyzing H_2O versus CO_2 is also discussed providing a fundamental background helpful in subsequent discussions.

Section 5.3 summarizes the overall performance of combined electrolysis in regards to stability and oxygen-production capability. A direct comparison is also made between the two cell-types. An analysis of the shape of performance curves motivates the calculation of thermal neutral voltages in section 5.4. The results of section 5.4 are also correlated to observations presented in section 4.7 of the alumina cell's electrodes.

Sections 5.5 and 5.6 look at two different theories proposed to explain the difference in combined electrolysis performance between the two cell-types. The results are applied in section 5.7, where methodologies for calculating the products of combined electrolysis are presented.

To explore the reasons governing the phenomenon discovered in the previous sections, section 5.8 discusses the nature of catalyst. Finally, further lessons learned are then applied in section 5.9 to explain GC data collected during CO_2/H_2 electrolysis experiments.

5.1 Electrolysis Initiation Voltage

A direct comparison of the electrolysis results presented in chapter 4 can not be made to previous works, for the electrodes, carrier gas, anode flush gas and operation temperature are different. However, in comparing trends, a striking difference between previously published data and the data presented here is the V_{min} required to initiate electrolysis. Take for example Isenberg's data presented in Figure 1-5. For a given operating temperature, V_{min} are a function of input gas composition while any of the electrolysis results presented here are not. For Isenberg's experiments, the carrier gas was chosen to match the exhausted product gas of electrolysis (H_2 for H_2O electrolysis and CO for CO_2 electrolysis); whereas, the experiments presented here either use a carrier gas completely uninvolved with the electrolysis reaction (not a reactant or product such as He or N_2) or one that is oxygen-providing itself (CO_2).

The difference in V_{min} trends can be readily explained by applying a first and second law thermodynamic analysis. Figure 5-1 is a schematic representing a control volume around an electrolysis cell. Each stream entering and leaving the cell must be taken into account. It should be noted that the molar ratio of the i^{th} gas entering the cell is represented with X_i and all streams exiting the cell are functions of these.

The gases entering the cell are:

1. The oxygen-providing gas to be electrolyzed (CO_2, H_2O or a combination of both).
2. The gas used to carry in the oxygen-providing molecules. This can be composed of two components: one that is "uninvolved" with the electrolysis reaction and another

that matches the product gas of electrolysis (i.e. CO in the case of CO_2 or H_2 in the case of H_2O).

3. The anode flush, which can also be broken into two components: an oxygen component and an inert component.

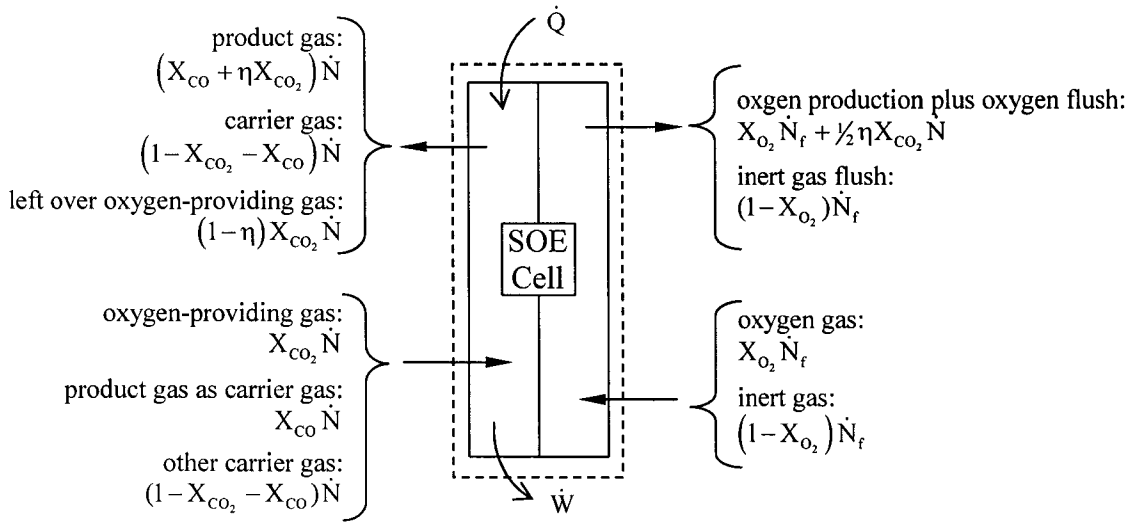

Figure 5-1 Thermodynamic system considered for an electrolysis cell.

The gases leaving the cell are:

1. The product gas. This includes that which is produced from electrolysis and that portion of the carrier gas used to carry in oxygen-providing molecules.
2. Any "uninvolved" carrier gas.
3. Leftover oxygen-providing gas not electrolyzed.
4. Oxygen, both from electrolysis and the anode flush.
5. Any inert gas flush.

To calculate the V_{min} required to initiate electrolysis, first assume that all streams are simple compressible substances since they are all gases at relatively low pressure (~1 atm). Second assume they enter and exit at the same operating temperature with a total

pressure of P_c and P_a at the cathode and anode, respectively. This assumption implies the gases arriving at the cell have had adequate time to be heated to operating temperature. In addition, it neglects any temperature changes due to heat exchange between the cell and gas molecules that can occur during the endothermic reactions of electrolysis or ohmic heating. However, since we are interested in the V_{min} required to initiate electrolysis, we will assume these losses do not occur and the cell can be modeled as "reversible". Finally assume the system is in steady state since performance data (IV curves) are usually meant to be an indication of steady state operation.

Through these stated assumptions and the application of the first and second law of thermodynamics, the minimum amount of voltage required to electrolyze an oxygen-providing gas can be calculated.

As an example for CO_2 electrolysis, the expression can be written as (see Appendix A.1 for derivation):

$$V_{min} = \frac{\Delta G^{\circ}_{T,rxn}}{2\Im} + \frac{\Re T}{2\Im}\frac{1}{\eta}\left\{\left[\eta \ln X_{CO_2} - (1-\eta)\ln(1-\eta)\right] + \left[\frac{X_{CO}}{X_{CO_2}}\ln X_{CO} - \left(\frac{X_{CO}}{X_{CO_2}} + \eta\right)\ln\left(X_{CO} + \eta X_{CO_2}\right)\right] + \left[-\frac{\eta}{2}\ln P_a + \frac{X_{O_2}}{X_{CO_2}}\frac{\dot{N}_f}{\dot{N}_{inlet}}\ln X_{O_2} - \left(\frac{X_{O_2}}{X_{CO_2}}\frac{\dot{N}_f}{\dot{N}_{inlet}} + \frac{\eta}{2}\right)\ln\left(\frac{\dot{N}_f/\dot{N}_{inlet} X_{O_2} + \eta/2 X_{CO_2}}{\dot{N}_f/\dot{N}_{inlet} + \eta/2 X_{CO_2}}\right)\right] + \frac{\dot{N}_f}{\dot{N}_{inlet}}\frac{(1-X_{O_2})}{X_{CO_2}}\left[\ln\left(\frac{\dot{N}_f/\dot{N}_{inlet} + \eta/2 X_{CO_2}}{\dot{N}_f/\dot{N}_{inlet}}\right)\right]\right\} \quad (5.1)$$

It can be shown that the expression can be used for H_2O electrolysis if the subscript CO_2 is replaced with H_2O and CO is replaced with H_2. The first term of equation (5.1) is

the difference between the standard Gibbs energies of formation of the oxygen-providing gas and its products after electrolysis at the operating temperature, T [19]. As an example, for CO_2 electrolysis:

$$\Delta G^{\circ}_{T,rxn} = \left(\Delta \bar{h}^{\circ}_{f} + \bar{h}_{T} - \bar{h}_{STP} - T\bar{s}^{\circ}_{T}\right)_{CO_2} - \left(\Delta \bar{h}^{\circ}_{f} + \bar{h}_{T} - \bar{h}_{STP} - T\bar{s}^{\circ}_{T}\right)_{CO} - \frac{1}{2}\left(\Delta \bar{h}^{\circ}_{f} + \bar{h}_{T} - \bar{h}_{STP} - T\bar{s}^{\circ}_{T}\right)_{O_2} \quad (5.2)$$

The second and third terms of equation (5.1) are entropy terms of the oxygen-providing and product gases on the cathode side, respectively. The fourth term represents the entropy mixing of the oxygen produced. The fifth term represents the entropy mixing of the inert anode flush gas. It should be noted that even though the example is for CO_2, the presence of these entropy terms is indifferent to the type of oxygen-providing gas.

In Figure 5-2 calculations using equation (5.1) for H_2O are compared to V_{min} required to initiate H_2O/H_2 electrolysis as reported in the literature [19]-[23]. The literature does not state anode pressure and flush rates so calculations assume 1 atm and a flush rate that matches the total inlet flow rate at the cathode. It is seen that V_{min} to electrolyze a mixture of H_2O in H_2 at an operating temperature of 1000°C is a function of the amount of H_2O in the input stream. The fact that experimental data is actually lower than the theoretical "minimum" could be due to differing anode pressures. Lower pressures will cause lower theoretical V_{min}. The magnitude of the anode flush has little effect on results.

A CO_2/CO experiment was conducted to instill further confidence in the derivation and applied assumptions of equation (5.1). The experiments were operated at a temperature of 750°C using different anode flushes: air and oxygen. The inlet

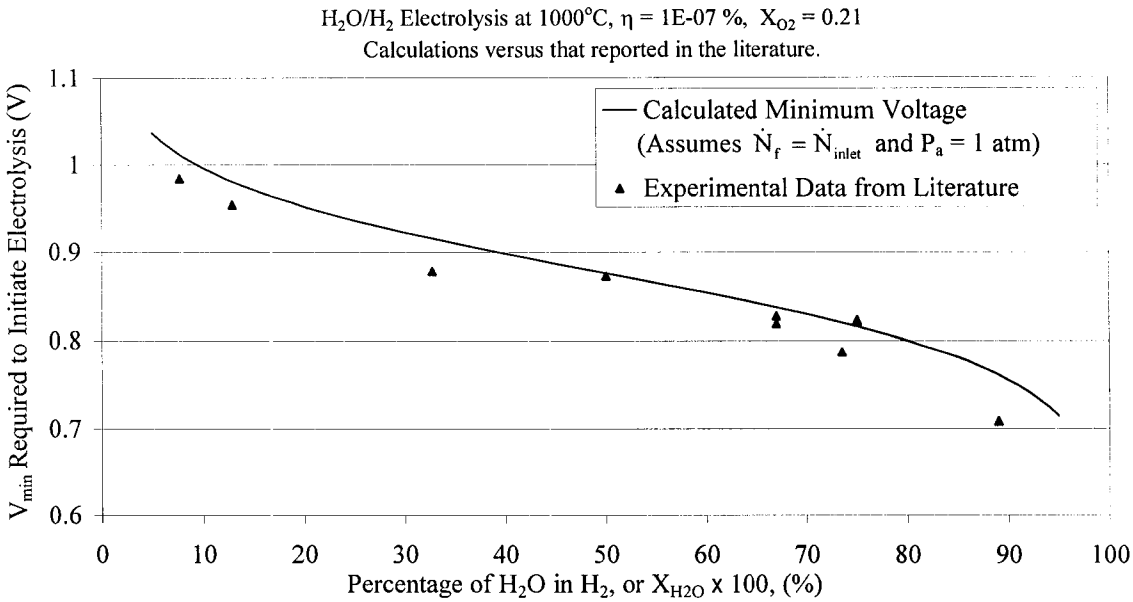

Figure 5-2 V_{min} for H_2O/H_2 electrolysis: Literature reported data versus calculations.

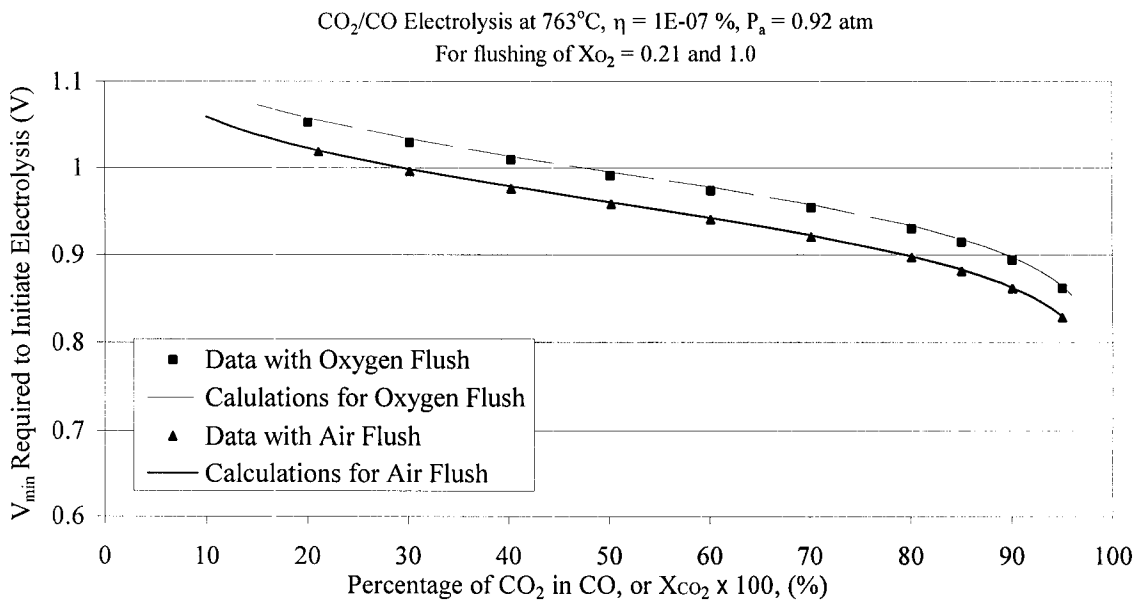

Figure 5-3 V_{min} for CO_2/CO Electrolysis: experimental results versus calculations.

composition was varied from about 20 to 95%. For each inlet composition, the current was set to zero and the voltage was allowed to achieve steady state. The resulting voltage is equivalent to the open circuit voltage because when the electrolysis circuit is broken, or "open", no current can flow. Any voltage above this value will initiate electrolysis and drive oxygen across the electrolyte, creating a current. Allowing current to vary, the voltage could then be nudged above this open circuit voltage and electrolysis would initiate. The open circuit voltage for both anode flushes matched theory very well, as shown in Figure 5-3.

However, these calculations do not explain why V_{min} of the experimental results presented in chapter 4 are not a function of H_2O or CO_2 concentration. Equation (5.1) is still valid, but the experiments are different from those presented in the literature. One should remember that the experiments presented here use a carrier gas that does not match the product gas of electrolysis (i.e. H_2 or CO), and is therefore "uninvolved" with the electrolysis reactions. This means the molar ratio of the portion of carrier gas that matches the product gas is zero. For the CO_2 electrolysis example this translates to $X_{CO} = 0$ and equation (5.1) reduces to:

$$V_{min} = \frac{\Delta G^{\circ}_{T,rxn}}{2\Im} + \frac{\Re T}{2\Im}\frac{1}{\eta}\left\{\left[-(1-\eta)\ln(1-\eta) - \eta\ln(\eta)\right] + \left[-\frac{\eta}{2}\ln P_a + \frac{X_{O_2}}{X_{CO_2}}\frac{\dot{N}_f}{\dot{N}_{inlet}}\ln X_{O_2} - \left(\frac{X_{O_2}}{X_{CO_2}}\frac{\dot{N}_f}{\dot{N}_{inlet}} + \frac{\eta}{2}\right)\ln\left(\frac{\dot{N}_f/\dot{N}_{inlet}\, X_{O_2} + \eta/2\, X_{CO_2}}{\dot{N}_f/\dot{N}_{inlet} + \eta/2\, X_{CO_2}}\right)\right] + \frac{\dot{N}_f}{\dot{N}_{inlet}}\frac{(1-X_{O_2})}{X_{CO_2}}\left[\ln\left(\frac{\dot{N}_f/\dot{N}_{inlet} + \eta/2\, X_{CO_2}}{\dot{N}_f/\dot{N}_{inlet}}\right)\right]\right\} \quad (5.3)$$

For the Cr-alloy cells, the anode was sealed and not flushed ($\dot{N}_f = 0$) so equation (5.3) reduces substantially:

$$V_{min} = \frac{\Delta G^{\circ}_{T,rxn}}{2\Im} + \frac{\Re T}{2\Im}\frac{1}{\eta}\left[-(1-\eta)\ln(1-\eta) - \eta\ln(\eta) - \frac{\eta}{2}\ln P_a\right] \qquad (5.4)$$

It should be noted that this is not a function of the percentage of input gas that is oxygen-providing, i.e. X_{CO_2}. Therefore, this explains why the data presented section 4.4 for the Cr-alloy cells initiate at the same voltage regardless of inlet composition. Also one should note that the take off point for electrolysis begins between 0.6 and 0.8 V (see Figure 4-2, Figure 4-3, Figure 4-5 through Figure 4-10, and Figure 4-12) which matches the prediction in Figure 5-4.

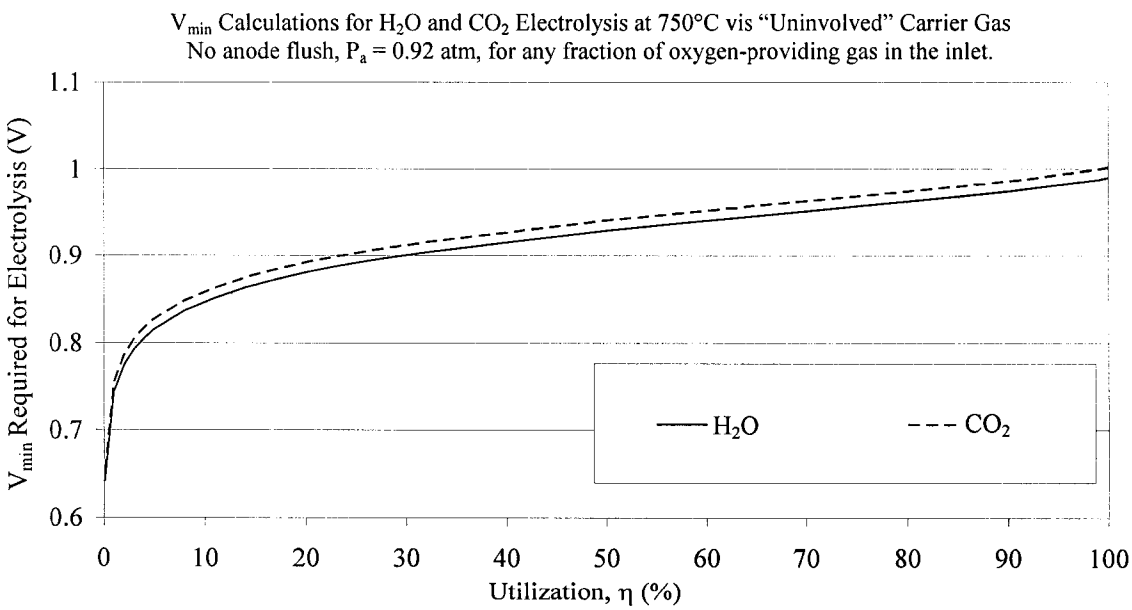

Figure 5-4 V_{min} calculations for Cr-alloy cell experiments as a function of utilization.

Alumina cells were tested similarly to the Cr-alloy cells in that the carrier gas was uninvolved with the electrolysis reaction. However, the anode was flushed with air. Had

the anode been flushed with oxygen (X_{O_2}=1), equation (5.3) would again reduce to equation (5.4). However, for any other concentration of oxygen in the anode flush ($X_{O_2} \neq 1$), the last three terms of equation (5.3) do not disappear. This leaves equation (5.3) as a function of the oxygen-providing molar concentration (i.e. X_{CO_2}). Why, then, would all the V_{min} required to initiate electrolysis as presented in section 4.5 appear not to be a function of inlet H_2O and/or CO_2?

The last three terms of equation (5.3) act to reduce the required voltage. For the conditions tested (X_{O_2} = 0.21), the reduction to the overall voltage by the last three terms is at maximum 5% (< 0.03V) of the total voltage. This contribution only varies with inlet concentration for large utilization. For example, at η = 99.9%, this variation is about 0.034 to 0.023 V from 0.1 to 99.9% inlet CO_2 molar concentration (X_{CO_2}). Therefore, the impact of the last three terms for the alumina cell testing performed here is insignificant. What is significant is the fact that the carrier gas does not contain any product gas.

Thus to optimize V_{min}, the input gas should be either 100% oxygen-providing or oxygen-providing gas carried into the cell by a gas completely uninvolved in the overall electrolysis reaction. These conclusions are important when evaluating H_2O electrolysis as a means for H_2 production because it is stating that it takes less energy to electrolyze H_2O via an uninvolved carrier gas. But it also has implications for a propellant/life support production plant on Mars. When H_2 is recycled back through the electrolysis

unit, it will act as a carrier gas that is involved with the electrolysis reactions and thus increase the cost of oxygen production.

5.2 Water Electrolysis versus Carbon Dioxide Electrolysis

H_2O electrolysis at a minimum performs on the order of 20% better than CO_2 electrolysis for either cell-type. This is at voltages around 1.8V. The percentage improvement in performance increases as the voltage is lowered. Direct comparison of the performance of the two cell-types can not be made since different levels of humidity were tested. However, it should be noted that alumina cells require flow rates on the order of 10 times that of the Cr-alloy cells to achieve stable performance.

H_2O electrolysis performing better than CO_2 electrolysis is not much of a surprise given the past performance observed with Ni electrodes at 1000°C [20]. If one were to look at the Gibbs free energy of dissociating CO_2 versus H_2O into CO/O_2 and H_2/O_2 respectively, at room temperature H_2O electrolysis is favored by requiring 11% less energy. However, at 750°C H_2O electrolysis is only favored by 1% and at 1000°C, CO_2 electrolysis is actually favored (see Figure 5-5). So at 750°C, the energy required to electrolyze both molecules is almost the same and the difference in performance can not be attributed to that.

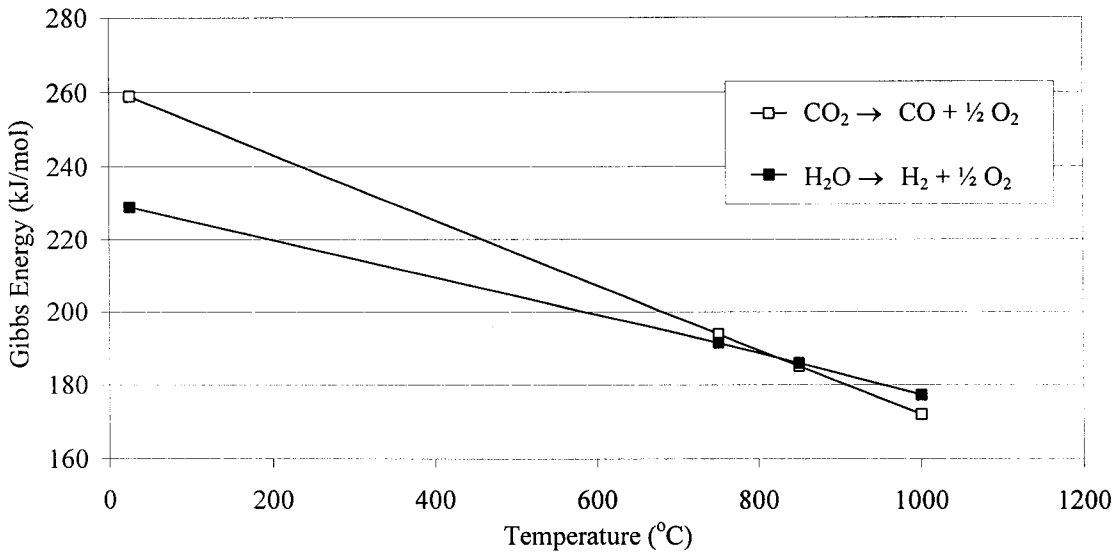

Figure 5-5 Gibbs energy required to break up CO_2 and H_2O versus temperature.

Another reason for the different levels of performance could be electrochemical in nature. Possibly the electrodes have different catalytic effects on the dissociation of H_2O versus CO_2. Using equation (5.1), V_{min} required for each reaction is plotted in Figure 5-6 as a function of utilization of the oxygen-providing gas. The experimental data is also plotted again, but this time as a function of utilization. It can be seen that for a given performance, a significant amount of voltage is required over the minimum. Part of this is because the flow rates are extremely high such that the cell is operating outside the mass limiting flow region. Thus, utilization is purposely tested at low values.

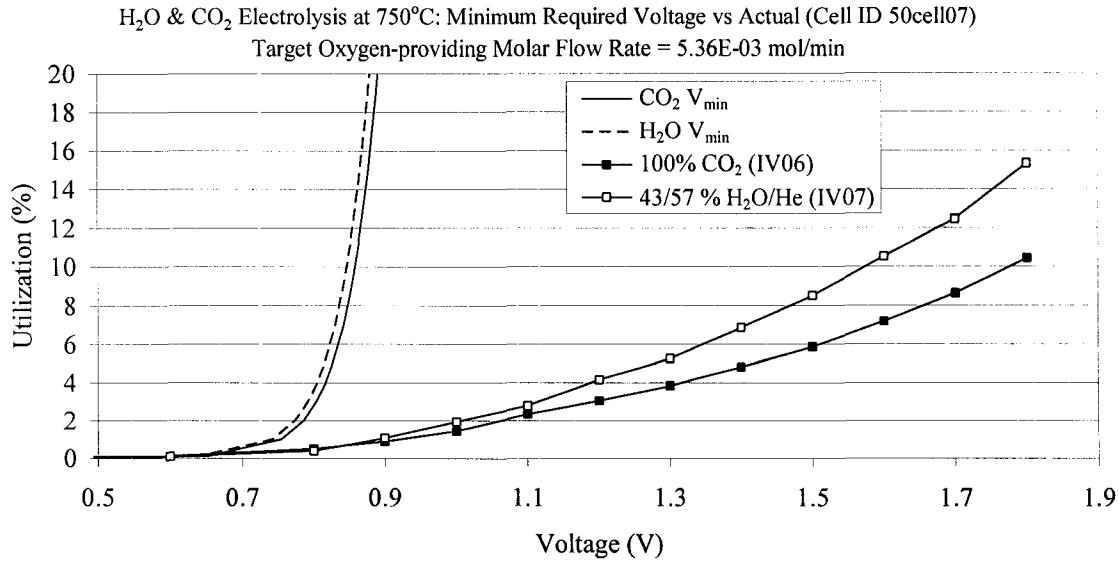

Figure 5-6 Theoretical V_{min} versus applied for both CO_2 and H_2O.

However, the extra voltage above the minimum is due to overpotentials, as mentioned in section 1.2. Concentration overpotentials should be negligible because of the high oxygen-providing molar flow rates into the cell as determined with the mass limiting experiments mentioned above. Ohmic overpotentials for the data presented in Figure 5-6 should be the same for a given utilization since the same cell was used to collect both sets of data. One should remember that utilization is dependent upon the current produced. Since both runs had the same target oxygen-providing molar flow rate, the current is the same for a given utilization. That leaves activation overpotentials, which may be different between the two molecules in the presence of Pt/YSZ electrodes.

Another consideration should be chemisorption of CO on Pt. The presence of CO could inhibit the CO_2 electrolysis reaction (equation (1.4)) from moving to the right. Adsorbed CO would not inhibit H_2O electrolysis from moving to the right.

5.3 Combined Electrolysis Performance

As evident in chapter 4, the performance that can be expected from combined electrolysis depends heavily upon the cell-type used. Differences are discussed within the following common issues.

5.3.1 Achieving Steady State Operations

Stable performance of combined electrolysis might be more easily or quickly achieved in Cr-alloy cells than in alumina cells. The conclusion is qualified with the word "might" because combined electrolysis in Cr-alloy cells was not rigorously tested for repeatability. One reason is because performance during tests appeared stable and there was no reason to suspect the performance was significantly changing or adapting over time. Combined electrolysis in alumina cells, on the other hand, gave the appearance of declining quickly during the tests. At the initiation of combined electrolysis testing, steady state operation was particularly difficult to achieve (if at all) at high voltages. Thus many combined electrolysis alumina tests were eventually performed to assure stable performance. In addition, just changing the mixture ratio of H_2O/CO_2 appears to cause the cell to need time to adjust before repeatable performance can be expected.

5.3.2 Relative to Other Inlet Mixtures

For the limited testing conducted, combined electrolysis is the best performing mixture in Cr-alloy cells. However, in alumina cells, combined electrolysis can be the worst depending upon mixture inlet and flow rate.

For Cr-alloy cells, combined electrolysis performance is not highly dependent upon the humidity concentration. Combined electrolysis definitely and fully outperforms CO_2 electrolysis by at least 40% (at 1.8V). Results presented in Figure 4-10 suggest 55/45% combined electrolysis also outperforms H_2O electrolysis at H_2O concentrations below 50/50% H_2O/He, though at most only by 7% (at 1.5V). Higher concentrations of H_2O electrolysis were not tested for Cr-alloy cells. Because Figure 4-13 and section 4.5.3 show that H_2O electrolysis is proportional to the amount of humidity in the inlet (regardless of cell-type), it is suspected that higher concentrations would test as well if not better than the 55/45% combined electrolysis tests.

For alumina cells, performance appears to be strongly dependent on the amount of H_2O in the mixture. All combined electrolysis tests underperforms high humidity (>83%) H_2O electrolysis. 70/30% H_2O/CO_2 performs worse by 14 – 30% whereas 30/70% H_2O/CO_2 performs worse by 50 – 60%. In general, the biggest percentage difference between the two inlet mixtures occurs at lower voltages. Though again, the fact that combined electrolysis underperforms H_2O electrolysis could be due to the humidity level in the H_2O electrolysis. Unlike the Cr-alloy cells, the comparison is against H_2O electrolysis that was tested at high humidity (83% or higher).

When compared to CO_2 electrolysis, combined electrolysis in alumina cells has mixed performance. Of the two stable cases achieved, combined electrolysis performance in alumina cells only fully outperforms CO_2 at a high H_2O content of 70/30%. The IV slope of combined electrolysis is shallower and more constant than that of CO_2 electrolysis so the percentage increase in performance goes down as voltage

increases (refer to Figure 4-24 (b)). As mentioned above, the lower humidity combined electrolysis (30/70% H_2O/CO_2) did not perform as well and thus for voltages above 1.1 V, combined electrolysis actually underperforms CO_2 electrolysis by up to 45%.

5.3.3 Performance Curve Trends

The shape of the combined electrolysis performance curves requires special attention. For the Cr-alloy cells, the combined electrolysis performance curves exhibit the same characteristics, regardless of humidity content, of both the H_2O and CO_2 electrolysis performance curves. Noticeable electrolysis commences around 0.6V and the slope rapidly increases until about 1.1 V where it remains constant. After about 1.4V, the slope starts to slightly increase again.

For the alumina cells, combined electrolysis performance curves also commence electrolysis near 0.6V; however, beyond that they differ from H_2O and CO_2 electrolysis trends. Combined electrolysis mixtures of high humidity (70% H_2O) exhibit shallower though relatively constant slopes. Combined electrolysis performance curves for low humidity (6 – 30% H_2O) exhibit an inflection point around voltage 1.3 – 1.4. By 1.5V, the performance of the alumina cell picks up and the second derivative of the IV slope turns positive. It is interesting to note that this occurs near the thermal neutral voltage of CO_2.

5.4 The Thermal Neutral Voltage Effect on Combined Electrolysis

As explained in section 2.1.2, the applied voltage is what determines the direction of heat transfer in electrolysis. When an electrolysis cell is operated above the thermal

neutral voltage, the cell will have to release heat in order to maintain the specified operating temperature. In the event that the heat can not be released quickly enough, the internal cell temperature will rise. A rise in temperature will encourage better performance since, as is shown in Figure 5-5, the energy required to break up either oxygen-providing molecule decreases with increasing temperatures. In addition, higher temperatures encourage faster electrode kinetics [13].

Equation (2.3) is used to evaluate what this thermal neutral voltage is for CO_2 electrolysis and H_2O electrolysis. For ideal gases, it can be assumed that enthalpy is independent of pressure. Values used here are taken from tables [54] at 750°C. Calculations are presented in Table 5-1 which show the thermal neutral voltage is higher for CO_2 than H_2O.

Table 5-1 Thermal Neutral Voltages for CO_2 and H_2O at 750°C

Oxygen-providing gas	**Thermal neutral voltage (V)**
CO_2	1.46
H_2O	1.30

Data was collected that actually corroborate the CO_2 result presented in Table 5-1. Figure 5-7 shows that temperature observations suggest the thermal neutral voltage for CO_2 electrolysis to be just below 1.5V. The data presented in Figure 5-7 was collected in the following manner.

A cell was placed in a furnace where the environment was controlled to 847.6 +/- 1.1°C with a Watlow Series 942 controller and K-type thermocouple. The measurements shown are from a second K-type thermocouple that was placed against the cell and shielded from the furnace's heating elements. At voltages below 1.5V, the cell

temperature appears to be lower (indicating thermal energy is being consumed by the endothermic reaction of breaking up CO_2). Above 1.5V, the cell temperature increases above the surrounding correlating to the evidence that the cell is giving off heat.

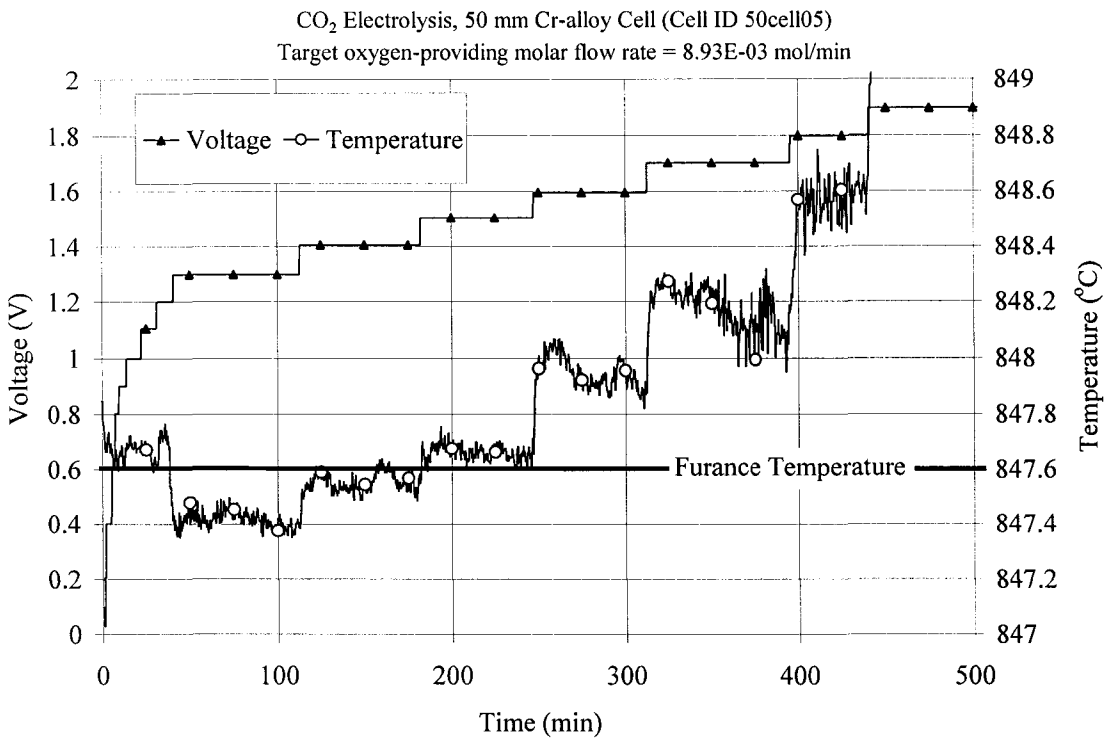

Figure 5-7 Temperature data suggests voltage determines heat transfer direction.

It should be noted that the data presented in Figure 5-7 merely supports the theory that operating above the thermal neutral voltage induces the cell to give off heat. It should not imply that operating above the thermal neutral voltage will always raise cell temperature. Higher cathode flow rates and/or higher anode flush rates could carry away any excess heat. Or, low current density may not produce enough heat to induce a measurable temperature change. So in other words, the operating voltage only dictates the direction of heat transfer, not its magnitude.

Section 5.3.3 reviews the shapes of the performance curves and suggests that for both Cr-alloy and alumina cells, the IV slopes for combined electrolysis begin increasing after 1.4V. For Cr-alloy cells, this occurs only slightly and for all humidity levels tested. For alumina cells, this is only observed in the low humidity tests (less than or equal to 30%), but the increase in slope is relatively substantial. Interestingly, for all cases this is after the thermal neutral voltage for CO_2 electrolysis (1.46V).

Then why would there not be an increase in slope after the thermal neutral voltage of H_2O (1.30V)? As it turns out, for pure H_2O electrolysis there is (for both cell-types). However, for combined electrolysis there is not. Maybe during combined electrolysis the increase in heat released from H_2O dissociated at voltage immediately above 1.3V is not enough to have a significant impact. Or possibly the extra heat is consumed by the neighboring CO_2 and only when both molecules are satisfied (i.e. have enough energy such that the dissociation will not rely on heat, which would happen at 1.46V) can energy be released as heat, thus increasing the internal temperature and performance.

This could explain also why the performance curve of combined electrolysis at higher humidity in alumina cells is so straight as compared to pure H_2O electrolysis. At low humidity, most of the H_2O gets dissociated easily. So easily that in fact it could appear as a cell starvation scenario (thus the flattening slope shown in Figure 4-24). Once the voltage gets higher, the CO_2 can be more readily electrolyzed and heat is given off as well (thus the inflection point). For high humidity, there is more water such that H_2O starvation does not occur. The slope does not increase because the CO_2 is still consuming the additional heat.

However, these trends are not seen in the Cr-alloy system. One reason could be due to the higher thermal conductivity of the manifolds. Thus any excess heating that may occur at higher voltages is dissipated. Another reason will be explored in section 5.8, after more foundation regarding the inner workings of combined electrolysis is presented.

In the mean time, another effect of operating above the thermal neutral voltage can be considered. In section 4.7, SEM images of the alumina electrodes reveal that not only the anode (where the exothermic formation of oxygen is occurring) but the cathode appears to coagulate. However, the porosity of the electrodes of the Cr-alloy more closely resembles a fresh unused electrode. Section 4.7 suggests the difference is in the thermal conductivity of the manifolds. But why would such an observation occur at the cathode where the electrolysis reactions are endothermic? One explanation could be that if operated above the thermal neutral voltage for long periods of time, heat will be dissipated and in alumina cells where the thermal conductivity is lower than in the Cr-alloy cells, the temperature could rise and possibly the cathode could meld together more.

5.5 Combined Electrolysis and Carbon Deposition

Combined electrolysis behaves differently depending upon the system. Section 5.3 shows the performance difference between the Cr-alloy and alumina systems is striking. Chromium-based systems electrolyze H_2O and CO_2 in roughly the same proportion as that entering the cell. Alumina cells however show a strong preference to H_2O over CO_2. More strikingly, combined electrolysis substantially underperforms CO_2 electrolysis in the alumina systems where in the Cr-alloy systems, it outperforms CO_2 electrolysis.

One question has been raised in an attempt to explain the differences observed between the systems. Could the alumina system be promoting carbon deposition? The presence of carbon on the electrode could reduce the number of three phase boundaries, decreasing the cell's performance. Is carbon deposition at SOE temperatures even possible? Concentrations of CO_2 in CO that are required to cause carbon to deposit as a function of temperature can be calculated from the carbon deposition reaction equilibrium constant (see the Appendix B.1). Figure 5-8 shows that at SOE operating temperatures carbon deposition is possible at low CO_2 concentrations in CO. But this is for a CO_2/CO mixture. What about a $CO_2/H_2O/CO/H_2$ mixture and how does one prove or disprove the probability of this actually occurring in either cell-type?

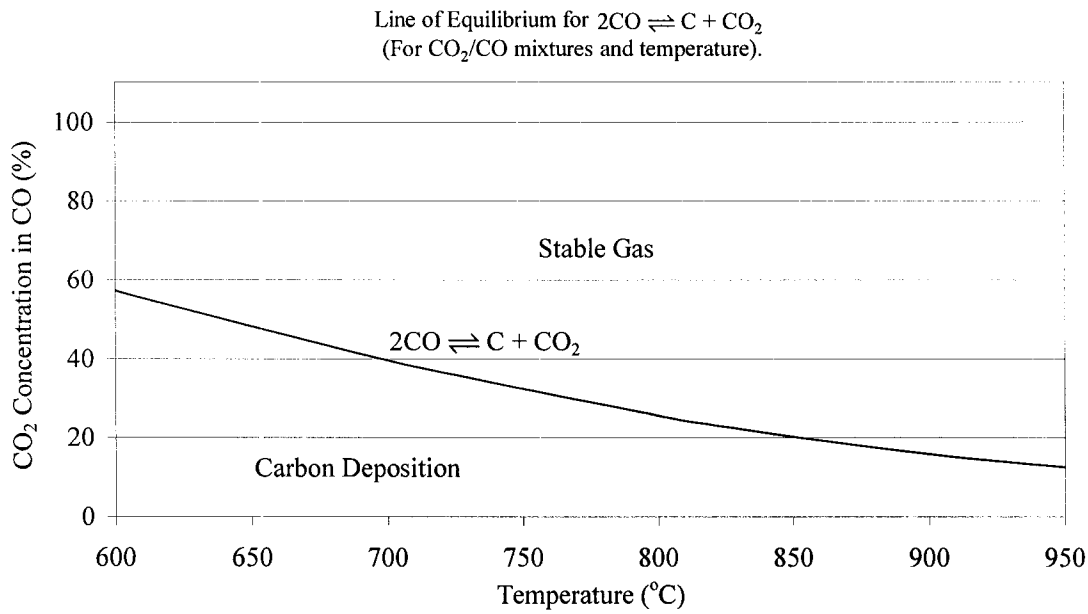

Figure 5-8 Temperature and CO_2/CO mixtures required for carbon deposition.

Consider the following system illustrated in Figure 5-9. A mixture of CO_2 and H_2O enters a SOE unit. Assume all oxygen is extracted from within the system and all that

comes out of the exhaust is CO and H_2, and left over undissociated CO_2 and H_2O. Assuming carbon deposition, what does theory predict an exhaust analysis will reveal about the mixture composition?

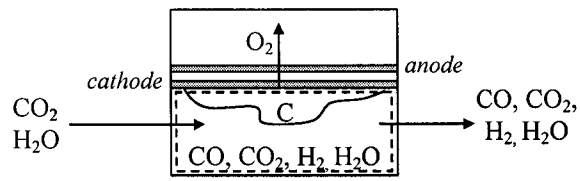

Figure 5-9 Illustration of carbon being deposited on the cathode side of a SOE cell.

Assume there are no air leaks and assume the catalysts or other cell materials don't evaporate. The gas inside the cell will be made up of formations composed of only three elements: carbon (C), hydrogen (H), and oxygen (O). The formation reactions for CO, CO_2, and H_2O using these elements are, respectively:

$$C + \tfrac{1}{2}O_2 \rightleftharpoons CO \qquad C + O_2 \rightleftharpoons CO_2 \qquad H_2 + \tfrac{1}{2}O_2 \rightleftharpoons H_2O \qquad (5.5),\ (5.6),\ (5.7)$$

If most of the O_2 is extracted such that the remaining amount can be assumed negligible then O_2 should be removed from reactions (5.5) – (5.7) to get two independent reactions:

$$\begin{array}{r} C + O_2 \rightleftharpoons CO_2 \\ +\quad 2H_2O \rightleftharpoons H_2 + O_2 \\ \hline C + 2H_2O \rightleftharpoons CO_2 + 2H_2 \end{array} \qquad \text{and} \qquad \begin{array}{r} C + O_2 \rightleftharpoons CO_2 \\ +\quad 2CO \rightleftharpoons 2C + O_2 \\ \hline 2CO \rightleftharpoons CO_2 + C \end{array} \qquad (5.8),\ (5.9)$$

Reaction quotients can be calculated for both reactions (5.8) and (5.9), respectively:

$$Q_{Eq.\,(5.8)} = \frac{P_{CO_2} P_{H_2}^2}{P_{H_2O}^2\, a_C} = \frac{P_{CO_2} P_{H_2}^2}{P_{H_2O}^2} \qquad (5.10)$$

$$Q_{Eq.\,(5.9)} = \frac{P_{CO_2}\, a_C}{P_{CO}^2} = \frac{P_{CO_2}}{P_{CO}^2} \qquad (5.11)$$

where the activity of the solid carbon is a_C and can be set to unity. The total pressure, P_T, is written as a function of the partial pressures:

$$P_T = P_{CO_2} + P_{H_2O} + P_{CO} + P_{H_2} \tag{5.12}$$

The reaction quotients, $Q_{Eq.(5.8)}$ and $Q_{Eq.(5.9)}$ of equations (5.10) and (5.11), can be calculated assuming the reactions are in equilibrium. The equilibrium constants $K_{P,Eq.(5.8)}$ and $K_{P,Eq.(5.9)}$ are then calculated using Gibbs standard state energy [15] for a given SOE operating temperature, T. This type of calculations is demonstrated in Appendix B.1. T and P_T will be considered known since data is collected for a specific set of operating conditions: T = 750°C and P_T = 0.91 atm. Three equations ((5.10) – (5.12)) and four unknowns (P_{CO2} , P_{H2O} , P_{CO} , and P_{H2}) remain.

The equations are solved as a function of the ratio of P_{H2}:P_{CO} and plotted in Figure 5-10. The solutions are reasonable. For example, as P_{H2}:P_{CO} increases, P_{H2} increases and P_{CO} decreases. Additionally, all partial pressures add up to P_T. The solution represented in Figure 5-10 describes the relationship of the partial pressures within the system. If a gas sample were to be extracted from an actual electrolysis system, measurements of partial pressure would match the calculations presented in Figure 5-10 if carbon were indeed deposited in the cell.

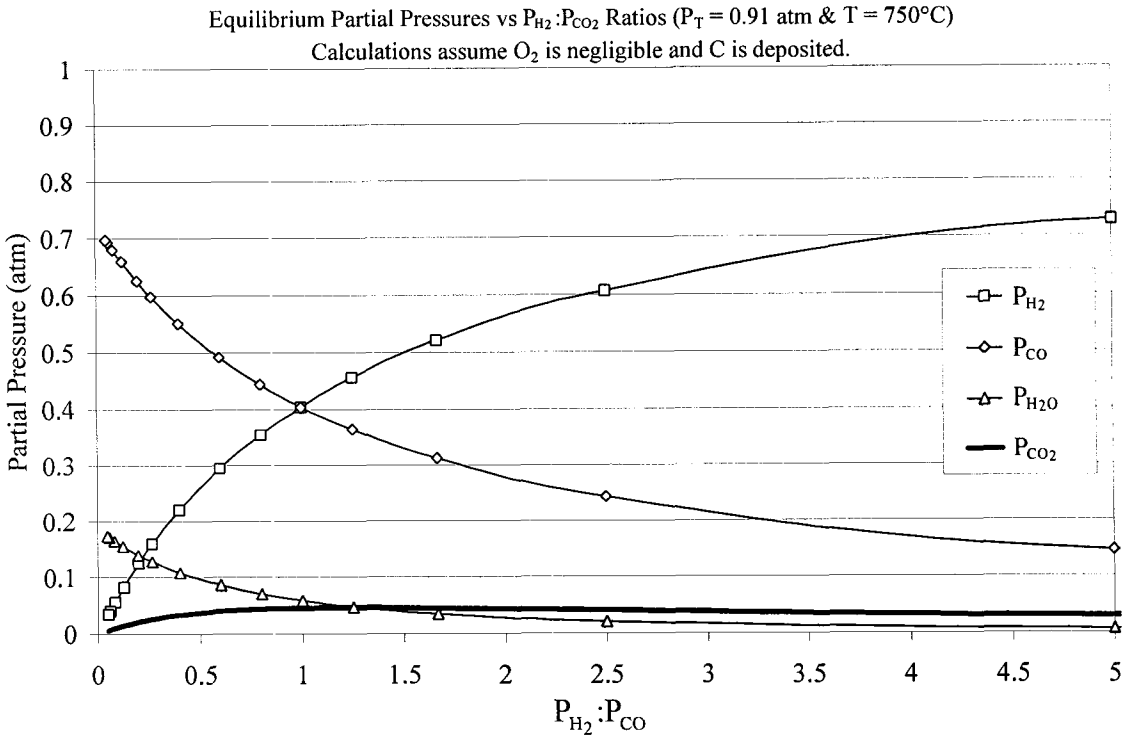

Figure 5-10 Calculated partial pressures of combined electrolysis exhaust assuming carbon deposition.

To compare actual experiments to calculations, a GC is used to analyze the constituents of the SOE cell exhaust. Because H_2O contaminates the columns of the GC, the exhaust of the SOE cell is first sent through a condenser. To appropriately compare the GC data to theory, H_2O should be removed from the theoretical solution. See Appendix A.2 for details of calculating the solutions after H_2O removal.

The solutions of the partial pressures of H_2, CO_2, and CO after removing H_2O are presented in Figure 5-11 as lines. Data collected from the exhaust of various combined electrolysis tests are plotted. As can be seen, the data do not agree with the theory. For example, if carbon were deposited in the cell, theory suggests the partial pressure of CO_2 exiting the cell (represented by a diamond line) would account for less than 0.2 atm of the

total pressure. However, the P_{CO_2} data (dark gray diamonds) indicate that in fact the partial pressure of CO_2 accounts for over 0.5 atm of the total pressure. Therefore, with such a mismatch between theory and data it is concluded that carbon is not being deposited in the cell.

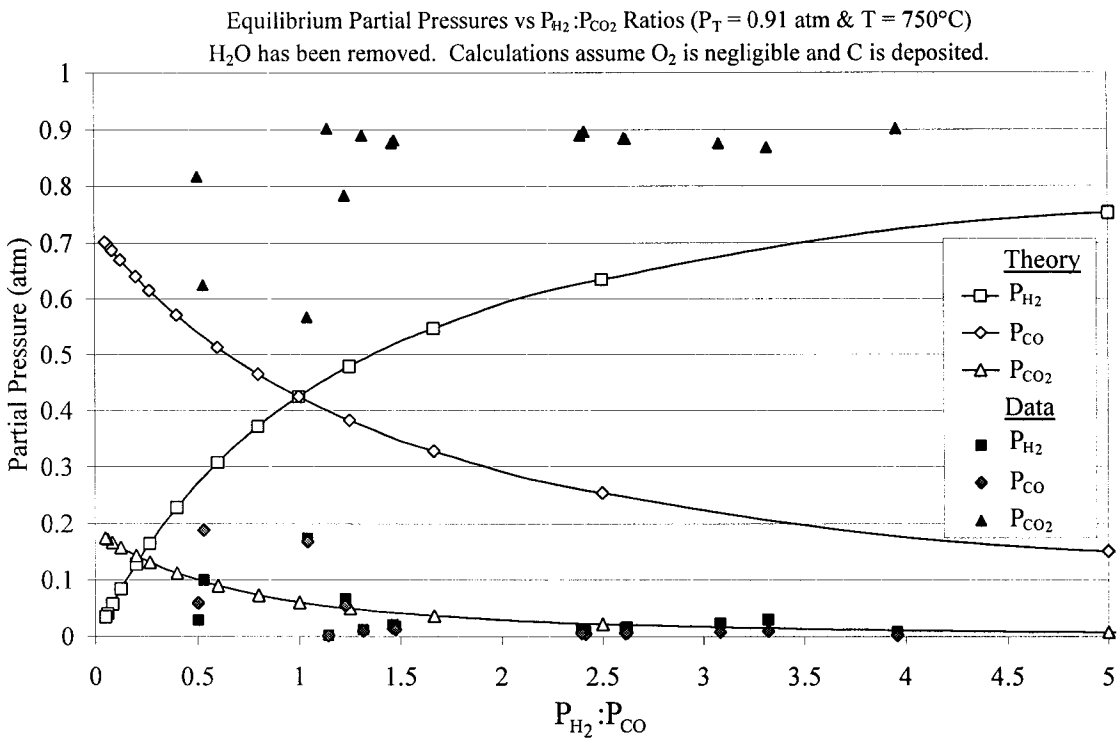

Figure 5-11 Partial pressure data does not match theory assuming carbon deposition.

5.6 Combined Electrolysis and the Water Gas Shift Reaction

In the proceeding section, a methodology was presented that concluded carbon is not being deposited in the cells during combined electrolysis. Consider now a system that is not depositing carbon in the SOE cell (as illustrated in Figure 5-12). The same procedure can be used as above but this time the reactions must be further reduced to remove the carbon, as is shown in equation (5.13). As mentioned in section 2.2, Equation (5.13) is

also known as the water gas shift reaction. Because there is only one independent reaction, there can only be one reaction quotient as written in equation (5.14).

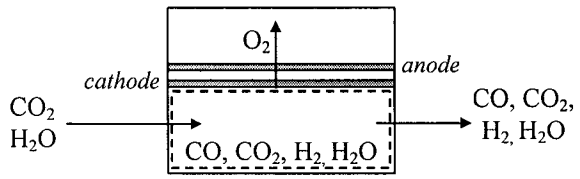

Figure 5-12 Illustration of no carbon deposited on the cathode side of a SOE cell.

$$\begin{aligned} C + 2H_2O &\rightleftharpoons CO_2 + 2H_2 \\ + \quad 2CO &\rightleftharpoons CO_2 + C \\ \hline H_2O + CO &\rightleftharpoons CO_2 + H_2 \end{aligned} \tag{5.13}$$

$$Q_{wgs} = \frac{P_{CO_2} P_{H_2}}{P_{H_2O} P_{CO}} \tag{5.14}$$

T and P_T are still considered known, with P_T described previously in equation (5.12). Furthermore, a value for Q_{wgs} can be calculated if the water gas shift reaction is assumed to be in equilibrium. For an operating temperature of 750°C, $K_{P,wgs} = 1.282$. This leaves only two equations ((5.12) and (5.14)) and the same four unknowns (P_{CO2}, P_{H2O}, P_{CO}, and P_{H2}). Solutions are found as a function of P_{CO2} and the ratio P_{H2}:P_{CO}. An example solution is provided in Appendix B.2. Water is then condensed out of the solution using the same method previously described in Appendix A.2. An example solution for three P_{H2}:P_{CO} ratios is plotted versus P_{CO2} in Figure 5-13. Figure 5-13 (a) plots the partial pressure of CO and Figure 5-13 (b) plots H_2. The calculations are qualitatively reasonable. For instance as a sanity check, the plot shows that as the P_{H2}:P_{CO} ratio

increases, the partial pressure of CO decreases and the partial pressure of the H_2 increases.

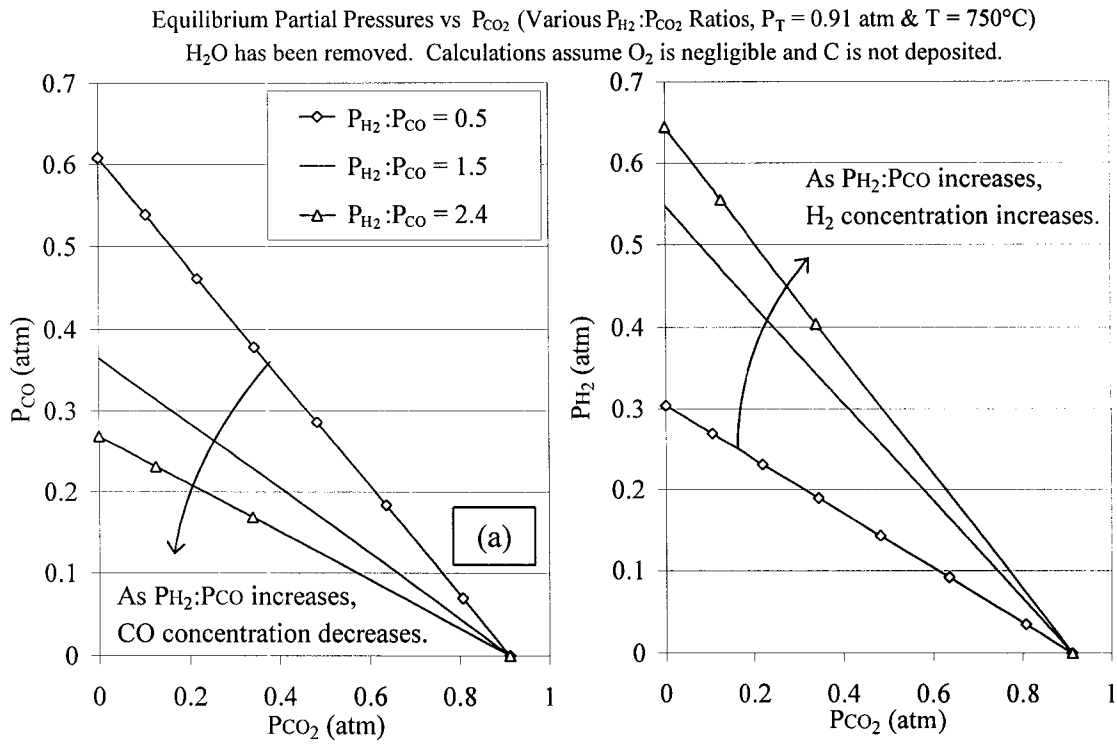

Figure 5-13 Exhaust partial pressures for combined electrolysis (no carbon deposition).

The data now can be plotted against the theory presented in Figure 5-13. As an example, Figure 5-14 shows a set of data with a P_{H_2}:P_{CO} ratio of 2.4. The raw data (shown using filled symbols) matches the theory very well. It should be noted that the GC detects not only CO_2, CO and H_2 but also air. If the detected O_2: N_2 ratio is near 0.21:0.78, then it can be assumed the air contamination occurs down stream of the electrolysis cell. If not, the oxygen would be electrolyzed and the ratio of O_2 to N_2 would be quite less. As it turns out the former is true, and thus the raw data obtained from the

GC are corrected for air leaks (see Appendix A.3). As shown in Figure 5-14, the "corrected" data (shown using open symbols) agrees extremely well.

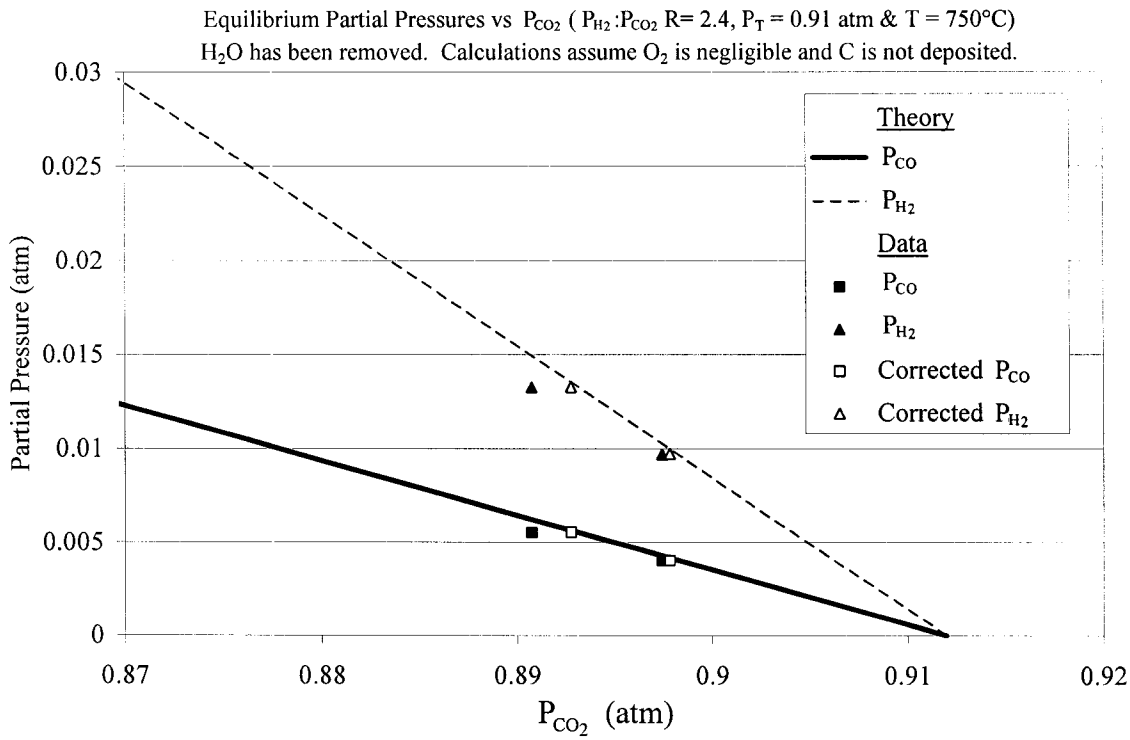

Figure 5-14 Combined electrolysis exhaust data matches theory (P_{H_2}:P_{CO} = 2.4).

Plotting the data against theory can be quite confusing when plotting both the partial pressures of H_2 and CO and then doing it for the many different P_{H_2}:P_{CO} ratios. Thus checking all the data would call for a multitude of plots (for example, one for each P_{H_2}:P_{CO} ratio as that done in Figure 5-14). Therefore, a means for normalizing the data as a function of P_{H_2}:P_{CO} is developed such that all data can be compared to theory on one plot.

Normalization is accomplished by dividing all solutions and data by the following non-dimensional function:

$$y = \exp\left(-.9\frac{1}{x}\right) + \frac{x}{9^x} \tag{5.15}$$

where y is the normalized P_{H_2} or P_{CO} and x is P_{H_2}:P_{CO} or P_{CO}:P_{H_2}, respectively. The details of the development of equation (5.15) are in Appendix A.4. The normalized results of P_{H_2} and P_{CO} are plotted in Figure 5-15 a) and b), respectively.

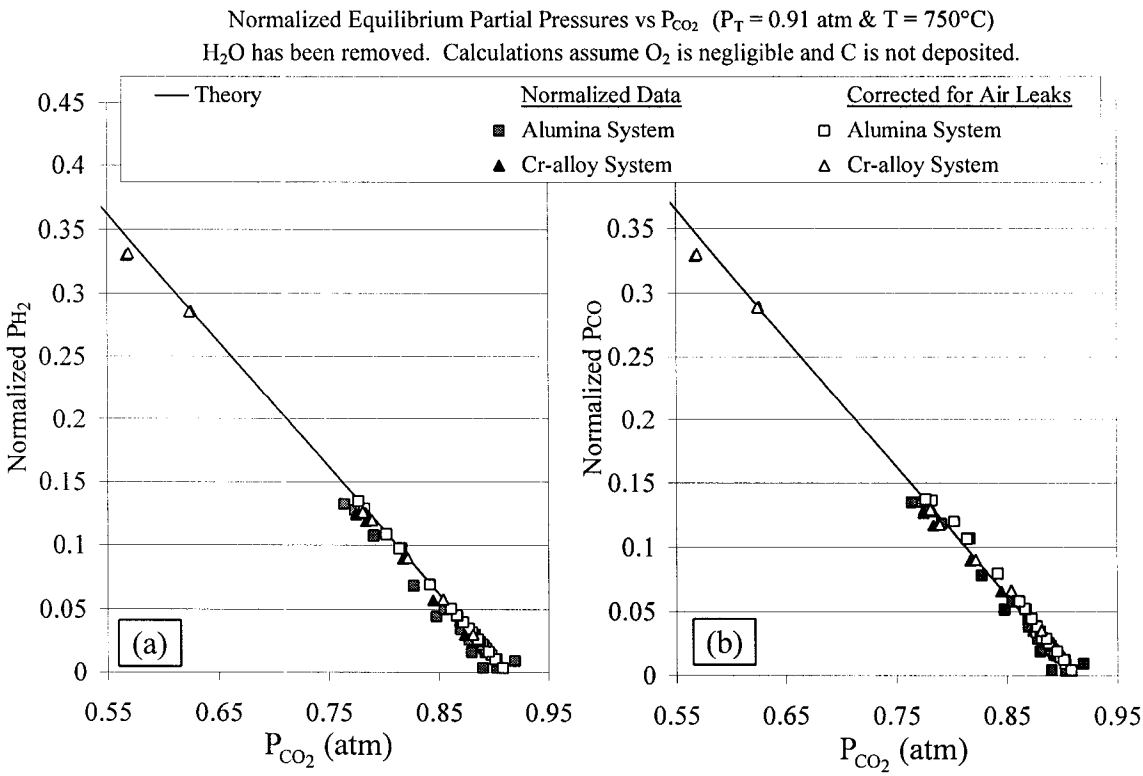

Figure 5-15 Normalized combined electrolysis exhaust P_{H_2} and P_{CO} comparison between experiment and theory.

Figure 5-15 shows the composition of H_2 to CO to CO_2 exhausting from combined electrolysis can be accurately calculated assuming no carbon is deposited in the cell. The data collected via experiments align quite well with theory. Considering the terrible

agreement between data with the theory of carbon deposition and the very good agreement with the non-carbon deposition theory, it can be concluded that no carbon is being deposited in the cell. Furthermore, it can be concluded that no constituent is deposited at all and in fact, all atoms are conserved across the cell. However, the analysis presented here gives no information regarding H_2O content. The data matched by this analysis was collected after the H_2O was removed from the exhaust.

As it turns out, any value of Q_{wgs} will produce the theoretical results presented in Figure 5-15. It was assumed that the independent reaction governing the exhaust, the water gas shift reaction, was in equilibrium. But in fact, this assumption does not need to be made (and is not the case for alumina cells, as will be shown later). The post-condensed solution that matches the data is independent of the value of Q_{wgs}. However, the solution containing H_2O is different for different values of Q_{wgs}. Even though the $P_{H_2}:P_{CO}$ ratio matches before and after H_2O is removed, the partial pressures do not. An example calculation is presented in Table 5-2 for two values of Q_{wgs}: 1.282 ($K_{P,wgs}$ at 750°C) and 100 (a randomly chosen different value from $K_{P,wgs}$).

Table 5-2 Normalized pressure calculations for different Q_{wgs}.

Qwgs	1.282	100	1.282	100	1.282	100
	Calculated Exhaust Partial Pressures (atm)		Partial Pressure after Water is Removed (atm)		Normalized Partial Pressure	
P_{CO_2}	0.200	0.600	0.616	0.616		
P_{CO}	0.019	0.058	0.060	0.060	0.344	0.344
P_{H_2}	0.077	0.230	0.236	0.236	0.296	0.296
P_{H_2O}	0.616	0.024	--	--		
Total	0.912	0.912	0.912	0.912		

Consequently, besides the conclusion that all atoms are conserved across the cell, the only other conclusions that can be made is that the water gas shift reaction characterizes the relative composition of CO to H_2 to CO_2 in combined electrolysis exhaust. No conclusion can be made regarding whether these constituents are in equilibrium. This result has an important consequence, for one final interesting observation is that the data in Figure 5-15 aligns well regardless of the cell-type even though a chromium-based system clearly behaves differently than an alumina-based system. What will be shown in the next section is that the reaction quotient for the Cr-alloy system is in equilibrium whereas for the alumina system *it is not*.

5.7 Predicting the Exhaust Composition of Combined Electrolysis

Ideally, when designing a combined electrolysis system to produce a given amount of oxygen, an engineer should know how the input composition will affect the exhaust composition. For instance, the exhaust will contain CO and CO_2. If the exhaust is lowered in temperature during a process down stream, carbon could deposit depending upon the CO to CO_2 ratio and materials present. Whether this is a desired effect or not is not the issue. What is the issue is to know how to get the desired ratio, or any exhaust composition for that matter, which best integrates combined electrolysis into a given system.

It will be shown in the following two sections that the exhaust of a Cr-alloy system achieves water gas shift equilibrium whereas the exhaust of an alumina system does not. Therefore, to achieve a predictable exhaust composition for a given oxygen production and inlet composition, one can use 1) a Cr-alloy cell or 2) an alumina cell followed by a

water gas shift reactor. The implementation of such predictions depends upon the combined electrolysis application. The combined electrolysis exhaust composition is a function of the inlet H_2O and CO_2 molar flow rates and oxygen production rate. Another way to set up the problem would be to specify absolute humidity of the inlet stream, total inlet molar flow rate and oxygen production. This is because specifying absolute humidity and total flow rate is the same thing as specifying CO_2 and H_2O flow rates individually. The set of variables chosen would be dictated by the application of the combined electrolysis and how the unit is implemented. Once decided, charts can be generated for easy table look up.

5.7.1 In Cr-alloy Cells

In order to calculate what exhausts from a combined electrolysis cell, the H_2O/CO_2 mixture ratio and total flow rate of the gas input as well as the O_2 production must be taken into account and are considered known. Molar rates will be used in this analysis rather than moles because oxygen production is a rate, and when operating a cell beyond its mass limiting range, the oxygen production rate is independent of the molar flow rate of the input gas. For a given input mixture ratio, the CO_2 and H_2O molar flow rates constrain the amount of C, H, and O entering the system. Through conservation of atoms, the following equations can be applied to the electrolysis cell:

$$\dot{N}_{CO_2}^{in} = \dot{N}_{CO_2}^{out} + \dot{N}_{CO}^{out} \tag{5.16}$$

$$\dot{N}_{H_2O}^{in} = \dot{N}_{H_2O}^{out} + \dot{N}_{H_2}^{out} \tag{5.17}$$

$$2\dot{N}_{O_2}^{out} = \dot{N}_{CO}^{out} + \dot{N}_{H_2}^{out} \tag{5.18}$$

These three equations contain four unknowns: $\dot{N}_{CO_2}^{out}$, $\dot{N}_{CO}^{out}$, $\dot{N}_{H_2O}^{out}$ and $\dot{N}_{H_2}^{out}$. One should note that $\dot{N}_{O_2}^{out}$ is the oxygen generation rate. Another equation is needed to solve for all four unknowns. From section 5.6, the water gas shift reaction was shown to govern the exhaust of combined electrolysis. Therefore, to provide a fourth equation, the definition of the reaction quotient for the water gas shift reaction (equation (5.14)) can be re-written in terms of molar flow rates when assuming ideal gases [55]:

$$Q_{wgs} = K_{P,wgs} = \frac{\dot{N}_{CO_2}^{out}\dot{N}_{H_2}^{out}}{\dot{N}_{CO}^{out}\dot{N}_{H_2O}^{out}} \tag{5.19}$$

Equations (5.16) - (5.19) can now be manipulated to solve for the molar flow rate of each component in the exhaust. As solved in this work, Appendix A.5 shows that $\dot{N}_{H_2O}^{out}$ is a solution to a 4th order polynomial function of the known variables $\dot{N}_{CO_2}^{in}$, $\dot{N}_{H_2O}^{in}$ and $\dot{N}_{O_2}^{out}$, and can be solved using a numerical root finder. The solutions to $\dot{N}_{CO_2}^{out}$, $\dot{N}_{H_2}^{out}$, and $\dot{N}_{CO}^{out}$ can then be calculated, and equations for doing so are also presented in Appendix A.5.

In order to test the validity of this model, solutions were calculated for experiments described in chapter 4 that had GC data to quantify the exhaust composition. For the experiments modeled, the operation temperature was 750°C which corresponds to a $K_{P,wgs}$ = 1.282. The molar flow rate solutions were converted to partial pressures and then as done in section 5.5, H_2O was condensed out and compared to experimental GC data that has been corrected for air leaks.

Figure 5-16 shows experimental data versus calculations for partial pressures of both H_2 (square markers) and CO (triangle markers). First, Cr-alloy experimental results agree to within 7 and 11% of the calculations for H_2 and CO partial pressures, respectively. Figure 5-17 compares CO_2 partial pressure of experimental data to theoretical calculations. P_{CO_2} calculations agree within 2% of the experimental data. These results verify that not only is the water gas shift reaction driving the exhaust but that for the Cr-alloy cells it is in equilibrium (one should remember that the equilibrium constant for the reaction at 750°C of $K_{P,wgs} = 1.282$ is used).

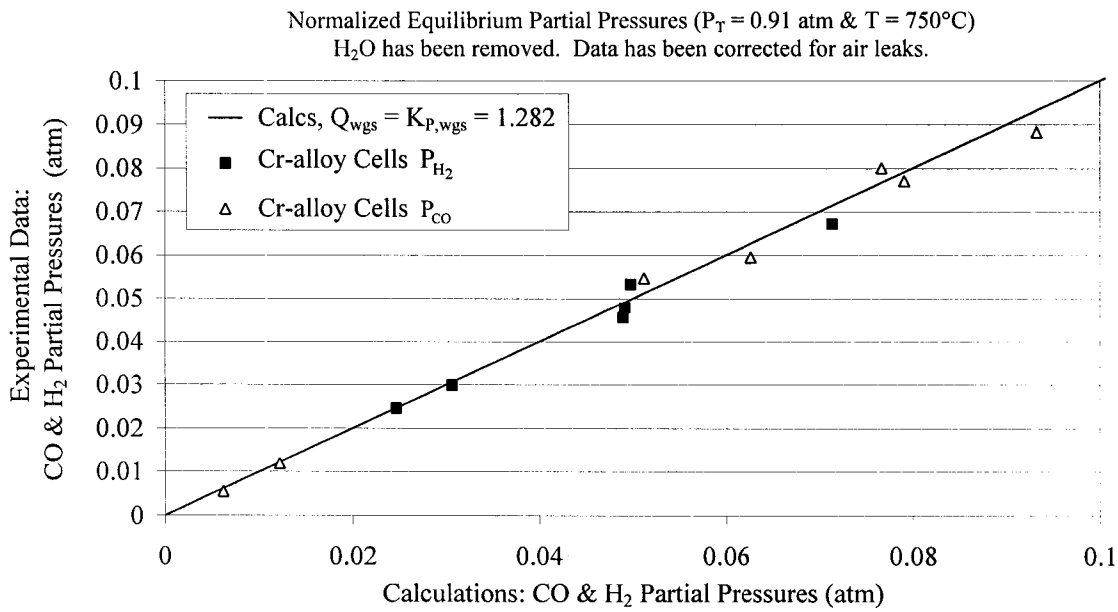

Figure 5-16 Cr-alloy cells: P_{CO} and P_{H_2} calculations versus experimental data.

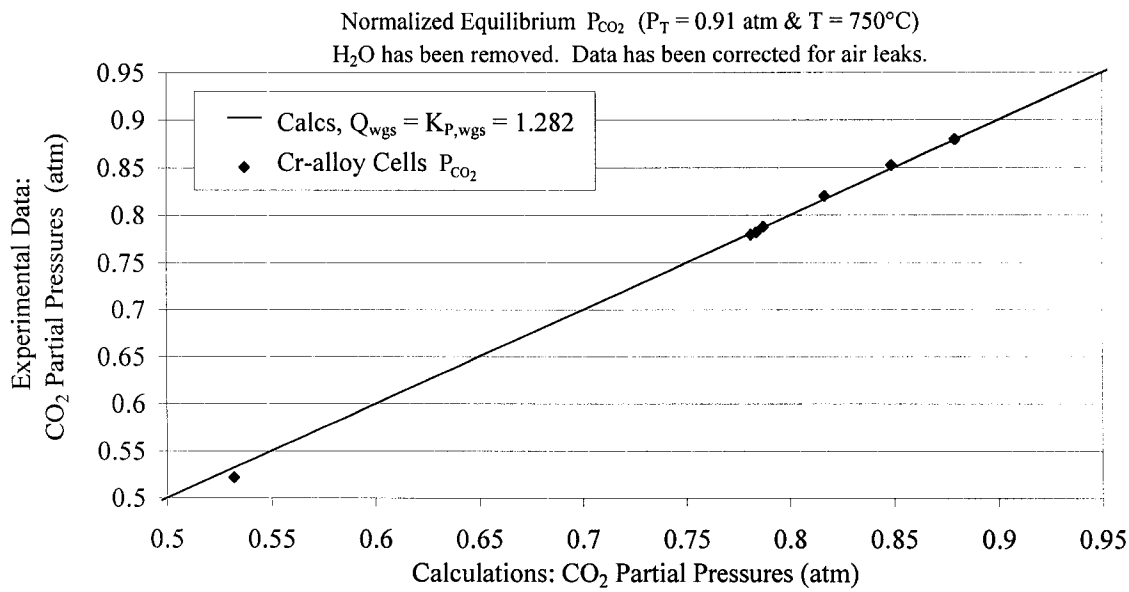

Figure 5-17 Cr-alloy cells: P_{CO_2} calculations compared to experimental data.

5.7.2 In Alumina Cells

The procedure outlined above does not explicitly work for the alumina cells. As shown in Figure 5-18, the experimental results from alumina cells do not agree, deviating up to 88 and 1358% from calculations for the partial pressures of H_2 and CO, respectively. Interestingly, Figure 5-19 shows P_{CO_2} calculations agree within 0.3% of the experimental data. Regardless, the method presented above can not be used to completely describe the relationship between the products in the exhaust of an alumina combined electrolysis cell.

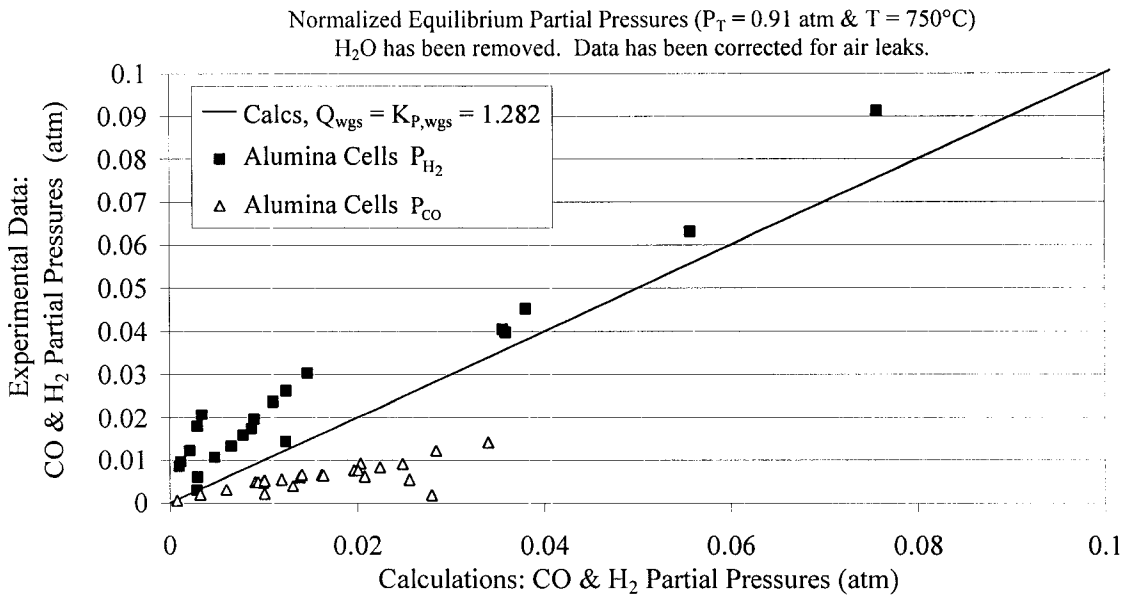

Figure 5-18 Alumina cells: P_{CO} and P_{H_2} calculations compared to experimental data.

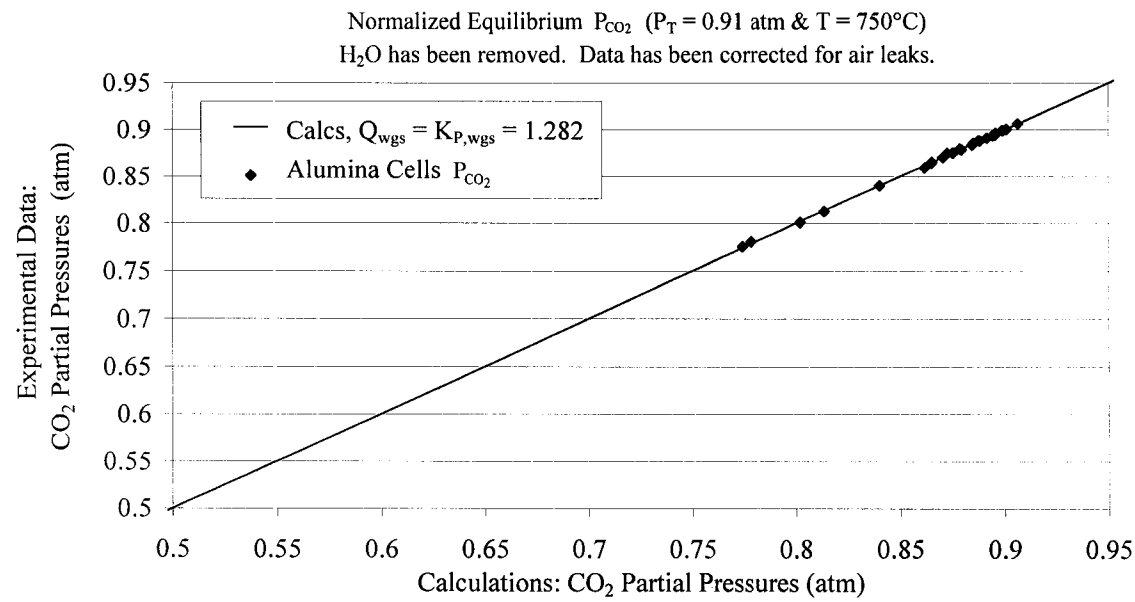

Figure 5-19 Alumina cells: P_{CO_2} calculations compared to experimental data.

However, since section 5.6 proves that the water gas shift reaction governs the output of both cells regardless of reaction completeness, possibly the reaction does not achieve equilibrium in the alumina cells. In order to evaluate how close the alumina cell is to equilibrium, the reaction quotient is used in place of equation (5.19):

$$Q_{wgs} = \frac{\dot{N}_{CO_2}^{out}\dot{N}_{H_2}^{out}}{\dot{N}_{CO}^{out}\dot{N}_{H_2O}^{out}} \tag{5.20}$$

Now the question becomes what reaction quotient will drive the calculations to match the P_{CO2}, P_{CO}, and P_{H2} measurements taken from the alumina cell's exhaust? The reaction quotients of the alumina cells in which GC data is available were thus solved. Figure 5-20 shows that the reaction quotient reduces over time suggesting that the cell can be conditioned. Whether or not the cell can be conditioned such that equilibrium of the water gas shift reaction and reliable prediction of the cell's exhaust composition can both be achieved will require more experimentation.

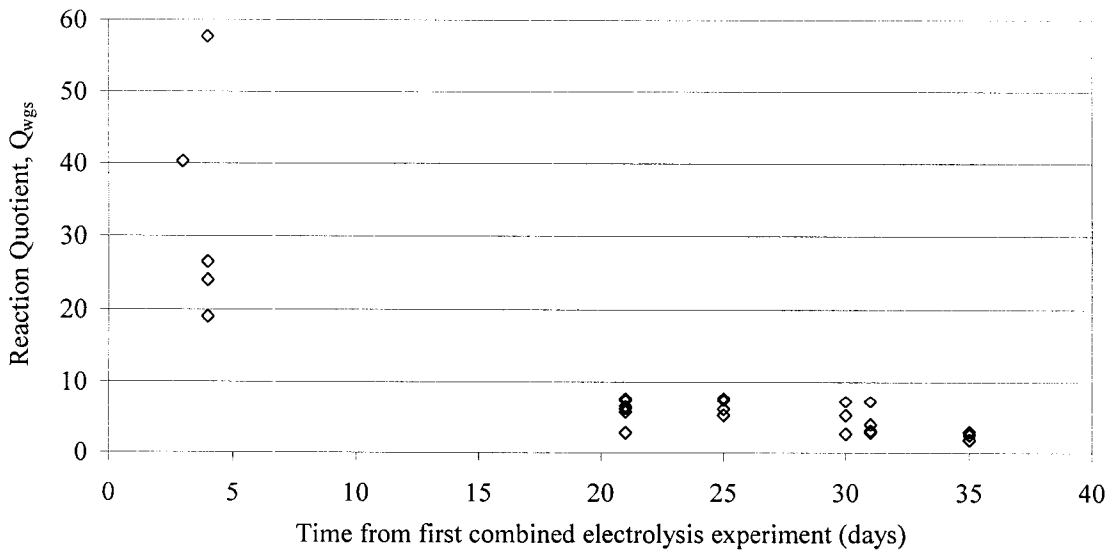

Figure 5-20 The Q_{wgs} of the alumina cell reduces over time.

However, there are several other variables that could influence an alumina cell's reaction rate including input humidity, input molar flow rate, oxygen production, and applied voltage. Of these, only voltage and absolute humidity appeared to be a factor. Figure 5-21 (a) shows that low absolute humidity could also be a cause of high reaction quotients. Figure 5-21 (b) suggests that raising the applied voltage (and thus relative oxygen production) increases reaction quotient.

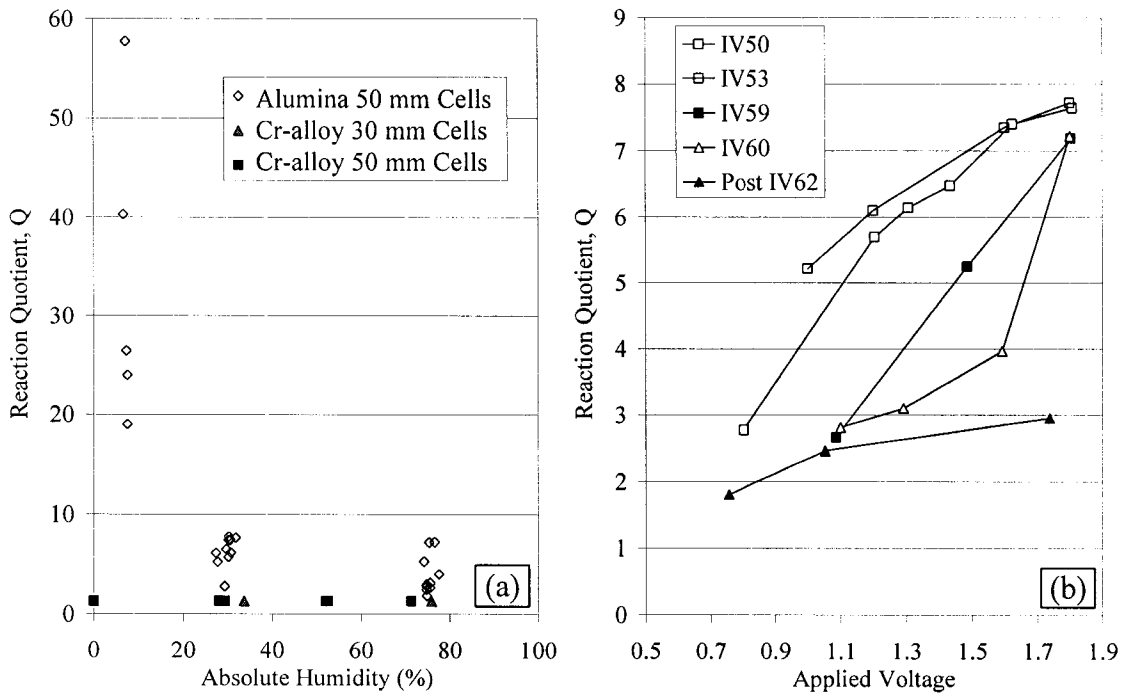

Figure 5-21 The water gas shift reaction quotient versus (a) absolute humidity and (b) applied voltage.

The bottom line is that the alumina cells are not achieving equilibrium and thus make it difficult to predict the exhaust output. The root of this cause is buried in the absence of an adequate catalyst for the water gas shift reaction. However, knowing this, the combined electrolysis exhaust of an alumina cell can be made to be predictable by routing it through a water gas shift reactor, as shown in Figure 5-22.

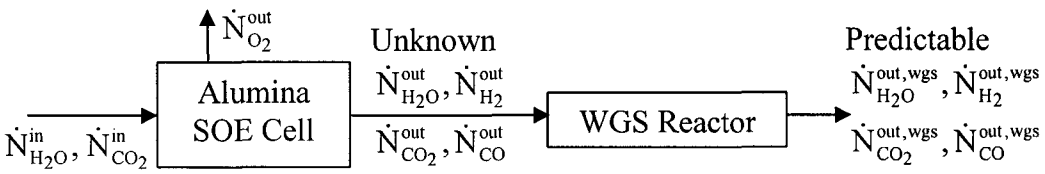

Figure 5-22 Illustration of an alumina cell in series with a water gas shift reactor.

Knowing the inlet composition to the alumina cell and the desired oxygen production, the outlet of the water gas shift reactor can be determined without knowing the reactor's inlet conditions. It might be asked, "How can the outlet of a water gas shift reactor be guaranteed when different cell-types may provide different exhaust compositions for the reactor's input?" The answer is if atoms are conserved across the electrolysis cell (i.e. no carbon or other deposition) then the exhaust composition for a given O_2 production rate and inlet gas mixture does not matter. A proof is provided in Appendix A.6. The four governing equations that can be solved for the exhaust of the water gas shift reactor are also presented in Appendix A.6.

5.7.3 Comparison of Methods

Section 5.7.1 describes how to calculate the exhaust of a Cr-alloy cell assuming equilibrium of the water gas shift reaction happens inside the cell itself. Section 5.7.2 describes how to calculate the exhaust of an alumina cell after it passes through a water gas shift reactor to force equilibrium. As it turns out, the calculations are exactly the same. The equations that govern the exhaust of the water gas shift reactor (see equations (A.52) – (A.55) in Appendix A.6) can be re-written as:

$$\dot{N}_{CO_2}^{in,SOE} = \dot{N}_{CO_2}^{out,wgs} + \dot{N}_{CO}^{out,wgs} \tag{5.21}$$

$$\dot{N}_{H_2O}^{in,SOE} = \dot{N}_{H_2O}^{out,wgs} + \dot{N}_{H_2}^{out,wgs} \tag{5.22}$$

$$2\dot{N}_{O_2}^{out,SOE} = \dot{N}_{CO}^{out,wgs} + \dot{N}_{H_2}^{out,wgs} \tag{5.23}$$

$$K_{P,wgs} = \frac{\dot{N}_{CO_2}^{out,wgs}\dot{N}_{H_2}^{out,wgs}}{\dot{N}_{CO}^{out,wgs}\dot{N}_{H_2O}^{out,wgs}} \tag{5.24}$$

For a given input gas mixture ($\dot{N}_{CO_2}^{in,SOE}$ and $\dot{N}_{H_2O}^{in,SOE}$) and oxygen production rate ($\dot{N}_{O_2}^{out,SOE}$), equations (5.21) – (5.24) match the equations derived to describe the exhaust of the Cr-alloy cells (equations (5.16) – (5.19)).

In other words, assuming the water gas shift reaction reaches equilibrium inside the cell itself or after the cell results in the same exhaust composition, for a given oxygen production rate and inlet gas mixture.

5.8 The Catalyst Effect on Combined Electrolysis

Section 5.3 summarizes that the performance between the Cr-alloy and alumina cells during combined electrolysis is markedly different. In section 5.6, the water gas shift reaction is shown to play an important role in determining the products of combined electrolysis. In section 5.7, it is shown that in a Cr-alloy cell system the water gas shift reaction achieves equilibrium but in an alumina cell system it does not.

The major difference between the two cells is the materials used for the construction of the manifolds and inlet/outlet tubes. As stated in section 3.4.2, the manifolds as well as the inlet and exhaust tubes of the alumina cell are made of alumina. Alumina is extremely stable at SOE operating temperatures. It does not react with carbon to form carbides. It also does not react with CO, CO_2 or H_2. It can react with H_2O to form

Al(OH)3, but the equilibrium constant at SOE operating temperatures is on the order of 1E-16. Such a low equilibrium constant makes the reaction highly improbable. Furthermore, alumina is not a known catalyst for the water gas shift reaction.

In contrast, both the manifolds and tubes of the Cr-alloy cells contain Cr and iron (Fe). The tubes also contain Ni. Cr is highly reactive with both H_2O and CO_2 to form the favorable chromium-oxide Cr_2O_3. For example, equilibrium calculations presented in Figure 5-23 and Figure 5-24 show that only the slightest presence of CO_2 in CO or H_2O in H_2 encourages the possibility of its formation. Furthermore, as exemplified in Figure 5-23, the formation of this oxide consumes the Cr such that other carbides can not form. For example, for $Cr_{23}C_6$ to form at 750°C, the mixture will have to contain at least 90% CO_2 (line with open squares). However, the line with filled triangles shows that if *any* CO_2 is present, Cr will *first* be consumed to form Cr_2O_3. Another chrome oxide is possible. CrO_2 can form at CO_2/CO concentrations near 100% CO_2 and H_2O/H_2 concentrations above 85% H_2O.

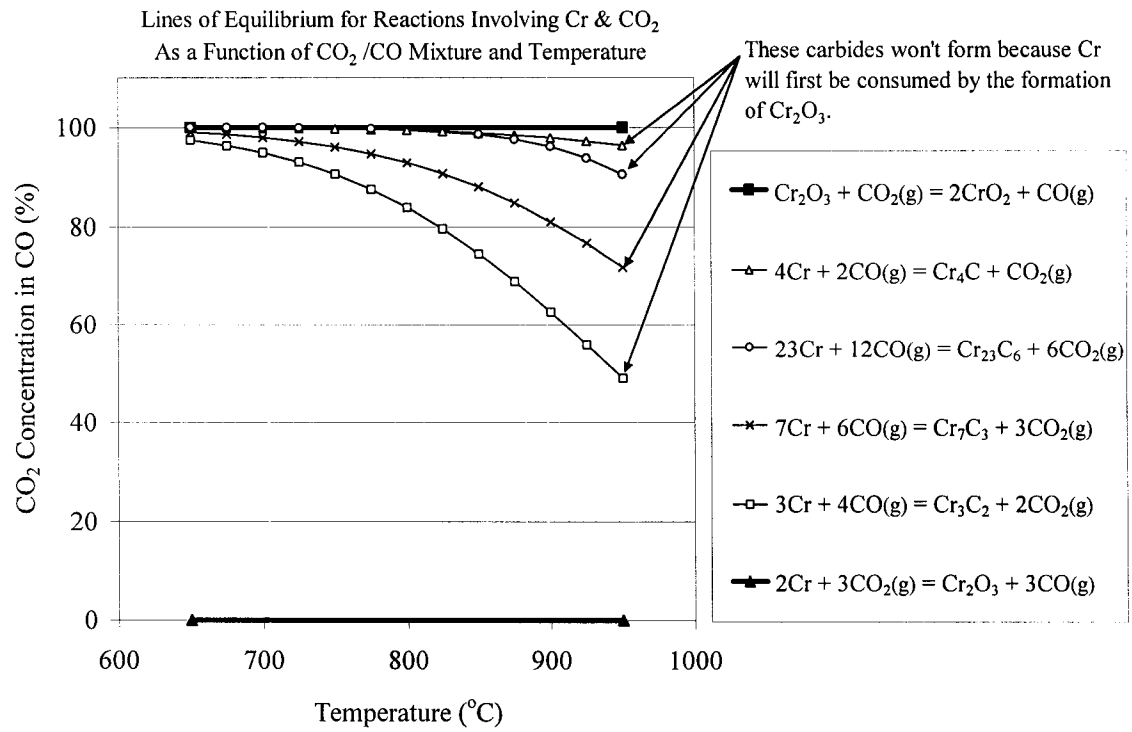

Figure 5-23 Equilibrium conditions for reactions between Cr and CO_2.

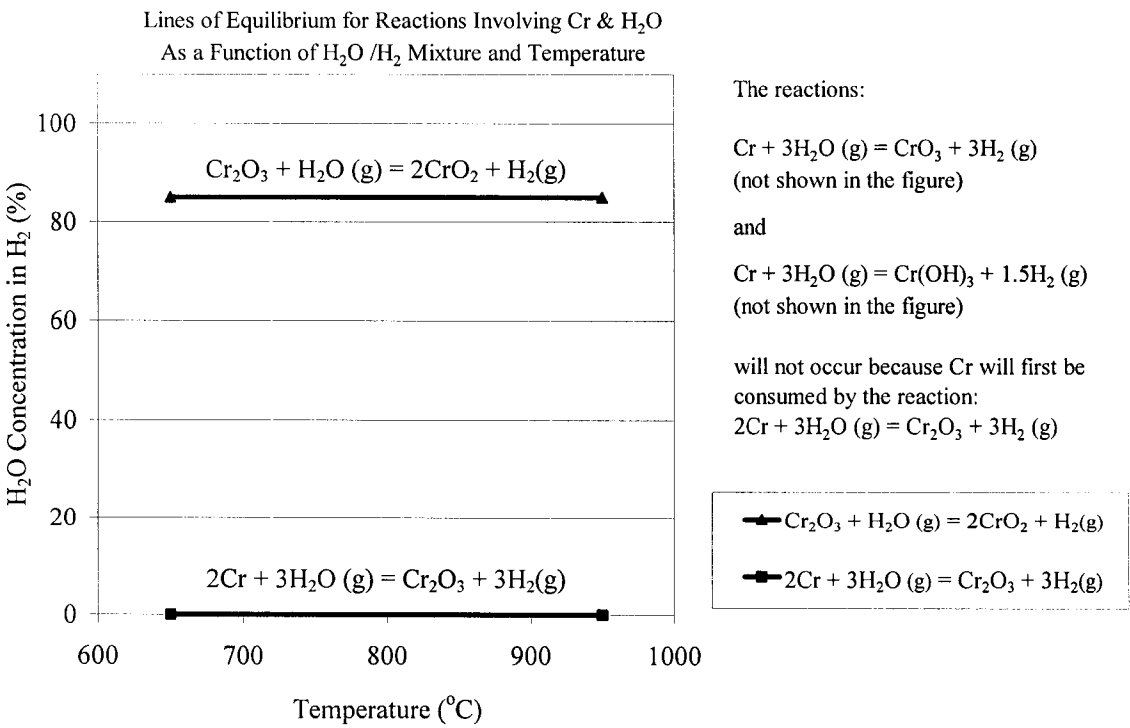

Figure 5-24 Equilibrium conditions for reactions between Cr and H_2O.

As it turns out, high temperature water gas shift catalysts are iron and chromium oxides [56]. For example, King states that the water gas shift reaction at temperatures above 300°C uses catalysts consisting of iron oxides "promoted by Cr_2O_3"[57]. The word "promoted" is used to imply the desire to push the water gas shift reaction in the forward direction such that CO is consumed. Higher temperatures favor CO production rather than H_2 production. To keep the reaction moving "forward" (H_2 production) the temperature is kept below 485°C [58]. However, SOE is operated at temperatures above 750°C where the equilibrium constant is on the order of 1 as shown in Figure 5-25. An equilibrium constant on the order of 1 implies the equilibrium composition will contain all gases CO_2, H_2O, H_2 and CO.

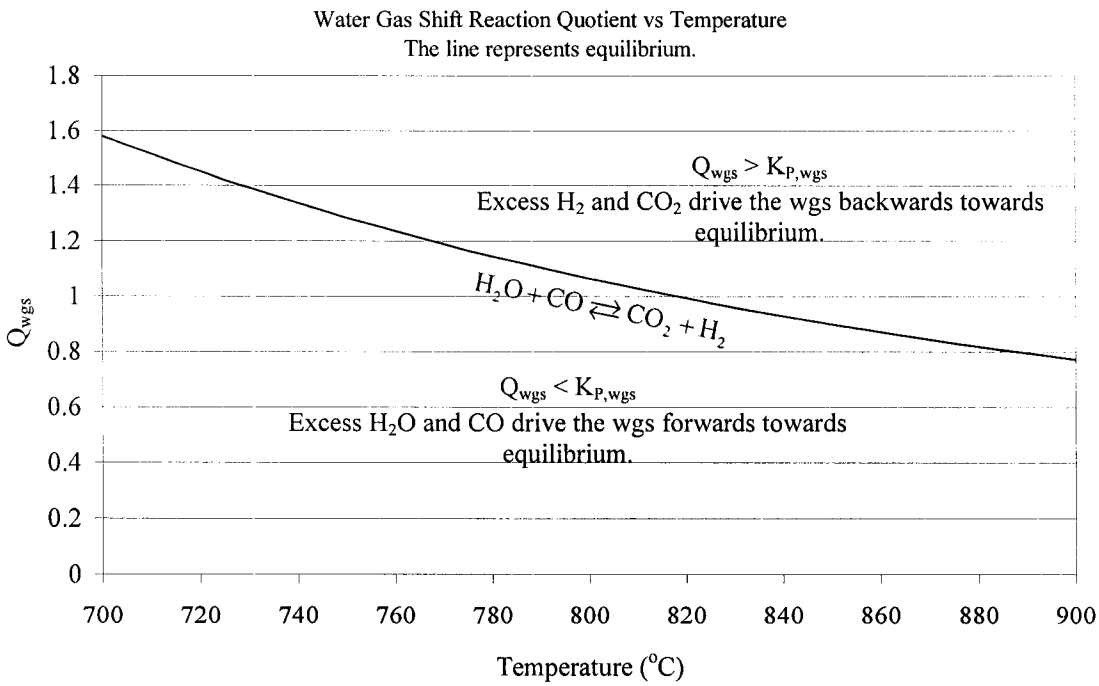

Figure 5-25 Equilibrium constant for the water gas shift reaction.

Results presented in sections 4.4.6 and 4.5.10 show that during combined electrolysis the alumina cells exhaust a greater concentration of H_2 than CO as compared to the Cr-alloy cells. Section 5.7 concluded that in fact, equilibrium is achieved in the Cr-alloy cells while the reaction quotient of the exhaust of alumina cells is greater than $K_{P,wgs}$. As shown in Figure 5-25, this means there is excess H_2 and CO_2 (as compared to the equilibrium composition). One could propose that chromium oxide is present in the Cr-alloy system, which pushes the composition of the mixture being electrolyzed to equilibrium.

Visual and X-ray analyses support this proposition. Despite the coating that was placed on the Cr-alloy manifolds, postmortem inspection reveals the manifolds turn green, as shown in Figure 5-26. The green color is indicative of chromium oxide which could occur if Cr migrates through the coating. Furthermore, X-ray analyses show that Cr migrates not only to the top Pt layer but also throughout the mixed Pt/YSZ layer. X-ray analyses are summarized in Appendix C

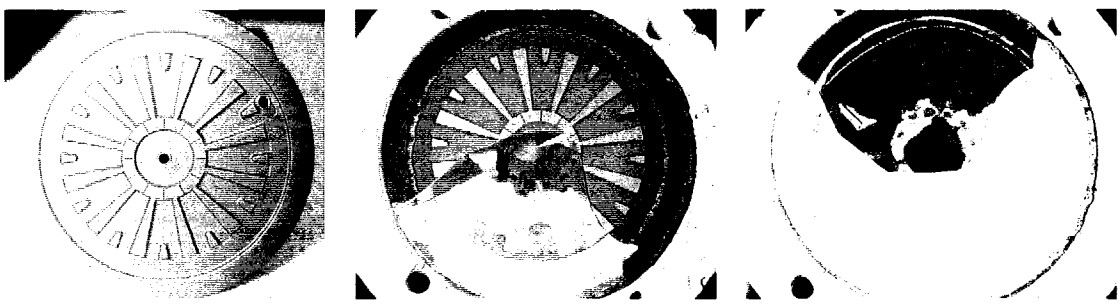

(unused) (50cell09) (50cell09)

Figure 5-26 Photos of Cr-alloy manifolds taken before and after electrolysis.

So it is evident that Cr_2O_3 exists in the Cr-alloy cells. But possibly the water gas shift reaction is not achieving equilibrium inside the cell, during electrolysis, but along

the exhaust tube. One should be reminded that the exhaust tube is Inconel, which contains both Fe and Cr. The exhaust tube could act as water gas shift "reactor", as described in section 5.7.2.

However, the two cell-types do not perform the same. If the water gas shift reaction is achieving equilibrium only upon leaving the cell, then why does for combined electrolysis the Cr-alloy cell outperform the alumina cell?

Section 5.4 hypothesizes that at low humidity combined electrolysis, alumina cells experience in essence a H_2O starvation. This is because gas chromatograph data indicate that alumina cells have a strong preference to H_2O molecules over CO_2 molecules. The question is then asked, should the same trends be seen in Cr-alloy performance curves?

If the water gas shift reaction is achieving equilibrium inside the cell, rather than along the exhaust tubes (in a reactor sense), then the H_2 produced by the H_2O electrolysis could react with CO_2 to produce more H_2O. One should remember that the equilibrium constant is on the order of unity so a significant portion of H_2O could be produced if mostly H_2O electrolysis were occurring at low voltages. Thus, H_2O starvation would not occur and an inflection point would not be observed.

If the water gas shift reaction truly does not achieve equilibrium until exhausting from the cell, another phenomenon could be helping the Cr-alloy cells: chemisorption of CO_2. Chemisorption is when molecules attach to a surface via a chemical bond. This is opposed to physisorption where the attachment is influence merely by van der Waals forces. The energy released during the adsorption process is an order of magnitude higher for chemisorption [59]. Such a process can fragment molecules which can aid in

reactions and thus supports catalysis. Table 5-3 shows that H_2, O_2 and CO all chemisorb onto pure Pt and Cr [59]. However, chemisorption of CO_2 does not occur on pure Pt. It should be noted that CO_2 does adsorb on an electronic promoted Pt surface [13] (which occurs when the Pt electrodes are placed in-between an electric potential) but maybe an electronic promoted Cr surface adsorbs CO_2 more easily. In Cr-alloy cells, possibly the chemisorption of CO_2 onto the migrated Cr throughout the electrode aids in CO_2 electrolysis at lower voltages and again, no inflection point in the IV performance curves is observed.

Table 5-3 Chemisorption abilities of different materials.

	O_2	CO	H_2	CO_2	N_2
Ti, Cr, Mo, Fe	+	+	+	+	+
Ni, Co	+	+	+	+	–
Pd, Pt	+	+	+	–	–
Mn, Cu	+	+	+	±	–
Al, Au	+	+	+	–	–
+ Strong chemisorption ± Chemisorption – No chemisorption					

5.9 Hydrogen Added to Carbon Dioxide Electrolysis Produces Water?

In section 4.5.1, the results of testing the effects of H_2 on CO_2 electrolysis are presented. An analysis was performed with the GC data in an attempt to understand the observations described.

If it is assumed that carbon is conserved across the cell (no carbon is deposited inside the cell) and that all the oxygen produced is from CO_2 only, then calculations using the data presented in Table 4-1 suggest there is too much CO for these assumptions to be

satisfied. Furthermore, the conservation of oxygen is violated in that oxygen leaving the cell falls short of what is supplied. However, if the water gas shift reaction is considered to occur between the CO_2 and H_2, then these results would make sense. The following explains.

When H_2 is added, it could combine with CO_2 to produce H_2O and CO via the water gas shift reaction. The initial presence of H_2O could increase the performance instantaneously since it is easier (requires less energy) to electrolyze than CO_2. Any left over H_2O not electrolyzed would partially account for the shortage of oxygen not detected in the exhaust and oxygen production. The creation of CO via the water gas shift reaction would also account for the excess CO detected.

The degradation in performance with the addition of H_2 could also be explained if H_2O were forming. This essentially creates a combined electrolysis atmosphere. As shown in section 5.3.1, the performance of initial tests of combined electrolysis in alumina cells requires time to become steady. Section 4.5.8 shows that for low humidity combined electrolysis significantly underperforms CO_2 electrolysis, followed by a period of degraded CO_2 electrolysis performance. The addition of H_2 to CO_2 electrolysis did not produce a *significant* decrease in performance probably because added quantities of H_2 were small but the trends are similar.

Finally, it is shown that there is a point where adding more H_2 induces no immediate response from the alumina cell. At such low H_2 concentrations (2%), if the water gas shift reaction were achieving equilibrium an immediate increase in response should still be seen. These observations corroborate the fact proved in section 5.7.2 that equilibrium

is not achieved in the alumina cells. For this reason, it would be interesting to electrolyze CO_2/H_2 in a Cr-alloy cell. An increase in performance would be a further indication that equilibrium is achieved inside the cell itself and the chrome oxide inside aids in oxygen production.

In summary, if the water gas shift reaction is considered, the results from the analysis of the GC data make sense because the analysis erroneously neglected any H_2O exhausting from the cell. In addition, some of the experimental observations can be explained. If this test were to be performed again, it may be helpful to use a humidity sensor to monitor change in humidity in the exhaust.

6 CONCLUSIONS

Several experiments and theoretical analyses were conducted on planar electrolysis cells as described herein operated at 750°C using 8% by mol YSZ electrolytes and 50/50 by weight Pt/YSZ electrodes. Two cell-types were tested that provided very different results. Therefore, general statements regarding combined electrolysis as a whole and independent of cell-type must be made carefully. Conclusions, mindful of the above, are drawn as follows.

6.1 Phenomenon Governing Combined Electrolysis

First and foremost, regardless of cell-type, combined electrolysis does not encourage carbon deposition and the make-up of its products is governed by the water gas shift reaction. The only difference between the two cell-types tested is that the exhaust composition of Cr-alloy cells achieve water gas shift reaction equilibrium whereas the exhaust composition of the alumina cells do not.

There are two possible reasons why the products of Cr-alloy cells appear to achieve the reaction equilibrium. One is that the Inconel exhaust tube acts as an adequate catalyst for the water gas shit reaction, providing the exhaust with more time to achieve equilibrium. A second scenario is that Cr-oxide inside the cell itself acts as a catalyst to push the electrolysis reaction to equilibrium. In actuality, probably both are happening. However, performance differences between the cells as presented in the following conclusions can be better explained with the second scenario.

6.2 Combined Electrolysis Preference to Water versus Carbon Dioxide

Alumina cells exhibit a strong preference to H_2O over CO_2. This result alleviates any concerns of significant H_2O build-up in a system like a Martian propellant production plant. Once the CH_4 is produced, the Sabatier reactor portion of the plant can be shut off and after a CO_2 electrolysis recovery period, the remaining oxygen required to satisfy the optimal 3.5:1 O/F ratio can be produced. On the other hand, had CO_2 been preferentially electrolyzed, H_2O would continually build up in the system requiring additional provisions of H_2 to produce the desired amount of CH_4. The H_2O could be extracted and used for life support supplies. But for a sample return, such a design is inefficient.

For Cr-alloy cells, exhaust data suggest only a slight preference to H_2O over CO_2. However, because of the uncertainly as to whether the water gas shift reaction is achieving equilibrium inside the cell or along the exhaust tubes, no solid conclusion can be made. Interpretation of the performance data supports the theory that equilibrium is attained inside the cell itself. The ability to electrolyze H_2O and CO_2 fairly equally allows for better utilization of CO_2, as compared to alumina cells. There may be an application where this is desired. However when implemented with a Sabatier reactor, the point is moot because all the carbon will be utilized (whether it is in the form of CO or CO_2) if the reactor is run H_2 rich.

6.3 Combined Electrolysis Performance Comparison between Cell-Types

Combined electrolysis performance of alumina cells is only competitive with Cr-alloy cells when the humidity in the mixture is high and the voltage is very low. This is

surprising, given the fact that CO_2 electrolysis performance of alumina cells is better than that of Cr-alloy cells.

One theory is that Cr-alloy cells have the ability to push the water gas shift reaction to equilibrium *during* electrolysis while the alumina cells do not. Alumina cells are shown to electrolyze more H_2O than CO_2 in essence depleting H_2O sources. However, if the water gas shift reaction reaches equilibrium during electrolysis, this means the H_2O supply will be replenished providing comparatively more H_2O to be electrolyzed. It is shown that for both cell-types, H_2O electrolysis outperforms CO_2 electrolysis. Thus for such a scenario performance would be boosted for combined electrolysis.

6.4 Combined Electrolysis Performance and Mixture Ratio

For a fixed oxygen-providing molar flow rate, combined electrolysis performance increases with humidity content. For Cr-alloy cells, the dependence on humidity content appears to be weak and can be neglected when considering its application in systems that will operate over a large range of H_2O/CO_2 mixture ratios. However for alumina cells, the dependency is strong. For example, decreasing the humidity content can drastically decrease oxygen production, depending upon operating voltage.

Again, the lack of a water gas shift reaction achieving equilibrium inside the alumina cell could be the culprit. At low humidity, the H_2O supply is easily diminished leaving only CO_2 to be electrolyzed as H_2O battles concentration gradients in order to reach reaction sites. Thus, performance declines. If the water gas shift reaction could be attained, H_2O could be replenished.

6.5 Combined Electrolysis Effect on Cell Health

CO_2 electrolysis performance appears to degrade immediately following combined electrolysis. However, additional CO_2 electrolysis encourages considerable (if not full) recovery. The limited amount of Cr-alloy data suggests the initial CO_2 electrolysis performance degradation is not as significant as for the alumina cells.

A proposed hypothesis to the cause of the degradation is that H_2 adsorption is the culprit, blocking reaction sites. When pure CO_2 gas is administered, the H_2 partial pressure in the overlying flow diminishes allowing H_2 to desorb over time. The equilibrium occurring inside the cell during electrolysis explains why combined electrolysis' encumbrance of subsequent CO_2 electrolysis is less for Cr-alloy cells than for alumina cells. If H_2 adsorption is the problem, the water gas shift reaction pushes H_2 to react with CO_2. This frees the reaction site for the newly formed H_2O molecule which is easily electrolyzed. H_2 is still then created but, assuming this scenario, reaction sites blocked by H_2 might be freed more quickly than in an alumina cell.

6.6 Establishing Reliable Combined Electrolysis Performance

Cr-alloy cells do not appear to have any difficulty establishing stable performance while executing combined electrolysis. However, combined electrolysis in alumina cells requires many performance tests before it exhibits repeatable performance. This conditioning takes a couple of days as opposed to a few hours as that exhibited by Cr-alloy cells.

Furthermore, even if a stable operation at one mixture ratio in an alumina cell is established, tests show the cells require additional time to achieve steady state after

changing mixture ratio or oxygen-providing molar flow rate. This suggests a single period of combined electrolysis pre-conditioning would not be enough to ensure performance capable of adapting quickly to changing input streams.

6.7 Prediction of Combined Electrolysis Products

The product gas of combined electrolysis can be guaranteed by routing it through a water gas shift reactor because it is proven that constituents are conserved across the electrolysis cell (i.e. no carbon or other deposition). In the case of the Cr-alloy cells, no additional reactor is needed since the water gas shift reaction equilibrium is proven to occur in the cell system.

6.8 Minimum Voltage Required for Combined Electrolysis

The minimum required voltage to initiate combined electrolysis is independent of the H_2O/CO_2 mixture ratio. This finding conveniently allows for any input mixture without concern for increased voltage requirements (and thus power). Such a situation will always arise as a system, that delivers input to a combined electrolysis unit, requires time to achieve equilibrium.

However, should a gas that is a byproduct of the electrolysis reaction be present in the carrier gas, the minimum required voltage to initiate electrolysis increases. The amount of increase is directly proportional to the concentration of this byproduct gas (i.e. H_2 if electrolyzing H_2O or CO if electrolyzing CO_2). This can have consequences for a propellant/life support production plant on Mars. Because H_2 is a precious commodity, it

is recycled back through the electrolysis unit becoming a part of the inlet gas. This, in turn, increases the voltage required for electrolysis and thus DC power.

6.9 Flow Rate Effects

If flow rate effects are to be minimized for a given investigation, it is best to establish and test above the mass limiting oxygen-providing molar flow rate for a given cell-type and *input mixture*. The values determined in this dissertation are only relevant to the cells used but the relative trends can be applied to similar systems. For Cr-alloy cells, flow rates matching the mass limiting flow rate of CO_2 electrolysis enables stable electrolysis for H_2O and combined electrolysis. However for alumina cells, stable H_2O electrolysis is shown to require flow rates higher than flow rates required for stable CO_2 and combined electrolysis. Such trends call for special consideration when designing a system that requires a SOE unit to perform electrolysis on different input gases. For example, such a system may need to be optimized to account for different performances for a fixed flow rate.

6.10 Combined Electrolysis versus Water Electrolysis

A definitive comparison between combined electrolysis and H_2O electrolysis was only performed with alumina cells. Alumina cells show combined electrolysis over a wide range of mixture ratio underperforms H_2O electrolysis of high humidity (83 – 91%).

High humidity electrolysis was not tested with Cr-alloy cells. However, it can be noted that for Cr-alloy cells one test shows combined electrolysis outperforms H_2O electrolysis of lower humidity (45%). Because it was later realized that for either cell-

type H_2O electrolysis is strongly dependent upon humidity content (H_2O in He for example), it is believed H_2O electrolysis of higher humidity would outperform combined electrolysis regardless of cell-type.

6.11 Combined Electrolysis versus Carbon Dioxide Electrolysis

For Cr-alloy cells, combined electrolysis fully outperforms CO_2 electrolysis. For alumina cells, combined electrolysis can outperform CO_2 electrolysis depending upon humidity and voltage.

High humidity combined electrolysis in alumina cells fully outperforms CO_2 electrolysis. However, low humidity only outperforms CO_2 electrolysis at low voltages and underperforms CO_2 electrolysis at mid to high voltages. The decreased performance of low humidity combined electrolysis at higher voltages does not preclude it from being useful. Quite the contrary, alumina cells may be just the answer for low voltage applications where DC power needs to be minimized or voltage supplies are limited.

6.12 Summary

So at this stage, if one were to design a Martian propellant production unit employing combined electrolysis, does one use a Cr-alloy or alumina cell? For life support, does the recommendation change?

The answer depends upon the constraints of the rest of the system in which combined electrolysis is to be implemented. For propellant production, one might optimize the system for a given CO_2/H_2O mixture ratio and then the cell that performs best at that ratio would be a likely candidate. For life support, humidity levels can

change dependent upon crew activity. If consistent performance regardless of humidity level is required, preliminary results show Cr-alloy cells should be pursued. However, if thermal energy is more easily available than electric potential energy, or DC power, an alumina cell can be consistently run at low voltages for all humidity levels.

Of course, the best combined electrolysis performance will probably be achieved by combing aspects of each cell-type into one. How to achieve this is yet to be found but future work, as suggested in the next section, will help. In the mean time, it is felt the work presented here provides a better general understanding of combined electrolysis. Decisions regarding how to best implement it will be better informed. Then the obtained data can help engineers perform first order analyses of system designs accounting for real life effects, rather than just extrapolating CO_2 or H_2O electrolysis data.

The objectives that were established at the beginning of this research have all been addressed. Though it is only a dent in the issues to be considered, it is with great hope that this work will aid in the pursuit of Mars exploration.

7 FUTURE WORK

Someone once said that good scientific research poses more questions than it answers. If that were the sole criteria of a good dissertation, then this dissertation could be judged a good one. Several questions that developed over the course of this research as well as further investigations await exploration.

First, is Cr acting as a catalyst to promote the water gas shift reaction *inside* the electrolysis cell such that oxygen production is improved? One idea is to test an alumina cell with an electrode that contains Cr additives. If a Cr additive boosts the alumina cell performance *and* the exhaust composition reaches equilibrium, then the answer to the question is yes. If only the cell performance is increased, then possibly the ability of CO_2 chemisoprtion on Cr is partially the reason for the increase in performance. Another idea is to add Inconel tubes to the alumina cells but this would not resolve the difference in performance seen between the two cell-types. No doubt an investigation of this sort could lead to the optimization of combined electrolysis SOE cells.

Does increasing the flow rate of combined electrolysis always deteriorate performance? This is shown to occur during testing of the alumina cells. Flow rate affects on combined electrolysis were not tested for Cr-alloy cells. Therefore, flow rate effects should be tested with Cr-alloy cells to determine if the phenomenon is universal or dependent upon cell-type. Also, stable electrolysis at the higher flow rates in the alumina cells should be pursued to establish the level of decline in performance. Because it was not pursued in this work, possibly the cell just needs time to adjust and performance may eventually equalize at a level that is not deteriorated at all. Or, maybe it just declines for

the given inlet mixture tested. Since adding H_2O to an input stream increases the total oxygen-providing molar flow rate, such information is critical in implementing combined electrolysis into a design that has fixed CO_2 input but changing humidity input.

In Cr-alloy cells, does combined electrolysis outperform H_2O electrolysis of high humidity? Higher humidity H_2O electrolysis needs to be tested against combined electrolysis to fairly assess their relative performances. At this juncture, it is shown that combined electrolysis in Cr-alloy cells barely outperforms 45% H_2O electrolysis. The application of pure H_2O electrolysis of any humidity in conjunction with combined electrolysis is probably not too relevant, but the investigation could provide insight to understanding the overall performance of combined electrolysis in general.

Further investigation is needed to completely quantify the performance of combined electrolysis for more H_2O/CO_2 mixture ratios. In this dissertation, only alumina cells have been rigorously tested at humidity of approximately 30% and 70%. Cr-alloy cells have not been rigorously tested at all. How combined electrolysis behaves at various humidity levels will help system engineers utilize the technology to its fullest advantage.

Another curious observation that needs study is the change in structure of the alumina electrodes as compared to that of the Cr-alloy electrodes. Changes in electrode structure can affect the long term stability of cells. The increased coagulated appearance could be explored through thermal modeling.

Finally, it is important to note that electrode kinetics is not investigated in this dissertation. These are dependent upon materials used (i.e. Pt versus Cr contamination), operating temperature (is heating effects encouraging faster reaction kinetics) and species

involved in the electrolysis reactions (competition between CO_2 and H_2O to adsorb and migrate to reaction sites, ease of CO versus H_2 to desorb, etc.). Thus the study of electrode kinetics should be applied to better explain the phenomena observed during combined electrolysis for the different cell-types.

APPENDIX A DERIVATIONS

A.1 Minimum Required Voltage for SOE

The first and second law of thermodynamics [55], [60] for an open system of simple compressible substances are, respectively:

$$\dot{Q} - \dot{W} + \sum_{in}\left(\dot{N}_i \bar{h}_i + \dot{m}_i g z + \dot{m}_i \frac{V^2}{2} \right) - \sum_{out}\left(\dot{N}_i \bar{h}_i + \dot{m}_i g z + \dot{m}_i \frac{V^2}{2} \right) = \frac{dE_{cv}}{dt} \tag{A.1}$$

$$\dot{S}_{gen} = \dot{S} + \sum_{out} \dot{N}_i \bar{s}_i - \sum_{in} \dot{N}_i \bar{s}_i - \sum_{j} \frac{\dot{Q}_j}{T_j} \geq 0 \tag{A.2}$$

where the signs of heat and work transfer follow the heat engine sign convention [60].

If one neglects the contributions from potential and kinetic energies as well as assumes steady state operation, the first law of thermodynamics for a system can be generally expressed as:

$$\dot{Q} - \dot{W} + \sum_{in} \dot{N}_i \bar{h}_i - \sum_{out} \dot{N}_i \bar{h}_i = 0 \tag{2.1}$$

Additionally if the system is assumed reversible, the second law of thermodynamics can be represented in general as:

$$0 = \sum_{out} \dot{N}_i \bar{s}_i - \sum_{in} \dot{N}_i \bar{s}_i - \frac{\dot{Q}}{T} \tag{A.3}$$

The assumption that the system is reversible implies no losses occur, thus the minimum amount of power required for the system can be calculated by combining equation (2.1) and (A.3):

$$\dot{W}_{min} = \sum_{in} \dot{N}_i \left(\bar{h}_i - T\bar{s}_i \right) - \sum_{out} \dot{N}_i \left(\bar{h}_i - T\bar{s}_i \right) \tag{A.4}$$

Using the definition of the molar Gibbs function [55],

$$\bar{g}_i = \bar{h}_i - T\bar{s}_i \tag{A.5}$$

equation (A.4) can be written as:

$$\dot{W}_{min} = \sum_{in} \dot{N}_i \bar{g}_i - \sum_{out} \dot{N}_i \bar{g}_i \tag{A.6}$$

Equation (A.4) or (A.6) can be applied to an electrolysis system to calculate V_{min} required to electrolyze an oxygen-providing molecule such as CO_2 or H_2O. Consider the system outlined in Figure 5-1. Each stream entering and leaving the cell must be taken into account. It should be noted that the molar ratios of the i^{th} gas entering the cell is represented with X_i and all streams exiting the cell are functions of these.

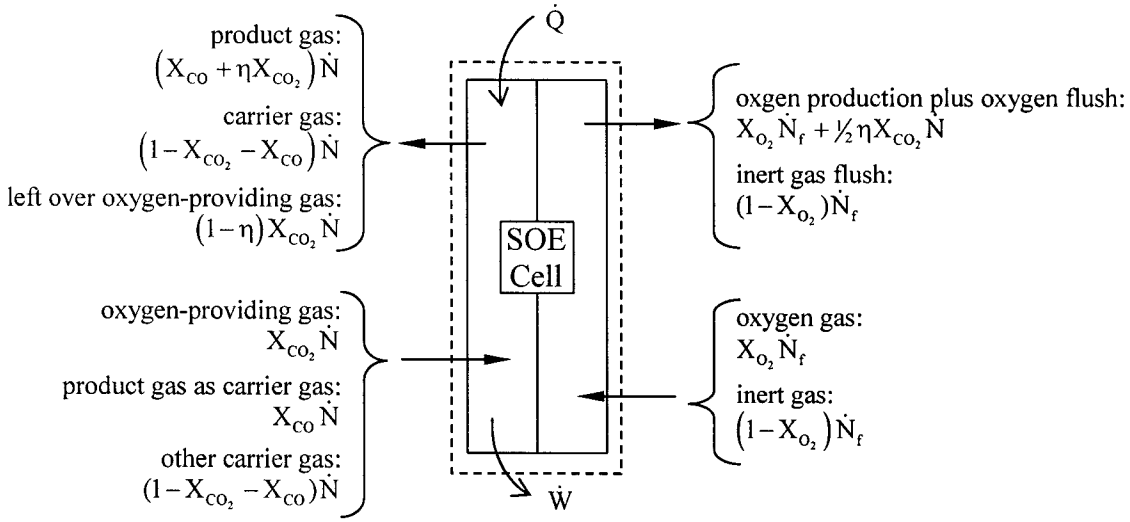

Figure 5-1 Thermodynamic system considered for an electrolysis cell.

It should be noted that because chemical reactions are occurring inside the cell, molar enthalpy is evaluated using the enthalpy of formation to avoid difficulties of different reference states from different thermodynamic tables:

$$\bar{h}_{i,T,P} = \Delta\bar{h}^{\circ}_{f,298,i} + \bar{h}_{T,P,i} - \bar{h}_{298K,1\,atm,i} \tag{A.7}$$

Additionally, entropy is calculated by integrating one of the Gibbs equations [61] isothermally from a reference pressure of 1 atm to the partial pressure of the constituent:

$$\bar{s}_{i,T} = \bar{s}^{\circ}_{i,T,1\,atm} - \Re \ln\left(\frac{P_i}{1\,atm}\right) \tag{A.8}$$

Condensing the expressions into Gibbs energy functions reveals leftover natural logarithm terms which are attributed to "entropy mixing". These entropy mixing terms are what separate the analysis of a simple Nernst oxygen partial pressure calculation to that of an engineering system.

For example, consider the electrolysis of CO_2. First the availability of CO_2 is calculated by writing the full availability of the entering and exiting CO_2 streams:

$$\begin{aligned}&\bar{g}_{CO_2,in} - \bar{g}_{CO_2,out} = \\ &X_{CO_2}\dot{N}_{inlet}\left[\left(\Delta\bar{h}^{\circ}_f + \bar{h}_T - \bar{h}_{STP} - T\bar{s}^{\circ}_T\right)_{CO_2} + \Re T \ln\left(P_c X_{CO_2}\right)\right] - \\ &(1-\eta)X_{CO_2}\dot{N}_{inlet}\left\{\left(\Delta\bar{h}^{\circ}_f + \bar{h}_T - \bar{h}_{STP} - T\bar{s}^{\circ}_T\right)_{CO_2} + \Re T \ln\left[P_c(1-\eta)X_{CO_2}\right]\right\}\end{aligned} \tag{A.9}$$

After combining like terms, equation (A.9) reduces to:

$$\begin{aligned}&\bar{g}_{CO_2,in} - \bar{g}_{CO_2,out} = \eta X_{CO_2}\dot{N}_{inlet}\left(\Delta\bar{h}^{\circ}_f + \bar{h}_T - \bar{h}_{STP} - T\bar{s}^{\circ}_T\right)_{CO_2} + \\ &X_{CO_2}\dot{N}_{inlet}\Re T\left\{\ln\left(P_c X_{CO_2}\right) - (1-\eta)\ln\left[P_c(1-\eta)X_{CO_2}\right]\right\}\end{aligned} \tag{A.10}$$

The same procedure can be done for the product gas (i.e. CO) and oxygen, respectively:

$$\begin{aligned}&\bar{g}_{CO,in} - \bar{g}_{CO,out} = -\eta X_{CO_2}\dot{N}_{inlet}\left(\Delta\bar{h}^{\circ}_f + \bar{h}_T - \bar{h}_{STP} - T\bar{s}^{\circ}_T\right)_{CO} + \\ &\dot{N}_{inlet}\Re T\left\{X_{CO}\ln\left(P_c X_{CO}\right) - \left(X_{CO} + \eta X_{CO_2}\right)\ln\left[P_c\left(X_{CO} + \eta X_{CO_2}\right)\right]\right\}\end{aligned} \tag{A.11}$$

$$\bar{g}_{O_2,in} - \bar{g}_{O_2,out} = -\frac{\eta}{2} X_{CO_2} \dot{N}_{inlet} \left(\Delta\bar{h}_f^\circ + \bar{h}_T - \bar{h}_{STP} - T\bar{s}_T^\circ \right)_{O_2} +$$
$$\dot{N}_{inlet} \Re T \left\{ X_{O_2} \frac{\dot{N}_f}{\dot{N}_{inlet}} \ln\left(P_a X_{O_2} \right) - \right.$$
$$\left. \left(X_{O_2} \frac{\dot{N}_f}{\dot{N}_{inlet}} + \frac{\eta}{2} X_{CO_2} \right) \ln\left[P_a \left(\frac{\dot{N}_f / \dot{N}_{inlet} X_{O_2} + \eta/2 X_{CO_2}}{\dot{N}_f / \dot{N}_{inlet} + \eta/2 X_{CO_2}} \right) \right] \right\} \qquad \text{(A.12)}$$

The first term on the right-hand side of equations (A.10) - (A.12) can be combined to form the Gibbs energy for a given reaction (i.e. $CO_2 \rightarrow CO + \frac{1}{2} O_2$) at the reaction temperature, T:

$$\Delta G_{T,rxn}^\circ = \left(\Delta\bar{h}_f^\circ + \bar{h}_T - \bar{h}_{STP} - T\bar{s}_T^\circ \right)_{CO_2} - \left(\Delta\bar{h}_f^\circ + \bar{h}_T - \bar{h}_{STP} - T\bar{s}_T^\circ \right)_{CO} -$$
$$\frac{1}{2} \left(\Delta\bar{h}_f^\circ + \bar{h}_T - \bar{h}_{STP} - T\bar{s}_T^\circ \right)_{O_2} \qquad (5.2)$$

Such that equations (A.10) - (A.12) can be combined and written as:

$$\bar{g}_{CO_2,in} - \bar{g}_{CO_2,out} + \bar{g}_{CO,in} - \bar{g}_{CO,out} + \bar{g}_{O_2,in} - \bar{g}_{O_2,out} =$$
$$\eta X_{CO_2} \Delta G_{T,rxn}^\circ +$$
$$X_{CO_2} \dot{N}_{inlet} \Re T \left\{ \ln\left(P_c X_{CO_2} \right) - (1-\eta) \ln\left[P_c (1-\eta) X_{CO_2} \right] \right\} +$$
$$\dot{N}_{inlet} \Re T \left\{ X_{CO} \ln\left(P_c X_{CO} \right) - \left(X_{CO} + \eta X_{CO_2} \right) \ln\left[P_c \left(X_{CO} + \eta X_{CO_2} \right) \right] \right\} +$$
$$\dot{N}_{inlet} \Re T \left\{ X_{O_2} \frac{\dot{N}_f}{\dot{N}_{inlet}} \ln\left(P_a X_{O_2} \right) - \right.$$
$$\left. \left(X_{O_2} \frac{\dot{N}_f}{\dot{N}_{inlet}} + \frac{\eta}{2} X_{CO_2} \right) \ln\left[P_a \left(\frac{\dot{N}_f / \dot{N}_{inlet} X_{O_2} + \eta/2 X_{CO_2}}{\dot{N}_f / \dot{N}_{inlet} + \eta/2 X_{CO_2}} \right) \right] \right\} \qquad \text{(A.13)}$$

Dependence on the cathode pressure can be removed when equation (A.13) is further reduced by expanding the natural logarithm terms, for example $\ln (P_c X_{CO}) = \ln P_c + \ln X_{CO}$. The terms that contain P_c then cancel:

$$X_{CO_2}\dot{N}_{inlet}\Re T\left\{\ln\left(P_c\right)-\left(1-\eta\right)\ln\left(P_c\right)\right\}+$$
$$\dot{N}_{inlet}\Re T\left\{X_{CO}\ln\left(P_c\right)-\left(X_{CO}+\eta X_{CO_2}\right)\ln\left(P_c\right)\right\}=0 \qquad \text{(A.14)}$$

Equation (A.13) reduces to:

$$\bar{g}_{CO_2,in}-\bar{g}_{CO_2,out}+\bar{g}_{CO,in}-\bar{g}_{CO,out}+\bar{g}_{O_2,in}-\bar{g}_{O_2,out}=\eta X_{CO_2}\Delta G^{\circ}_{T,rxn}+$$
$$\dot{N}_{inlet}\Re T\left\{\left[X_{CO_2}\ln X_{CO_2}-\left(X_{CO_2}-\eta X_{CO_2}\right)\ln\left(X_{CO_2}-\eta X_{CO_2}\right)\right]+\right.$$
$$\left[X_{CO}\ln X_{CO}-\left(X_{CO}+\eta X_{CO_2}\right)\ln\left(X_{CO}+\eta X_{CO_2}\right)\right]+$$
$$\left.\left[X_{O_2}\frac{\dot{N}_f}{\dot{N}_{inlet}}\ln\left(P_a X_{O_2}\right)-\left(X_{O_2}\frac{\dot{N}_f}{\dot{N}_{inlet}}+\frac{\eta}{2}X_{CO_2}\right)\ln\left(P_a\frac{\dot{N}_f/\dot{N}_{inlet}X_{O_2}+\eta/2\,X_{CO_2}}{\dot{N}_f/\dot{N}_{inlet}+\eta/2\,X_{CO_2}}\right)\right]\right\} \qquad \text{(A.15)}$$

The carrier gas "uninvolved" in the electrolysis reaction ends up playing no part in the thermodynamic process and completely drops out of equation (A.4). For example, summing only the right side of equation (A.4) for the uninvolved carrier gas (assume it is N_2):

$$\bar{g}_{N_2,in}-\bar{g}_{N_2,out}=$$
$$\left(1-X_{CO_2}-X_{CO}\right)\dot{N}_{Total}\left\{\left(\Delta h_f^{\circ}+h_T-h_{STP}-Ts_T^{\circ}\right)_{N_2}+\Re T\ln\left[P_c\left(1-X_{CO_2}-X_{CO}\right)\right]\right\}-$$
$$\left(1-X_{CO_2}-X_{CO}\right)\dot{N}_{Total}\left\{\left(\Delta h_f^{\circ}+h_T-h_{STP}-Ts_T^{\circ}\right)_{N_2}+\Re T\ln\left[P_c\left(1-X_{CO_2}-X_{CO}\right)\right]\right\}$$
$$=0 \qquad \text{(A.16)}$$

The only stream not yet taken into account is the inert flush. This stream does not drop out because its partial pressure changes with the addition of more molecules from oxygen production. Thus an entropy mixing term appears:

$$\overline{g}_{\text{inert flush,in}} - \overline{g}_{\text{inert flush,out}} =$$

$$\left(1-X_{O_2}\right)\dot{N}_f \Re T\left\{\ln\left[P_a\left(1-X_{O_2}\right)\right]-\ln\left[P_a\left(\frac{\left(1-X_{O_2}\right)^{\dot{N}_f/\dot{N}_{inlet}}}{\dot{N}_f/\dot{N}_{inlet}+\eta/2\,X_{CO_2}}\right)\right]\right\}=$$

$$\dot{N}_f \Re T\left[\left(1-X_{O_2}\right)\ln\left(\frac{\dot{N}_f/\dot{N}_{inlet}+\eta/2\,X_{CO_2}}{\dot{N}_f/\dot{N}_{inlet}}\right)\right] \qquad \text{(A.17)}$$

Plugging equations (A.15) - (A.17) into equation (A.6), the minimum power required for CO_2 electrolysis is:

$$\dot{W}_{min} = \eta X_{CO_2}\dot{N}_{inlet}\Delta G^{\circ}_{T,rxn} +$$

$$X_{CO_2}\dot{N}_{inlet}\Re T\left\{\left[\ln X_{CO_2}-(1-\eta)\ln\left(X_{CO_2}-\eta X_{CO_2}\right)\right]+\right.$$

$$\left[\frac{X_{CO}}{X_{CO_2}}\ln X_{CO}-\left(\frac{X_{CO}}{X_{CO_2}}+\eta\right)\ln\left(X_{CO}+\eta X_{CO_2}\right)\right]+$$

$$\left[\frac{X_{O_2}}{X_{CO_2}}\frac{\dot{N}_f}{\dot{N}_{inlet}}\ln\left(P_a X_{O_2}\right)-\left(\frac{X_{O_2}}{X_{CO_2}}\frac{\dot{N}_f}{\dot{N}_{inlet}}+\frac{\eta}{2}\right)\ln\left(P_a\frac{\dot{N}_f/\dot{N}_{inlet}X_{O_2}+\eta/2\,X_{CO_2}}{\dot{N}_f/\dot{N}_{inlet}+\eta/2\,X_{CO_2}}\right)\right]+$$

$$\left.\frac{\dot{N}_f}{\dot{N}_{inlet}}\left[\left(\frac{1-X_{O_2}}{X_{CO_2}}\right)\ln\left(\frac{\dot{N}_f/\dot{N}_{inlet}+\eta/2\,X_{CO_2}}{\dot{N}_f/\dot{N}_{inlet}}\right)\right]\right\} \qquad \text{(A.18)}$$

The minimum work required per mol of CO_2 electrolyzed can be calculated by diving minimum power of equation (A.18) by the molar flow rate of CO_2 electrolyzed (or the oxygen-providing portion of the total inlet that is utilized). The voltage required to produce this minimum work is then calculated by further dividing by $2\Im$:

$$V_{min} = \dot{W}_{min}\frac{1}{\dot{N}_{CO_2}2\Im} = \frac{\dot{W}_{min}}{\eta X_{CO_2}\dot{N}_{inlet}2\Im} \qquad \text{(A.19)}$$

A unit analysis of equation (A.19) best explains from where the factor of two originates:

$$[V]=\left[\frac{J}{s}\right]\left[\frac{s}{\text{mol of } CO_2}\right]\left[\frac{\left(\begin{matrix}CO_2 \text{ molecule}\\ \text{electrolyzed}\end{matrix}\right)}{2e^-}\right]\left[\frac{\text{mol of } CO_2}{6.022x10^{+23}\ \text{molecules}}\frac{e^-}{1.6x10^{-19}\,C}\right]\left[\frac{V\text{-}C}{J}\right] \qquad (A.20)$$

Combining equations (A.18) and (A.19) and reducing P_a terms (like was previously done with the P_c terms), V_{min} required to electrolyze CO_2 is:

$$V_{min}=\frac{\Delta G^{\circ}_{T,rxn}}{2\Im}+\frac{\Re T}{2\Im}\frac{1}{\eta}\left\{\left[\eta\ln X_{CO_2}-(1-\eta)\ln(1-\eta)\right]+\right.$$
$$\left[\frac{X_{CO}}{X_{CO_2}}\ln X_{CO}-\left(\frac{X_{CO}}{X_{CO_2}}+\eta\right)\ln\left(X_{CO}+\eta X_{CO_2}\right)\right]-\frac{\eta}{2}\ln P_a$$
$$\left[\frac{X_{O_2}}{X_{CO_2}}\frac{\dot{N}_f}{\dot{N}_{inlet}}\ln X_{O_2}-\left(\frac{X_{O_2}}{X_{CO_2}}\frac{\dot{N}_f}{\dot{N}_{inlet}}+\frac{\eta}{2}\right)\ln\left(\frac{\dot{N}_f/\dot{N}_{inlet}X_{O_2}+\eta/2\,X_{CO_2}}{\dot{N}_f/\dot{N}_{inlet}+\eta/2\,X_{CO_2}}\right)\right]+$$
$$\left.\frac{\dot{N}_f}{\dot{N}_{inlet}}\frac{(1-X_{O_2})}{X_{CO_2}}\left[\ln\left(\frac{\dot{N}_f/\dot{N}_{inlet}+\eta/2\,X_{CO_2}}{\dot{N}_f/\dot{N}_{inlet}}\right)\right]\right\} \qquad (5.1)$$

A.2 Water Removal from a Theoretical Solution

The original solution as a function of P_{H_2}:P_{CO} yields P_{CO_2}, P_{H_2O}, P_{CO}, and P_{H_2}. Their sum is P_T, or 0.91 atm. The H_2O is condensed at ambient pressure. Thus as the H_2O condenses, the total pressure of the exhaust after condensation must remain at 0.91 atm. Subsequently, changes in the partial pressures of the gas occur, now denoted P_i'.

$$P_T = P_{CO_2} + P_{H_2O} + P_{H_2} + P_{CO} \tag{A.21}$$

Assign a new variable is assigned to the sum of the partial pressures excluding P_{H_2O}:

$$P'_T = P_{CO_2} + P_{H_2} + P_{CO} \tag{A.22}$$

Re-arranging:

$$1 = \frac{P_{CO_2} + P_{H_2} + P_{CO}}{P'_T} \tag{A.23}$$

$$P_T \cdot 1 = P_T \cdot \frac{P_{CO_2} + P_{H_2} + P_{CO}}{P'_T} \tag{A.24}$$

But P_T also can be written:

$$P_T = P'_{CO_2} + P'_{H_2} + P'_{CO} \tag{A.25}$$

Thus,

$$P'_{CO_2} = \frac{P_T}{P'_T} \cdot P_{CO_2} \tag{A.26}$$

$$P'_{CO} = \frac{P_T}{P'_T} \cdot P_{CO} \tag{A.27}$$

$$P'_{H_2O} = \frac{P_T}{P'_T} \cdot P_{H_2O} \tag{A.28}$$

A.3 Correcting Gas Chromatograph Data for Air Leaks

The raw data from the GC yields measurements of P_{CO_2}, P_{H_2O}, P_{CO}, P_{H_2}, P_{N_2} and P_{O_2}. Their sum is P_T, or 0.91 atm. If it is assumed that air leaked into the GC sample, then the data can be "corrected" as follows, now denoted P_i'. (The method is similar to that presented in Appendix A.2):

$$P_T = P_{CO_2} + P_{H_2O} + P_{H_2} + P_{CO} + P_{N_2} + P_{O_2} \tag{A.29}$$

$$P'_T = P_{CO_2} + P_{H_2} + P_{CO} \tag{A.30}$$

$$1 = \frac{P_{CO_2} + P_{H_2} + P_{CO}}{P'_T} \tag{A.31}$$

$$P_T \cdot 1 = P_T \cdot \frac{P_{CO_2} + P_{H_2} + P_{CO}}{P'_T} \tag{A.32}$$

But P_T also can be written:

$$P_T = P'_{CO_2} + P'_{H_2} + P'_{CO} \tag{A.33}$$

Thus,

$$P'_{CO_2} = \frac{P_T}{P'_T} \cdot P_{CO_2} \tag{A.34}$$

$$P'_{CO} = \frac{P_T}{P'_T} \cdot P_{CO} \tag{A.35}$$

and

$$P'_{H_2O} = \frac{P_T}{P'_T} \cdot P_{H_2O} \tag{A.36}$$

A.4 Normalizing Partial Pressures of Combined Electrolysis Exhaust

First the normalization of the P_{H_2} data will be considered. As exemplified in Figure A-1, all theoretical trends are linear. Dividing each linear P_{H_2} solution by its slope would result in a line with the slope of 1. Thus, if all solutions were divided by their unique slope, the solutions would all align on the same line.

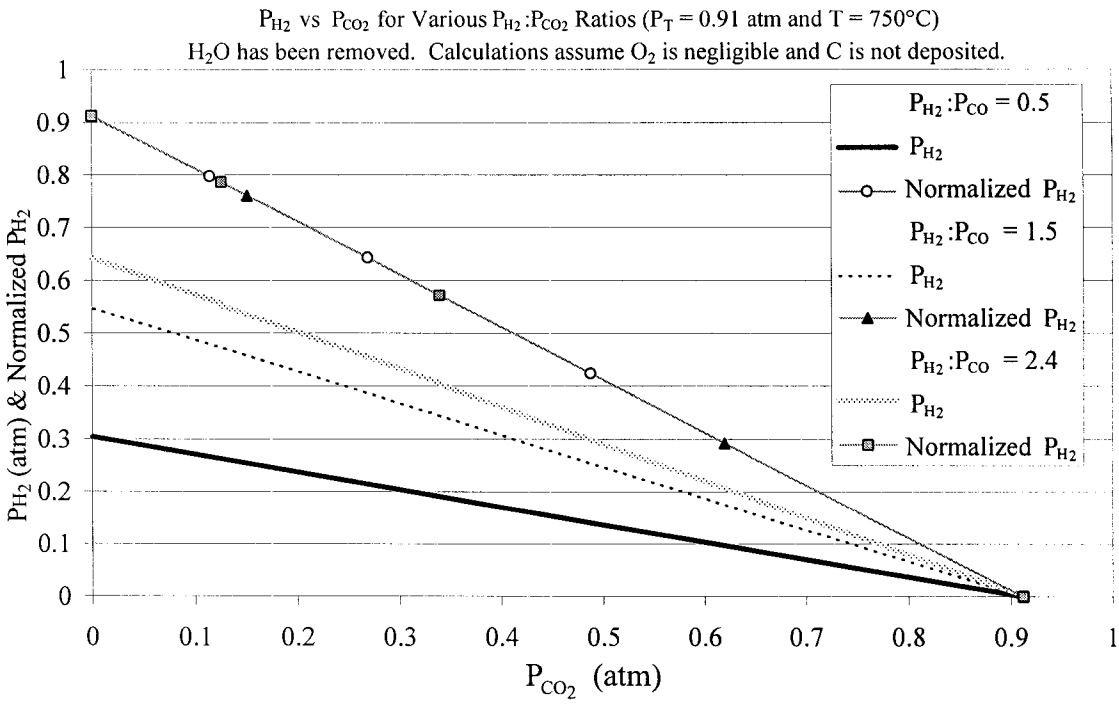

Figure A-1 Example of normalizing P_{H_2} .

As demonstrated in Figure A-1, the slope of each P_{H_2} solution depends upon the P_{H_2}:P_{CO} ratio. Rather than calculating the slope for each P_{H_2}:P_{CO} solution, it would be helpful to come up with an expression as a function of P_{H_2}:P_{CO} that describes the slope. Then, this function can be used to normalize the solutions and the data.

The normalization function is created by plotting in Figure A-2 the slope of each P_{H_2} solution (like those shown in Figure A-1) versus its $P_{H_2}:P_{CO}$ ratio. An exponential function can be used to fit the plot:

$$\frac{d(P_{H_2})}{d(P_{CO_2})} = \exp\left(-.9\frac{1}{(P_{H_2}:P_{CO})}\right) + \frac{(P_{H_2}:P_{CO})}{9^{(P_{H_2}:P_{CO})}} \qquad R^2 = 0.998 \qquad \text{(A.37)}$$

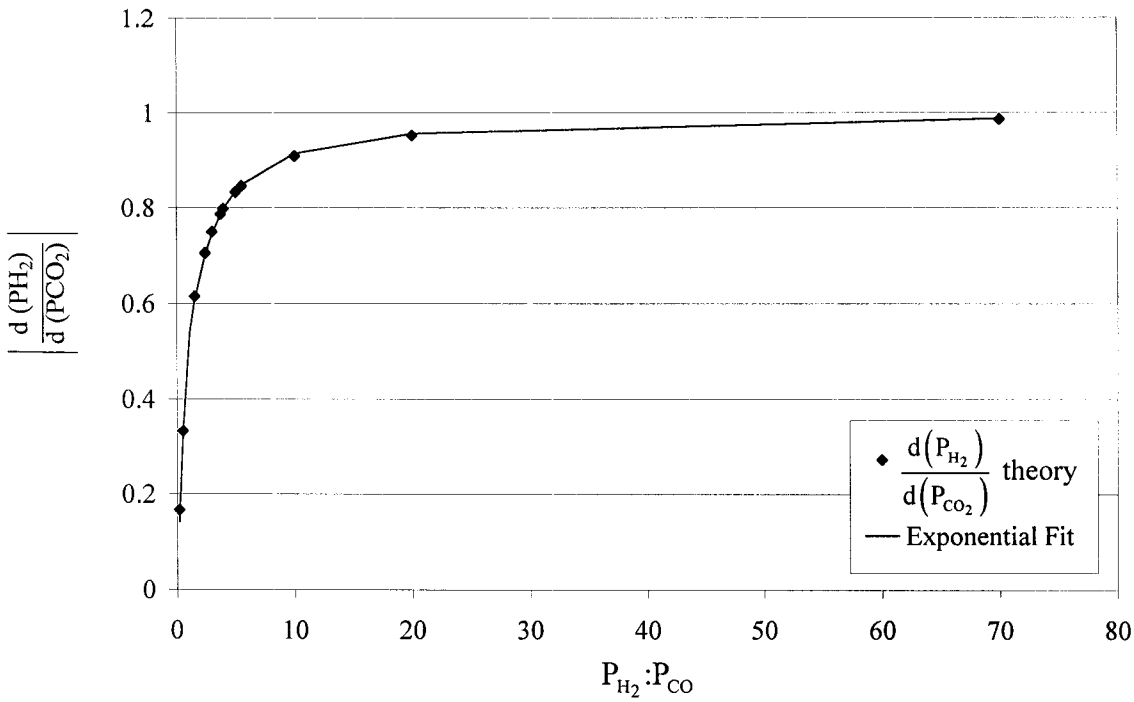

Figure A-2 Slope of P_{H_2} solution versus $P_{H_2}:P_{CO}$ ratio.

The fit was accomplished through recognizing the exponential trend in Figure A-2. A term was added which allows the "elbow" (around $P_{H_2}:P_{CO}$ of 2 to 10) to be better fit yet forces the function to 1 as $P_{H_2}:P_{CO}$ approaches infinity and to 0 as $P_{H_2}:P_{CO}$ approaches 0. The 0.9 factor used in the exponential term might be the total pressure of the anode (approximately 0.91 atm in the case of the data presented here). More investigations are needed to correlate any physics of the problem to the function.

The same procedure can be applied to the normalization of P_{CO}. However, if the slope dP_{CO}/dP_{CO_2} is plotted versus $P_{CO}:P_{H_2}$ (rather than $P_{H_2}:P_{CO}$), then the points align with the same curve-fit previously performed in Figure A-2. This alignment is demonstrated in Figure A-3. For the P_{CO} normalization, the same function can be used but now it is a function of $P_{CO}:P_{H_2}$.

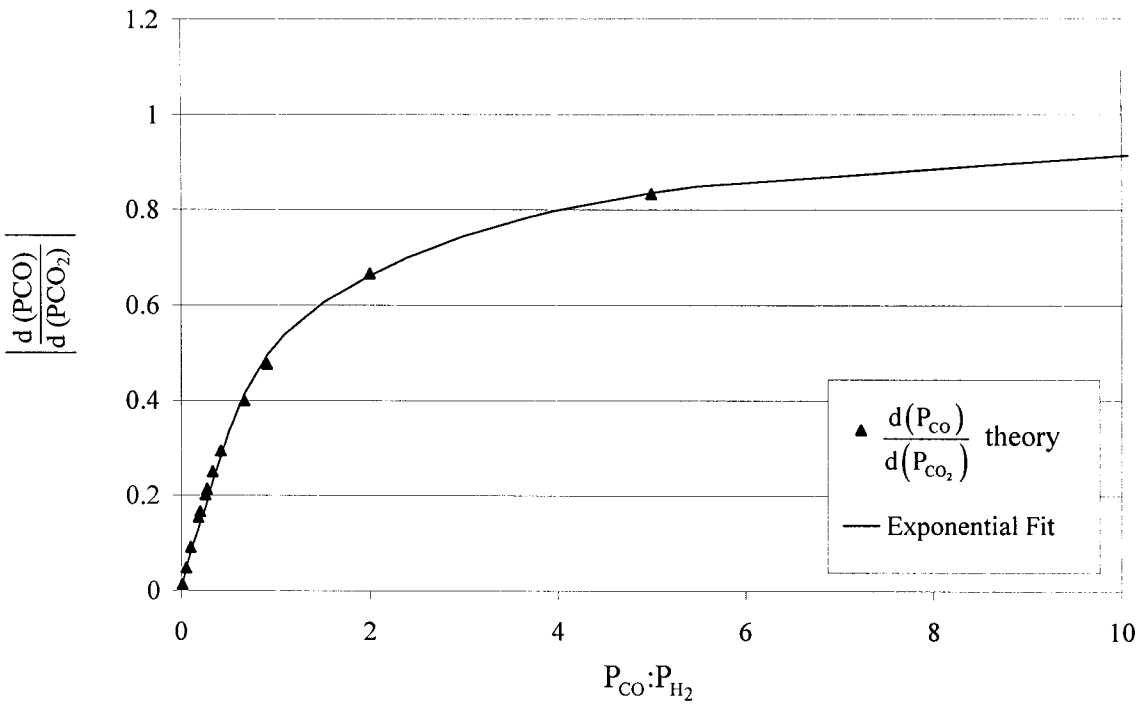

Figure A-3 Change in P_{CO} as a function of $P_{H_2}:P_{CO}$

A.5 Solving for Combined Electrolysis Exhaust Composition

The following four equations represent expressions for the conservation of C, H and O in the electrolysis cell and the equilibrium constant for the water gas shift reaction, respectively.

$$\dot{N}_{CO_2}^{in} = \dot{N}_{CO_2}^{out} + \dot{N}_{CO}^{out} \tag{A.38}$$

$$\dot{N}_{H_2O}^{in} = \dot{N}_{H_2O}^{out} + \dot{N}_{H_2}^{out} \tag{A.39}$$

$$2\dot{N}_{O_2}^{out} = \dot{N}_{CO}^{out} + \dot{N}_{H_2}^{out} \tag{A.40}$$

$$K_{P,wgs} = \frac{\dot{N}_{CO_2}^{out}\dot{N}_{H_2}^{out}}{\dot{N}_{CO}^{out}\dot{N}_{H_2O}^{out}} \tag{A.41}$$

Equation (A.41) can be rearranged to solve for $\dot{N}_{CO}^{out}$ which can then be inserted into equation (A.40) and solved for $\dot{N}_{H_2}^{out}$.

$$\dot{N}_{CO}^{out} = \frac{\dot{N}_{CO_2}^{out}\dot{N}_{H_2}^{out}}{K_{P,wgs}\dot{N}_{H_2O}^{out}} \tag{A.42}$$

$$\dot{N}_{H_2}^{out} = \frac{2\dot{N}_{O_2}^{out}K_{P,wgs}\dot{N}_{H_2O}^{out}}{\dot{N}_{CO_2}^{out} + K_{P,wgs}\dot{N}_{H_2O}^{out}} \tag{A.43}$$

Equation (A.43) is then inserted into equation (A.39) and rearranged to solve for $\dot{N}_{CO_2}^{out}$.

$$\dot{N}_{H_2O}^{in} = \dot{N}_{H_2O}^{out} + \frac{2\dot{N}_{O_2}^{out}K_{P,wgs}\dot{N}_{H_2O}^{out}}{\dot{N}_{CO_2}^{out} + K_{P,wgs}\dot{N}_{H_2O}^{out}} \tag{A.44}$$

$$\dot{N}_{CO_2}^{out} = K_{P,wgs}\left(\frac{\left(\dot{N}_{H_2O}^{out}\right)^2 + 2\dot{N}_{O_2}^{out}\dot{N}_{H_2O}^{out} - \dot{N}_{H_2O}^{in}\dot{N}_{H_2O}^{out}}{\dot{N}_{H_2O}^{in} - \dot{N}_{H_2O}^{out}}\right) \tag{A.45}$$

Equation (A.42) ($\dot{N}_{CO}^{out}$), equation (A.43) ($\dot{N}_{H_2}^{out}$), and finally equation (A.45) ($\dot{N}_{CO_2}^{out}$) can all be plugged into equation (A.38).

$$\dot{N}_{CO_2}^{in} = \dot{N}_{CO_2}^{out} + \frac{\dot{N}_{CO_2}^{out}\dot{N}_{H_2}^{out}}{K_{P,wgs}\dot{N}_{H_2O}^{out}} \tag{A.46}$$

$$\dot{N}_{CO_2}^{in} = \dot{N}_{CO_2}^{out} + \frac{2\dot{N}_{O_2}^{out}\dot{N}_{CO_2}^{out}}{\dot{N}_{CO_2}^{out} + K_{P,wgs}\dot{N}_{H_2O}^{out}} \tag{A.47}$$

$$0 = \left(\dot{N}_{CO_2}^{out}\right)^2 + \left(K_{P,wgs}\dot{N}_{H_2O}^{out} + 2\dot{N}_{O_2}^{out} - \dot{N}_{CO_2}^{in}\right)\dot{N}_{CO_2}^{out} - \dot{N}_{CO_2}^{in}K_{P,wgs}\dot{N}_{H_2O}^{out} \tag{A.48}$$

$$\begin{aligned} 0 = {} & K_{P,wgs}\left(\frac{\left(\dot{N}_{H_2O}^{out}\right)^2 + 2\dot{N}_{O_2}^{out}\dot{N}_{H_2O}^{out} - \dot{N}_{H_2O}^{in}\dot{N}_{H_2O}^{out}}{\dot{N}_{H_2O}^{in} - \dot{N}_{H_2O}^{out}}\right)^2 \\ & + \left(K_{P,wgs}\dot{N}_{H_2O}^{out} + 2\dot{N}_{O_2}^{out} - \dot{N}_{CO_2}^{in}\right)\left(\frac{\left(\dot{N}_{H_2O}^{out}\right)^2 + 2\dot{N}_{O_2}^{out}\dot{N}_{H_2O}^{out} - \dot{N}_{H_2O}^{in}\dot{N}_{H_2O}^{out}}{\dot{N}_{H_2O}^{in} - \dot{N}_{H_2O}^{out}}\right) \\ & - \dot{N}_{CO_2}^{in}\dot{N}_{H_2O}^{out} \end{aligned} \tag{A.49}$$

The resulting expression shown in equation (A.49) is a fourth order function in $\dot{N}_{H_2O}^{out}$ of known variables $\dot{N}_{CO_2}^{in}$, $\dot{N}_{H_2O}^{in}$, $K_{P,wgs}$, and $\dot{N}_{O_2}^{out}$. Using a numerical root finder, $\dot{N}_{H_2O}^{out}$ can now be obtained. The solutions to $\dot{N}_{CO_2}^{out}$, $\dot{N}_{H_2}^{out}$, and $\dot{N}_{CO}^{out}$ can then be calculated using equations (A.45), (A.43) and (A.42) in that order.

A.6 Water Gas Shift Reactor Guarantees Exhaust Composition

"How can the outlet of a water gas shift reactor be guaranteed when different cell-types may provide different exhaust compositions for the reactor's input?" The answer is if atoms are conserved across the electrolysis cell (i.e. no carbon deposition) then the

exhaust composition for a given oxygen production and inlet gas mixture ratio does not matter.

Consider two cells performing combined electrolysis that produce the same amount of O_2, $\dot{N}_{O_2}^{out,SOE}$, for a given input of $\dot{N}_{CO_2}^{in,SOE}$ and $\dot{N}_{H_2O}^{in,SOE}$. However, assume cell 1 and cell 2 exhibit different preferences to H_2O over CO_2. The CO_2 utilization of cell 1 and 2 can be represented as $\eta_{CO_2}^{(1)}$ and $\eta_{CO_2}^{(2)}$, respectively. Similarly, the H_2O utilization of cell 1 and 2 can be represented as $\eta_{H_2O}^{(1)}$ and $\eta_{H_2O}^{(2)}$, respectively. Then the expressions for the flow rates of the products and leftover oxygen-providing gas leaving the cells can be written as:

For Cell 1:

$$\dot{N}_{CO}^{out,SOE} = \eta_{CO_2}^{(1)} \dot{N}_{CO_2}^{in,SOE}$$
$$\dot{N}_{H_2}^{out,SOE} = \eta_{H_2O}^{(1)} \dot{N}_{H_2O}^{in,SOE}$$
$$\dot{N}_{CO_2}^{out,SOE} = \left(1-\eta_{CO_2}^{(1)}\right) \dot{N}_{CO_2}^{in,SOE}$$
$$\dot{N}_{H_2O}^{out,SOE} = \left(1-\eta_{H_2O}^{(1)}\right) \dot{N}_{H_2O}^{in,SOE}$$

For Cell 2:

$$\dot{N}_{CO}^{out,SOE} = \eta_{CO_2}^{(2)} \dot{N}_{CO_2}^{in,SOE}$$
$$\dot{N}_{H_2}^{out,SOE} = \eta_{H_2O}^{(2)} \dot{N}_{H_2O}^{in,SOE}$$
$$\dot{N}_{CO_2}^{out,SOE} = \left(1-\eta_{CO_2}^{(2)}\right) \dot{N}_{CO_2}^{in,SOE}$$
$$\dot{N}_{H_2O}^{out,SOE} = \left(1-\eta_{H_2O}^{(2)}\right) \dot{N}_{H_2O}^{in,SOE}$$

The flow rates leaving the cell are the inputs to the water gas shift reactor. The conservation of carbon and hydrogen across the reactor can be applied to derive equations for products of the reactor exhaust. For example, for the conservation of carbon across any cell:

$$\begin{aligned}\dot{N}_{CO}^{in,wgs} + \dot{N}_{CO_2}^{in,wgs} &= \dot{N}_{CO}^{out,SOE} + \dot{N}_{CO_2}^{out,SOE} \\ &= \eta_{CO_2} \dot{N}_{CO_2}^{in,SOE} + \left(1-\eta_{CO_2}\right) \dot{N}_{CO_2}^{in,SOE} \\ &= \dot{N}_{CO_2}^{in,SOE} \\ &= \dot{N}_{CO}^{out,wgs} + \dot{N}_{CO_2}^{out,wgs}\end{aligned} \tag{A.50}$$

The conservation of oxygen across the reactor can also be applied. For example, the equation for the conservation of O_2 across the reactor following any cell becomes:

$$\begin{aligned}
\dot{N}_{CO}^{in,wgs} + 2\dot{N}_{CO_2}^{in,wgs} + \dot{N}_{H_2O}^{in,wgs} &= \dot{N}_{CO}^{out,SOE} + 2\dot{N}_{CO_2}^{out,SOE} + \dot{N}_{H_2O}^{out,SOE} \\
&= \dot{N}_{CO_2}^{in,SOE} + \dot{N}_{CO_2}^{out,SOE} + \dot{N}_{H_2O}^{out,SOE} \\
&= \dot{N}_{CO_2}^{in,SOE} + \left(1-\eta_{CO_2}\right)\dot{N}_{CO_2}^{in,SOE} + \left(1-\eta_{H_2O}\right)\dot{N}_{H_2O}^{in,SOE} \\
&= 2\dot{N}_{CO_2}^{in,SOE} + \dot{N}_{H_2O}^{in,SOE} - \eta_{CO_2}\dot{N}_{CO_2}^{in,SOE} - \eta_{H_2O}\dot{N}_{H_2O}^{in,SOE} \\
&= 2\dot{N}_{CO_2}^{in,SOE} + \dot{N}_{H_2O}^{in,SOE} - 2\dot{N}_{O_2}^{out,SOE} \\
&= \dot{N}_{CO}^{out,wgs} + 2\dot{N}_{CO_2}^{out,wgs} + \dot{N}_{H_2O}^{out,wgs}
\end{aligned}$$

or

$$2\dot{N}_{CO_2}^{in,SOE} + \dot{N}_{H_2O}^{in,SOE} = 2\dot{N}_{O_2}^{out,SOE} + \dot{N}_{CO}^{out,wgs} + 2\dot{N}_{CO_2}^{out,wgs} + \dot{N}_{H_2O}^{out,wgs} \qquad \text{(A.51)}$$

In addition, both reactors must satisfy the equilibrium constant. Thus four equations for four unknowns are as follows ($\dot{N}_{H_2}^{out,wgs,(i)}$, $\dot{N}_{CO}^{out,wgs,(i)}$, $\dot{N}_{CO_2}^{out,wgs,(i)}$, and $\dot{N}_{H_2O}^{out,wgs,(i)}$):

For Cell 1:	For Cell 2:	
$N_{CO_2}^{in,SOE} = \dot{N}_{CO}^{out,wgs,(1)} + \dot{N}_{CO_2}^{out,wgs,(1)}$	$N_{CO_2}^{in,SOE} = \dot{N}_{CO}^{out,wgs,(2)} + \dot{N}_{CO_2}^{out,wgs,(2)}$	(A.52)
$N_{H_2O}^{in,SOE} = \dot{N}_{H_2}^{out,wgs,(1)} + \dot{N}_{H_2O}^{out,wgs,(1)}$	$N_{H_2O}^{in,SOE} = \dot{N}_{H_2}^{out,wgs,(2)} + \dot{N}_{H_2O}^{out,wgs,(2)}$	(A.53)
$2\dot{N}_{CO_2}^{in,SOE} + \dot{N}_{H_2O}^{in,SOE} =$ $2\dot{N}_{O_2}^{out,SOE} + \dot{N}_{CO}^{out,wgs,(1)} +$ $2\dot{N}_{CO_2}^{out,wgs,(1)} + \dot{N}_{H_2O}^{out,wgs,(1)}$	$2\dot{N}_{CO_2}^{in,SOE} + \dot{N}_{H_2O}^{in,SOE} =$ $2\dot{N}_{O_2}^{out,SOE} + \dot{N}_{CO}^{out,wgs,(2)} +$ $2\dot{N}_{CO_2}^{out,wgs,(2)} + \dot{N}_{H_2O}^{out,wgs,(2)}$	(A.54)
$K_{P,wgs} = \dfrac{\dot{N}_{CO_2}^{out,wgs,(1)}\dot{N}_{H_2}^{out,wgs,(1)}}{\dot{N}_{CO}^{out,wgs,(1)}\dot{N}_{H_2O}^{out,wgs,(1)}}$	$K_{P,wgs} = \dfrac{\dot{N}_{CO_2}^{out,wgs,(2)}\dot{N}_{H_2}^{out,wgs,(2)}}{\dot{N}_{CO}^{out,wgs,(2)}\dot{N}_{H_2O}^{out,wgs,(2)}}$	(A.55)

The two sets of equations are the same. The different utilizations of H_2O versus CO_2 for the two cells completely drop out. Thus, the process by which the two cells produce

oxygen given a fixed input mixture ratio does not influence the output of the water gas shift reactor, as long as constituents are conserved across the cell.

APPENDIX B SAMPLE CALCULATIONS

B.1 Calculating Reaction Equilibrium Constants

For a reaction at 298K:

$$\Delta G^{\circ}_{rxn,T} = \Delta H^{\circ}_{rxn} - T\Delta S^{\circ}_{rxn} \tag{B.1}$$

Example, for $CO_2 = CO + \frac{1}{2}O_2$:

$$\Delta H^{\circ}_{rxn} = \sum_{products} N_i \Delta \bar{h}^{\circ}_{f,i} - \sum_{reactants} N_i \Delta \bar{h}^{\circ}_{f,i}$$

$$= (1\,\text{kmol})(-110530\ {}^{kJ}/_{kmol}) + (\tfrac{1}{2}\,\text{kmol})(0\ {}^{kJ}/_{kmol}) - (1\,\text{kmol})(-393520\ {}^{kJ}/_{kmol})$$

$$= 282.990\,\text{kJ}$$

Similarly,

$$\Delta S^{\circ}_{rxn} = (1)(197.56) + (\tfrac{1}{2})(205.04) - (1)(213.97)$$

$$= 0.08611\ {}^{kJ}/_{K}$$

$$\Delta G^{\circ}_{rxn,298K} = 282.99 - (298)0.08611 = 257.3\,\text{kJ}$$

But equation (B.1) can also be written as:

$$\Delta G^{\circ}_{rxn,T} = -\Re T \ln(K_p) \tag{B.2}$$

Example, for $CO_2 = CO + \frac{1}{2}O_2$:

$$257.3\,\text{kJ} = -8.314\ {}^{kJ}/_{kgmol-K}\,(298K)\ln(K_p)$$

$$K_p = 7.881E-46 \quad \rightarrow \quad \log(K_p) = -45.107$$

Compare to values tabulated in Wark [55]: $\log(K_p) = -45.066$

For a reaction not at standard temperature, for example 1000K:

$$\Delta G^{\circ}_{rxn,1000} = 282.99 - 1000(0.08611) = 196.88\ {}^{kJ}/_{kgmol}$$

$$= -8.314(1000)\ln(K_p)$$

$$K_p = 5.196E-11 \quad \rightarrow \quad \log(K_p) = -10.284$$

Compare to Wark again: $\log(K_p) = -10.221$

B.2 Combined Electrolysis Exhaust Solution Assuming No Carbon Deposition

Combined solid oxide electrolysis is assumed to be operated at a temperature and pressure of 750°C (1023 K) and 0.91 atm, respectively. It is also assumed that no carbon is deposited inside the cell. Using equations (5.12) and (5.14), the partial pressures of CO, H_2O and H_2 in the exhaust can be solved as a function of P_{CO_2} and the P_{H_2}:P_{CO}. For the sample calculation presented here, a P_{H_2}:P_{CO} ratio of 0.5 is assumed. Example solutions as a function of P_{CO_2} are plotted in Figure A-4.

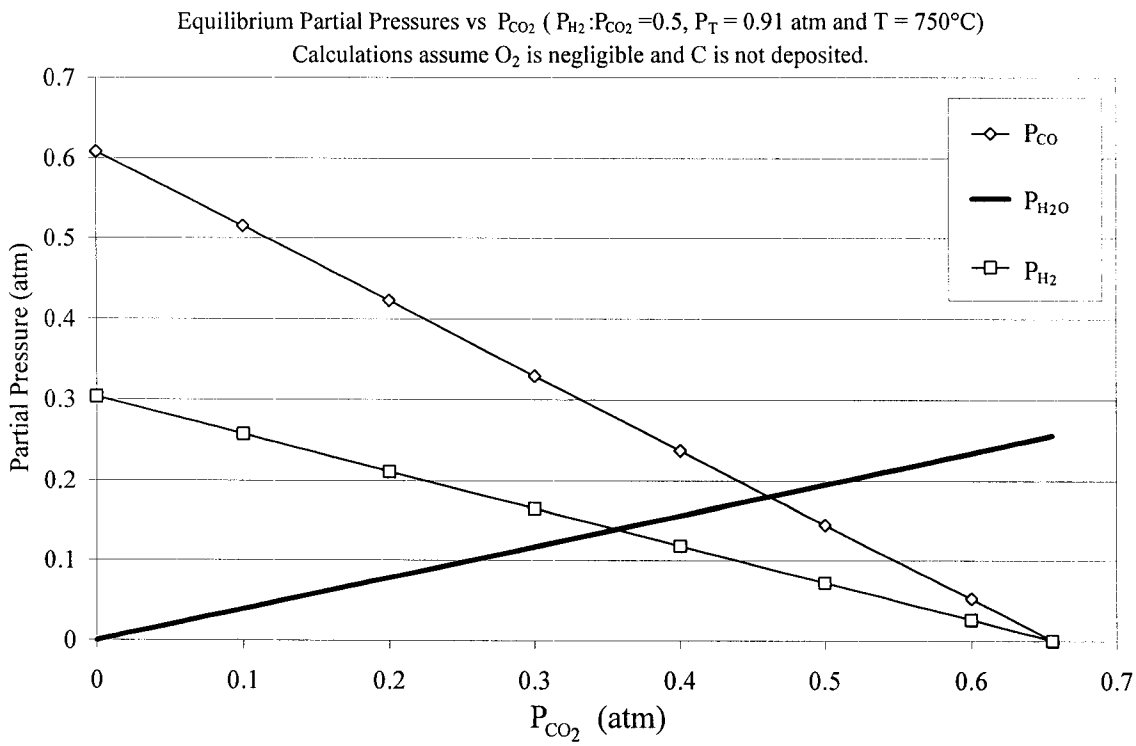

Figure A-4 Example partial pressure solution assuming no carbon deposition.

APPENDIX C SUMMARY OF X-RAY ANALYSES

C.1 Sodium and Silicon Electrode Contamination

A field-emission scanning electron microscope (Hitachi S-4500/Thermo-Noran Digital Imaging/EDS) was used to conduct the analyses. This is a cold field emission electron gun capable of magnification up to 500,000 times. The accelerating voltages range from 0.5 to 30 KV with 4.0 nm resolution at 1KV.

X-ray analyses were performed on a pure platinum electrode that had been exposed to distilled water. SEM imaging showed the sample analyzed appeared to have a normal-looking underlying Pt surface that was littered with little crystal structures. The first three X-ray analyses were performed on one location. The fourth X-ray analysis was performed on another area of the electrode. Results show sodium (Na) and silicon (Si) contamination. An example plot of the elements detected is shown in Figure A-5. Details follow.

Analysis 1: An area analysis was first performed. Mostly Pt (up to 8000 counts) was detected but some Mn, Na, and O was found as well (all under 500 counts).

Analysis 2: A pin-point analysis of a crystal was performed and revealed 1800 counts of Mn. Pt (1800), Na (400) and O (700) were also detected. It should be noted that in pin-pointing crystals, X-rays requires higher voltage and that makes crystals look transparent so their composition is hard to detect.

Analysis 3: Another pin point analysis was performed showing 1050 counts of Si. Pt (1800), O (500), Na (500) and Mn (200) as well as Zr (200) and Y (100) were detected.

Analysis 4: An area analysis was done on yet another image showing almost 800 counts of Na and 700 of O. Pt (800), Si (150), and Mn (150) were detected as well.

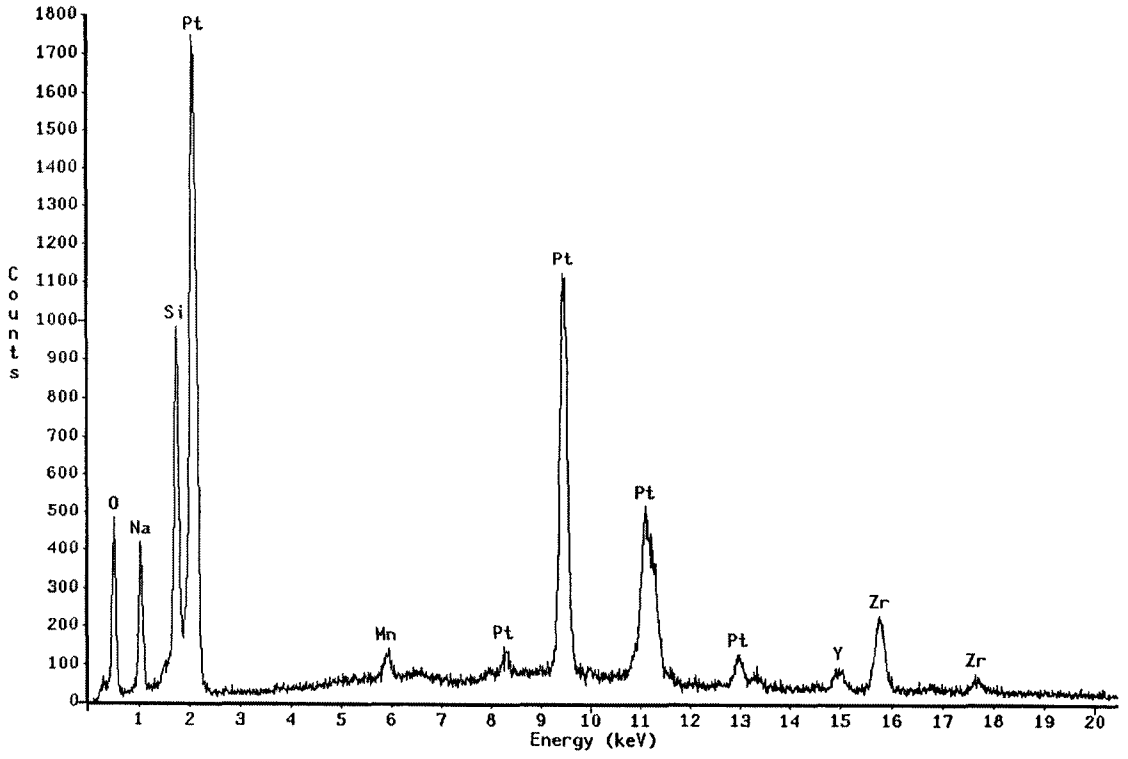

Figure A-5 Pin-point X-ray analysis of a Pt electrode showing contamination.

Possible suspects of contamination are the water, PC-7 Epoxy paste® (Protective Coating Co.) and silicon tubing. Protective Coating Co. says PC-7 contains trace amounts (parts per million) of inert fillers. A common filler used contains magnesium silicate, a very stable compound. Regardless, the sealant was replaced with Varian Vacuum Technologies "Torr Seal" (#9530001), silicon tubing was replaced with Tygon® tubing, and the distilled water was replaced with deionized water. No contamination has been detected since.

C.2 Cr-alloy versus Alumina Electrodes

A field-emission scanning electron microscope (Hitachi S-4500/Thermo-Noran Digital Imaging/EDS) was used to conduct the analyses. This is a cold field emission electron gun capable of magnification up to 500,000 times. The accelerating voltages range from 0.5 to 30 KV with 4.0 nm resolution at 1KV.

The electrodes on all samples are composed of two layers. The PEN is sintered only after both layers have been applied. The mixed layer contains 50/50% by weight Pt and YSZ. Thus, the mixed layer should contain oxygen, Pt, Zr, and Y. The 2^{nd}, or top layer, is pure Pt. It has always been suspected (and detected in the past) that the Pt paste contains Manganese (Mn).

One "control" PEN is analyzed (50PEN_11). This PEN has not been used in an electrolysis system. One PEN from an alumina cell is analyzed (IAcell04). The alumina system delivers the input gas via alumina manifolds (Al_2O_3). The manifolds are flat and press a Pt gauze against the electrodes. One PEN from a Cr-alloy cell is also analyzed (50cell09). The manifolds of this system are made of a chromium-alloy covered with a proprietary Pt-based coating (the other constituents are unknown). The manifold has channels of which input gas may pass and thus are directly pressed against the electrodes.

PEN preparation and hours at operating temperature for each is described in Table A-1. All were sintered exactly the same. The PEN used in the alumina system was "pre-sintered" at 150°C for 30 minutes in order to insure the PEN was completely dried before sintering. This should not result in a difference in electrode structure since the melting temperature of Pt is much higher at 1772°C (2045K) [33]. The chromium system

experienced the most time at temperature with 640 hours at 750°C and over a 1000 hours at 850°C. The alumina system never resided at 850°C for any length of time and was operated for 370 hours at 750°C. The control PEN was never exposed to high temperatures after it was sintered.

Table A-1 Preparation of electrodes used in X-ray analyses.

	Cr-Alloy System (50cell09)	**Alumina System (IAcell04)**	**Control PEN (50PEN_11)**
PRESINTER	None	T_{room} to 150°C at 1°C/min; 30 min soak; 150°C to T_{room} at 1 °C/min	None
SINTER	T_{room} to 800°C at 3°/min; 800 to 1200°C at 1°/min; 1 hr soak; 1200 to 800°C at 1°/min; 800°C to T_{room} at 3°/min; end	same	same
OPERATING TEMPERATURE	First Thermal Cycle: ~ 2 hrs at 950°C ~ 60 hrs at 850°C ~ 642 hrs at 750°C Second Thermal Cycel: ~ 1344 hrs at 850°C	First Thermal Cycle: ~ 2 hrs at 950°C ~ 370 hrs at 750°C	None

Low accelerating voltages do not penetrate as deeply into the sample as high accelerating voltages. Therefore, low voltages may be an indication of surface molecules rather than molecules deep in the sample. A cross section was analyzed but usually the X-ray analyses were placed on a pore since the pore would have been exposed to electrolysis gases. Two accelerating voltages were used: 5KV and 25KV.

Quantitative Analyses were not performed. It is difficult to assess relative quantities because sample areas, accelerating voltages, counts, etc are all different. Results are summarized qualitatively in Table A-2 for the pure platinum layer and the mixed Pt/YSZ

layer, showing only what elements were detected. Key observations are summarized below.

Analysis 1: A mixed layer, at low voltage (5KV), was first analyzed. The only significant difference between all three systems was that Cr was detected in the mixed layers of the Cr system. This implies Cr migrates to inside the electrode because the mixed layer is not in direct contact with Cr. Other observations are as follows:

- No aluminum was detected in the shallow reaches of the X-ray analysis. This makes sense because the mixed layer is not directly exposed to alumina for either system.
- Zr and Pt were both detected in all mixed layers.
- Carbon, though very little, was detected in all of the mixed layers.
- Oxygen was detected in all layers with peaks almost the size of Pt. Large peak sizes could be attributed to the significant source of oxygen that exists in YSZ.

Analysis 2: A mixed layer, at high voltage (25KV), was next analyzed. The higher voltage verified that the only significant difference between all samples was the presence of Cr in the mixed layers. Other observations are as follows:

- Zr, Pt, Y, and Mn were detected in all mixed layers.
- Carbon was more pronounced with the higher voltage analysis though still small.
- All mixed layers had slightly bigger O_2 peaks than C peaks, but not as big as Pt peaks.

Analysis 3: A Pt layer, at low voltage (5KV), was analyzed. The first significant difference is that aluminum was detected in all alumina system samples. This could be plausible since the Pt layer is in direct line-of-sight of the alumina manifolds (one should remember that there is a Pt gauze between it and the manifold).

In general, more oxygen was detected in the lower voltage samplings than in the higher voltage samplings. This could indicate oxides on the surfaces of the pores. More oxygen was also detected in both systems than in the control.

O_2 to Al peaks were approximately the same for the anode and cathode. Gary Chandler, a principle research specialist of the Material Science and Engineering Department at The University of Arizona, commented that usually O_2 peaks are smaller than Al peaks for Al_2O_3. This could be an indication that the oxygen belongs to a Pt-oxide, rather than all belonging to alumina. This theory seems more valid since *both* systems exhibited large oxygen peaks, especially as compared to the control.

For the PEN (control) platinum layer O_2:C peak comparison is low compared to the used PENs.

Finally, no Cr was detected with the low accelerating voltages.

Analysis 4: Lastly, a Pt layer, at high voltage (25KV) was finally analyzed. Cr was confirmed on the platinum layer of the chromium system. There was no oxygen detected in the control sample. There was oxygen detected on the anodes of both systems. Oxygen was not detected on the cathode of the chromium system. No high voltage analysis was performed on the Pt layer of the alumina cathode. In general, oxygen peaks were smaller than those detected with the lower accelerating voltage.

Table A-2 Constituents detected via an X-ray analysis.

	Notes	Acc. Voltage (kV)	C	O	Pt	Zr	Y	Mn	Al	Ni	Cr	Fe	Si
MIXED													
PEN		5	■	■	■	■							
Al Anode		5	■	■	■	■							
Al Cathode	1	5	■	■	■	■	■		■				
Cr Anode	9	5	■	■	■	■							
Cr Cathode	9	5	■	■	■	■					■		
PEN		25	■	■	■	■	■	■					
Al Anode		25	■	■	■	■	■	■					
Cr Cathode	2, 9	25	■	■	■	■	■	■			■	■	
Cr Anode	9	25	■	■	■	■	■	■			■		
PLATINUM													
PEN		5	■	■	■								
Al Anode		5	■	■	■				■				
Al Cathode	3	5	■	■	■				■				
Al Cathode	4	5	■	■	■				■				■
Cr Anode	9	5	■	■	■								
Cr Cathode	5, 9	5	■	■	■								
PEN		25	■		■					■			
Al Anode	6	25	■	■	■			■		■			
Al Cathode	7,8	25	■	■	■			■		■			
Cr Anode	9	25	■	■	■						■		
Cr Cathode	9	25	■		■					■	■	■	

Table Legend:

■ Detected

1 Area analysis made.

2 Mysterious peak could be Gd, Pm, Nd, or more likely Mn.

3 O_2 is usually smaller than Al for Al_2O_3. Here O_2 is big! Probably Pt-oxide?

4 Si is possibly Pt.

5 Very thin layer, not porous.

6 No Al. Focused on Pore.

7 No print of analysis made. No Al shown. Like anode with several Pt Peaks.

8 Higher voltage goes deeper thus could blow right by Al_2O_3 if on surface.

9 Electrode orientation not certain -could be anode or cathode.

NOMENCLATURE

a_c	activity of solid carbon, 1
E_{CV}	all energy associated with a control volume
g	gravitational constant
$\bar{g}_i$	molar Gibbs function of the i^{th} constituent
$\Delta G^{\circ}_{T,rxn}$	change in Gibbs standard energy for a reaction at temperature T
$\bar{h}_i$	molar enthalpy of the i^{th} constituent
$\bar{h}_{STP}$	molar enthalpy of at standard temperature and pressure, 298K and 1 atm
$\bar{h}_T$	molar enthalpy at temperature
Δh°_f	standard enthalpy of formation
I	current
K_p	equilibrium constant
$\dot{m}_i$	mass flow rate of i^{th} constituent
$\dot{N}_f$	anode flush molar flow rate
$\dot{N}_i$	molar flow rate of the i^{th} gas in moles per time
$\dot{N}_{inlet}$	electrolysis cell inlet gas mixture molar flow rate
P_a	total pressure of anode
P_c	total pressure of cathode
P_i	partial pressure of the i^{th} constituent
P_T	total pressure
$\dot{Q}$	heat transfer into a system
Q	reaction quotient
$\Re$	universal gas constant, 8.314 kJ/kmol-K
$\bar{s}_i$	molar entropy of i^{th} constituent
$\bar{s}^{\circ}_T$	molar entropy at temperature and 1 atm
$\dot{S}_{gen}$	entropy generation rate
t	time
T	temperature
$\dot{W}$	work transfer by a system to the environment
V_{min}	minimum voltage required for electrolysis
X_i	molar fraction of i^{th} constituent entering an electrolysis cell
Y_i	molar fraction of i^{th} constituent leaving an electrolysis cell
η	fraction of oxygen-providing gas electrolyzed, called "utilization"
σ_m	standard deviation of the mean
$\Im$	Faraday's constant, 96485 C/mol

REFERENCES

[1] Hamilton Standard Division of United Aircraft Corporation, "Tradeoff Study and Conceptual Designs of Regenerative Advanced Life Support Systems (AILSS)", NASA-CR1459, January, 1970.

[2] Ash, R. L., Dowler, W. L., and Varsi, G., "Feasibility of Rocket Propellant Production on Mars", Acta Astronautica, Vol. 5, 1978, Pp. 706 – 724.

[3] Reddig, M. and MacKnight, A., "Investigation of Mars In-Situ Propellant Production", SAE Paper 972496, July 1997.

[4] Clark, D. L., "In-Situ Propellant Production on Mars: A Sabatier/Electrolysis Demonstration Plant", AIAA Paper 97-2764, July 1997.

[5] Zubrin, R., Frankie, B., and Kito, T., "Mars In-Situ Resource Utilization Based on the Reverse Water Gas Shift: Experiments and Mission Applications", AIAA Paper 97-2767, July 1997.

[6] England, C., "Mars Atmosphere Resource Recovery System (MARRS)", AIAA Paper 2001-0942 January 2001.

[7] Green, S. T., Deffenbaugh, D. M., and Miller, M. A., "A Comparison of Five ISPP Systems for a Mars Sample Return Mission", AIAA Paper 99-2410, June 1999.

[8] Frisbee, Robert H., "Mass and Power Estimates for Mars In-Situ Propellant Production Systems", AIAA Paper 87-1900, June 1987.

[9] Sanders, J. B., "Integrated Propulsion and ISRU Propellant Production System for Mars Sample Return", AIAA Paper 95-2641, July 1995.

[10] Sridhar, K. R., Iacomini, C. S., and Finn, J. E., "Combined H_2O /CO_2 Solid Oxide Electrolysis for Mars In Situ Resource Utilization", Journal Propulsion and Power, Vol. 20, No. 3, 2004 (Tentative).

[11] Richter, R., "Basic Investigation into the Production of Oxygen in a Solid Electrolyte Process", AIAA-81-1175, AIA 16th Thermophysics Conference, June 23 – 25, Palo Alto, CA, 1981.

[12] Sridhar, K. R., and Vaniman, B. T., "Oxygen production on Mars using solid oxide electrolysis", Solid State Ionics, V 93, 1997, pp. 321-328.

[13] Tao, G., "Investigation of CO_2 Electrolysis Reaction Kinetics in Solid Oxide Electrozlyer (SOE)", Ph.D. Dissertation, The University of Arizona, 2003, pp. 18 – 32, 107-108.

[14] Rieger, P. H., *Electrochemistyr, 2nd Edition*, Chapman & Hall, Inc., New York, p. 380, 1994.

[15] Kotz, J. and Treichel, P. Jr., *Chemistry & Chemical Reactivity, 3rd Edition*, Saunders College Publishing, New York, 1996, p. 928.

[16] Sridhar, K. R., and Miller, S. A., "Solid Oxide Electrolysis Technology for ISRU and Life Support", SAE Paper 941255, June 1994.

[17] Vaniman, B., "Performance Characterization of Solid Oxide Electrochemical Cells", Masters Thesis, The University of Arizona, 1995, p. 24.

[18] Spacil, H. S. and Tedmon, Jr., "Electrochemical Dissociation of Water Vapor in Solid Oxide Electrolyte Cells: I. Thermodynamics and Cell Characteristics", Journal of Electrochemical Society, Vol 116, pp. 1618-1626, 1969.

[19] Spacil, H. S. and Tedmon, Jr., "Electrochemical Dissociation of Water Vapor in Solid Oxide Electrolyte Cells: II. Materials, Fabrication, and Properties", Journal of Electrochemical Society, Vol 116, pp. 1627-1633, 1969.

[20] Isenberg, A. O., "Energy Conversion Via Solid Oxide Electrolyte Electrochemical Cells At High Temperatures", Solid State Ionics, Vol. 3/4, August, pp. 431-437, 1980.

[21] Erdle, E., Koch, A., and Schaefer, W., "Preparation and Operation of Zirconia High-Temperature Electrolysis Cells for Hydrogen Production", Proceedings of the 2nd International Conference on the Science and Technology of Zirconia, Stuttgart, Federal Republic of Germany, June 21-23, pp. 685-690, 1984.

[22] Dönitz, W. and Erdle, E., "High-Temperature Electrolysis of Water Vapor – Status of Development and Perspectives for Application", Int. J. Hydrogen Energy, Vol. 10, No. 5, pp. 291-295, 1985.

[23] Maskalick, N. J., "High Temperature Electrolysis Cell Performance Characterization", Int. J. Hydrogen Energy, Vol. 11, No. 9, pp. 563-570, 1986.

[24] Barbi, G. B, and Mari, C. M., "High Temperature Water Electrolysis: Cathodic Behaviour Of Pt/Yttria Stabilized Zirconia (YSZ) Interface", Solid State Ionics, Vol. 6, No. 4, July, pp. 341-351, 1982.

[25] Bonner, M., Botts, T., McBreen, J., Mezzina, A., Salzano, F., and Yang, C., "Status of Advanced Electrolytic Hydrogen Production in the United States and Abroad", Int. J. Hydrogen Energy, Vol. 9, No. 4, pp. 269-275, 1984.

[26] Barbi, G. B., and Mari, C. M., "A Parameter for Defining the Energetic Efficiency of the Cathodic Process at High Temperature, High Current Density Electrolysis of Steam", Int. J. Hydrogen Energy, Vol. 9, No. 11, pp. 895-899, 1984.

[27] Salzano, F. J., Skaperdas, G. and Mezzina, A., "Water Vapor Electrolysis at High Temperature: Systems Consideration and Benefits", Int. J. Hydrogen Energy, Vol. 10, No. 12, pp. 801-809, 1985.

[28] Wendt, H. and Plzak, V., "Hydrogen Production by Water Electrolysis", Kerntechnik, Vol. 56, No. 1, pp. 22-28, 1991.

[29] Ashari, H., Naito, H., and Miura, H., "Hydrogen Production From High-Temperature Steam Electrolysis Using Solar Energy", Int. J. Hydrogen Energy, Vol. 16, No. 9, pp. 603-608, 1991.

[30] Eguchi, K., Hatagishi, T., and Arai, H., "Power Generation and Steam Electrolysis Characteristics of an Electrochemical Cell with a Zirconia- or Ceria-based Electrolyte", Solid State Ionics, Vol. 86-88, pp. 1245-1249, 1996.

[31] Momma, A., Kato, T., Kaga, Y., and Nagata, S., "Polarization Behavior of High Temperature Solid Oxide Electrolysis Cells (SOEC)", Journal of the Ceramic Society of Japan, Vol. 105, No. 5, pp. 369-373, 1997.

[32] Maskalick, N. J., Buzzelli, E. S., Zuckerbrod, D., Bonner, M., Mezzina, A., and Salzano, F., "Hydrogen Production Employing High-Temperature Solid Oxide Cells", 19th Intersociety Energy Conversion Engineering Conference: Advanced Energy Systems - Their Role in Our Future, San Francisco, CA, USA, pp. 1415-1420, 1984.

[33] Incropera, F. and DeWitt, D., Introduction to Heat Transfer, 3rd Ed., John Wiley & Sons, New York, 1996, pp. 45, 57, 745-747, 758-761.

[34] http://www.webelements.com/webelements/elements/text/Pt/heat.html

[35] Sridhar, K. R., and Miller, S. A., "Solid Oxide Electrolysis Technology for ISRU and Life Support", SAE Paper 941255, June, 1994.

[36] Vaniman, B., "Performance Characterization of Solid Oxide Electrochemical Cells", MastersThesis, The University of Arizona, p. 24, 1995.

[37] Hickey, D., "The Development of a Solid Oxide Reversible Electrolysis/Fuel Cell Stack", Masters Thesis, The University of Arizona, 2002, pp. 32 – 34, 81.

[38] Elikan, L., Morris, J. P., and Wu, C. K., "Development of a solid electrolyte carbon dioxide and H_2O reduction system for oxygen recovery (Solid electrolyte oxygen

regeneration system with electrolyzer, carbon deposition reactor, and palladium membranes for separating hydrogen)", NASA-CR-2014, Wahsington D.C., 1972.

[39] Hibino, T., Kuwahara, Y., Otsuka, T., Ishida, N., and Oshima, T., "Nox Detection Using the Electrolysis of Water Vapor in a YSZ Cell: Part II. Electrochemical Oxygen Pump", Solid State Ionics, Vol. 107, pp. 217-220, 1998.

[40] Zubrin, R., B. Frankie, and T. Kito, "Mars In-Situ Resource Utilization Based on the Reverse Water Gas Shift: Experiments and Mission Applications", AIAA Paper 97-2767, July 1997.

[41] McElroy, J.F., "SPE® electrolyzers in support of Mission form Planet Earth", *Journal of Power Sources*, Vol. 36, No. 3, 1991, pp. 219 – 233.

[42] Takahashi, T., "Water Electrolysis", *Solar-Hydrogen Energy Systems,* 1st ed., edited by T. Ohta, Pergamon Press, New York, 1979, pp. 51 – 53.

[43] Feldman, W. C., Boynton, W. V. , Tokar, R. L., Prettyman, T. H., Gasnault, O., Squyres, S. W., Elphic, R. C., Lawrence, D. J., Lawson, S. L., Maurice, S., McKinney, G. W., Moore, K. R. and Reedy, R. C., "Global Distribution of Neutrons from Mars: Results from Mars Odyssey", *Science*, Vol. 297, Issue 5578, July 5, 2002, pp. 75-78.

[44] Titus, T. N., Kieffer, H. H., and Christensen, P. R., "Exposed Water Ice Discovered near the South Pole of Mars", *Science*, Vol. 299, Issue 5609, February 14, 2003, pp. 1048-1051.

[45] Meyer, T., and McKay, C., "Using the Resources of Mars For Human Settlement", *Strategies for Mars: A Guide to Human Exploration*, edited by C. R. Stoker and C. Emmart, Vol. 86, Univelt Inc., San Diego, CA, 1996, p. 398.

[46] Clark, D. L., "In-Situ Propellant Production on Mars: A Sabatier/Electrolysis Demonstration Plant", AIAA Paper 97-2764, July 1997.

[47] Iacomini, C. and Sridhar, K. R., "Electrolyzer Power Requirements for Oxidizer Production On Mars", 42nd AIAA Aerospace Sciences Meeting and Exhibit, Reno, NV, 5 – 8 January 2004.

[48] "Solar System Exploration Roadmap", JPL 400-1077, NASA, Jet Propulsion Laboratory, California Institute of Technology, Pasadena, CA, May 2003, pp. 37, 41.

[49] Isenberg, A. O., and Verostko, C. E., "Carbon Dioxide and Water Vapor High Temperature Electrolysis", SAE Paper 891506, July 1989.

[50] Isenberg, A. O., and Cusick, R. J., "Carbon Dioxide Electrolysis with Solid Oxide Electrolyte Cells for Oxygen Recovery in Life Support Systems", SAE Paper 881040, July 1988.

[51] Sridhar, K. R., Gottmann, M., and Baird, R.S., "2001 Mars In-Situ Oxygen Production Flight Demonstration", AIAA Paper 99-2413, June 1999.

[52] McElroy, J.F., Molter, T. M., and Roy, R. J., "SPE Water Electrolyzers for Closed Environment Life Support", Proceedings of the 21st International Conference on Environmental Systems, Society of Automotive Engineers, Inc., Warrendale, PA, 1991, p. 261-270.

[53] Scott Specialty Gases, Material Safety Data Sheets, 630-08-0/E-5, Plumsteadville, PA, March 16th, 2001.

[54] Wark, K. Jr., *Tables and Figures to Accompany Thermodynamics*, McGraw-Hill, New York, 1988, pp. 12 – 20, 22, 29, 41.

[55] Wark, K., Jr., *Thermodynamics, 5th Ed.*, McGraw-Hill Publishing Company, New York, 1988, p. 177, 498, 547, 606 –607.

[56] Rofer-DePoorter, C. K., "Untangling the Water Gas Shift From Fischer-Tropsch: A Gordian Knot?", *Catalytic Conversions of Synthesis Gas and Alcohols to Chemicals*, ed. by Herman, R. G., Plenum Press, New York, 1984, p. 97.

[57] King, R. B., "Homogeneous Transition Metal Catalysis: From The Water Gas Shift Reaction To Nuclear Waste Vitrification", Journal of Organometallic Chemistry, vol. 586 (1), 1999, pp. 2 – 17.

[58] Thomas, C. L., Catalytic Processes and Proven Catalysts, Academic Press, New York, 1970, p. 104.

[59] Atkins, P., and de Paula, J., Physical Chemistry, Seventh Edition, W.H. Freeman and Company, New York, 2002, p. 1002.

[60] Bejan, A., *Advanced Engineering Thermodynamics,2nd Ed.*, John Wiley & Sons, Inc., New York, 1997, p. 6, 67.

[61] Wark, K. Jr., Advanced Thermodynamics for Engineers, McGraw-Hill, New York, 1995, p. 192.